Master Thesis in Biophysical Chemistry

Characterization of complex solutions using relaxation- and diffusion weighted NMR Spectroscopy.

By

Hans-Tore F. Hansen

Department of Chemistry

University of Bergen

May 2017

Acknowledgements

First and foremost, I would like to thank my supervisor John Georg Seland for great guidance, NMR knowledge, ideas and assistance with required software.

I would like to thank my co-supervisor professor Tanja Barth for providing the biooil as well as insight in the Lignin-to-Liquid process.

I would like to thank the rest of the NMR group for inspiring presentations during lunch meetings. I would particularly like to thank chief engineer Olav A. Bjørklund for keeping the instruments up and running and Nils Åge Frøystein for help with shimming as well as inspiring me to pursue NMR spectroscopy during the KJEM140 course.

I would like to thank my friends Jørgen, Maren, Morten and Einar for social activities.

Last, but not least, I would like to thank my family for all the support during my years in Bergen.

Thank you all!

Bergen, May 2017

Hans-Tore F. Hansen

Abstract

The need for a sustainable replacement to the conventional fossil fuels is required. Biooils is a potential replacement. The biooil analyzed in this thesis is made from lignin, which is a by-product of paper production. This process is called Lignin-to-Liquid. A method to efficiently examine the oils with respect to molecular size distribution is required. In this thesis, high field relaxation and diffusion measurements are performed on diluted and non-diluted samples of crude oils. The crude oils have previously been examined with true boiling point distillation or compositional analysis. The same experiments are also performed on a biooil with unknown composition in attempt to characterize it with respect to molecular size distribution.

Spectral relaxation and diffusion measurements show that the chemical differences and more electronegative nature of the biooils causes aggregation at lower concentration than the crude oils. From the spectral diffusion and relaxation measurements no differences in molecular sizes was seen for the crude oils. The results from the T_1-T_2 correlation experiments showed a higher T_1/T_2 ratio of the lowest concentration sample of all the crude oils.

Spectral relaxation measurements of the non-diluted oils showed minor variation of T_1 relaxation times. High variation was seen in the T_2 relaxation times and the shortest T_2 relaxation times were found in the most electronegative region of the aliphatic region, as well as in the most electronegative part of the aromatic region. The T_1-T_2 correlation relaxation measurements replicated the spectral relaxation measurements for the non-diluted samples, meaning it is a viable time-saving option for non-diluted samples. Diffusion measurements of the non-diluted samples showed low variation, however when normalizing with the viscosity results were the same as previous analysis with respect to molecular size distribution.

In the analysis of the diluted samples the biooil is very different from the crude oils due to it aggregating at lower concentrations. The difference is made clearer due to the viscosity difference of the solvents. In the analysis of the non-diluted samples the biooil appear to be quite equal to the Grane crude with respect to molecular size distribution, although it is chemically different.

Symbols and abbreviations

Symbol

P	Angular magnetic momentum
I	Angular momentum quantum number (1/2 for protons)
$\hbar$	Planck's constant divided by 2π ($1{,}0546 \times 10^{-34} m^2 kg/s$)
μ	Magnetic moment
γ	Magnetogyric ratio ($26{,}7522 \times 10^{7} rad T^{-1} s^{-1}$ for protons)
B_0	Static magnetic field, flux density
B_{eff}	Effective static magnetic field, flux density
μ_z	Magnetic moment in the field direction
m	Magnetic quantum number (±1/2 for protons)
ΔE	Energy difference between the spin states
α	Low energy spin state (m=1/2)
β	High energy spin state (m=-1/2)
ν	Frequency
ν_L	Larmor frequency
ν_{ref}	Reference frequency
N_α	Amount of spins occupying the α spin state
N_β	Amount of spins occupying the β spin state
k_B	Boltzmann constant ($1{,}3806 \times 10^{-23} J/K$)
T	Temperature (Kelvin)
σ	Shielding coefficient
Θ	Pulse flip angle
τ_p	Pulse duration
I	Intensity
D	Diffusion coefficient
D^0	Diffusion coefficient, unlimited dilution
r	Molecular radius
η	Viscosity

δ	Gradient duration
g	Gradient strength
p	Coherence order
ϕ	Phase change
Λ	Jerk of a helix
τ_c	Correlation time
$\overline{B_{loc}^2}$	Average local field strength
ω	Frequency
W_0	Zero-quantum transition
W_1	Single-quantum transition
W_2	Double-quantum transition
b	Dipole-dipole coupling constant
$J(0)$	Spectral density, zero-quantum transitions
$J(\omega_0)$	Spectral density, single-quantum transitions
$J(2\omega_0)$	Spectral density, double-quantum transitions
T_1	Longitudinal (spin-lattice) relaxation
T_2	Transverse (spin-spin) relaxation

Abbreviations

NMR	Nuclear magnetic resonance
FID	Free induction decay
ppm	Parts per million ($x10^{-6}$)
DMSO-d6	Deuterated dimethyl sulfoxide
Toluene-d8	Deuterated toluene
rf	Radio frequency
HOD	Hydrogen oxygen deuterium
LtL	Lignin-to-Liquid
SARA	Saturates, aromatics, resins and asphalthenes
TMS	Tetramethylsilane
DOSY	Diffusion-oriented spectroscopy
ft	Fourier transform

TAN	Total acid number (mgKOH/g)
MW	Molecular weight (g/mol)
ir	Inversion recovery
sr	Saturation recovery
cpmg	Carr-Purcell-Maiboom-Gill
TS	TopSpin
DS	Dynamics Center

Table of contents

Chapter 1

Introduction

1.1: Background

The need for a sustainable replacement to the conventional fossil fuels is required. Biooils is a potential replacement. The biooil analyzed in this thesis is made from lignin, which is a by-product of paper production. This process is called Lignin-to-Liquid (LtL). The biooils are highly complex mixtures and conventional mapping of components such as gas chromatography is not ideal due to the high fraction of the biooil not being transferred into the gas phase [1,2]. An ideal result of the LtL-process is a biooil with high H/C-ratio, low O/C ratio and consisting of small molecules [3]. However, it's not only the biooils' properties as a fuel that is of importance; several enriching products such as vanillin is also a potential product of the LtL-process [1].

NMR spectroscopy is a very versatile method of sample analysis. Unlike many other methods of analysis NMR is non-destructive, meaning the samples can be stored and used to perform different experiments at separate times and different instruments. In this thesis, the focus is studying the dynamics of complex fluids but NMR is also commonly used in structure elucidation, mixture analysis, analysis of mechanism and kinetics of reactions and analysis of inter-and intramolecular exchange. In a liquid, the molecules' ability to move is dependent on the radius of the molecule [4]. This is the basis for diffusion measurements, where the self-diffusion coefficient of each different molecule in a solution is measured [5]. In addition, the molecular size also affects its ability to rotate in solution. The molecules' ability to rotate in solution is the basis for relaxation measurement in this thesis, where the correlation time of each molecule varies with size [6].

The most common methods of characterizing crude oils are true boiling point distillation, elemental analysis and API gravity. Experimental results are then compiled into assays, which can be very detailed [7]. In order to describe the contents of saturates, aromatics, resins and aspaltenes (SARA) liquid chromatography is commonly used [8-11] analysis' using quantitative ^{1}H and ^{13}C are also reported [7,12-14].

1.2: Previous work.

The biooil analyzed was prepared by Solmaz Ghoreishi using the Lignin-to-Liquid (LtL) process [15]. Crude summary reports of the Ekofisk and Grane crude were performed by Statoil [15,16]. The Field Stockton viscosity approximation and composition analysis were received from PhD candidate Zachary P. Alcorn at the Department of Physics and Technology, UiB.

Analysis of crude oil dynamics using diffusion and especially relaxation are reported [2,17], and results show a broad distribution of diffusion coefficients and relaxation times as a result of the viscosity of the oil and the composition [2,18,19]. Oxygen and paramagnetic species present in the sample aids in relaxation causing shorter relaxation times. The contribution of oxygen on relaxation times has been measured to be in the order of seconds for slowly relaxing oils and negligible for fast relaxing oils. The effect was found to be the same for both transverse and longitudinal relaxation and does not change the distribution, it only shifts it towards lower relaxation times [18].

Low field analysis of T_1-T_2 correlation has showed that different classes of oil (i.e. light, heavy, very heavy) have different shapes of T_1-T_2 correlation distributions [19]. Differences in T_1-T_2 distributions are also seen between the different components in crudes. Saturates and aromatic components have

broad distributions of both T_1 and T_2 relaxation times, while resins have a narrower interval of T_1 relaxation times [19].

Previous analysis' using high field diffusion and relaxation NMR to determine the molecular size distribution of biooils made with different catalysts with the LtL-process have been performed. Results showed a decrease in T_1/T_2 ratio with increased temperature during the LtL-process. Results also showed differences in T_1/T_2 ratio between the different catalysts used [20].

1.3: Aim of the project.

- Examining relaxation behavior on standard samples containing known hydrocarbons at known concentrations.
- Optimizing diffusion experiment parameters.
- Determining effects of increased concentration of three crude oils and one biooil using ^1H diffusion, relaxation and T_1-T_2 correlation experiments
- Use diffusion and relaxation experiments maintaining spectral information on non-diluted oils to locate functional groups causing aggregation.
- Characterize molecular size distribution of a biooil comparing with results from crude oils of known composition.

Chapter 2

Theory

2.1: NMR Spectroscopy background.

In 1946, two groups of physicists (Block *et al* from Stanford and Purcell *et al* from Harvard) observed magnetic resonance signals for the first time. In 1952, they received the Nobel Prize in physics for their work [21].

2.2: Angular momentum and magnetic momentum.

Nuclei with angular momentum quantum number I≠0 have angular magnetic momentum P. In this thesis, the signal from ^{1}H is detected, which have an angular momentum quantum number of I=1/2. The formula for angular magnetic momentum P as a function of angular momentum quantum number I is listed below, where $\hbar$ is Planck's constant divided by 2π (1,0546x10^{-34}m^{2}kg/s)

$$P = \sqrt{I(I+1)}\hbar \qquad \text{Eq.2.1}$$

The magnetic moment μ is related to the angular magnetic moment P and the magnetogyric ratio γ of the nuclei detected. The magnetogyric ratio of protons are 26,7522x10^{7}radT^{-1}s^{-1}.

$$\mu = \gamma P = \gamma \hbar \sqrt{I(I+1)} \qquad \text{Eq.2.2}$$

Equation 2.2 clearly states there are no magnetic moment μ unless the angular momentum quantum number I≠0.

2.3: Nuclei in static magnetic fields and resonance conditions

When nuclei with angular momentum quantum number I≠0 experiences a static magnetic field B_0 oriented along the z-axis of a Cartesian coordinate system the magnetic moment μ will reorient itself in the B_0 direction. The magnetic moment μ_z in the direction of the main magnetic field is

$$\mu_z = \gamma m \hbar \qquad \text{Eq.2.3}$$

In equation 2.4, m represents the different energy levels the spins can occupy. For each nucleus, 2I+1 spin energy states are available. For nuclei with I=1/2 spins that align themselves in the same direction as the magnetic field are said to be in the α-state (m=1/2) and spins that align themselves in the opposite direction of the field are said to be in the β-state (m=-1/2). The difference in energy ΔE between these spin energy states is given by

$$\Delta E = -\Delta m \gamma \hbar B_0 \qquad \text{Eq.2.4}$$

For nuclei with I=1/2 Δm=1 so equation 2.5 can be rewritten as

$$\Delta E = -\gamma \hbar B_0 \qquad \text{Eq.2.5}$$

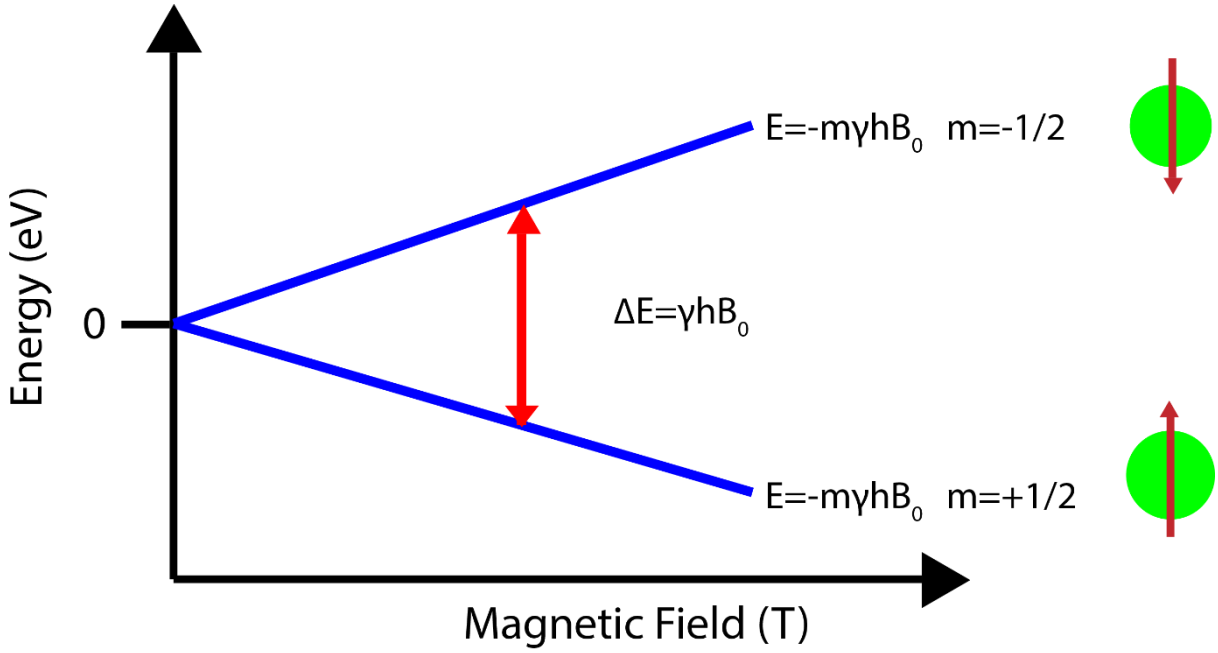

Figure 2.3.1: Difference in energy ΔE between the two possible spin energy states m=+1/2 (α) and m=-1/2 (β) for nuclei with I=1/2. [23]

The energy difference between the spin energy states can be rewritten in terms of frequency units

$$\Delta E = h\upsilon \qquad \text{Eq.2.6}$$

Transitions between the spin energy states occurs at the Larmor frequency ν_L

$$\nu_L = \left|\frac{\gamma}{2\pi}\right| B_0 \qquad \text{Eq.2.7}$$

The equilibrium of the spin energy states follows Boltzmann's statistics

$$\frac{N_\beta}{N_\alpha} = e^{-\frac{\Delta E}{k_B T}} \approx 1 - \frac{\Delta E}{k_B T} = 1 - \frac{\gamma \hbar B_0}{k_B T} \qquad \text{Eq.2.8}$$

Since the difference in energy ΔE is very small compared to the thermal energy k_BT at practical working temperatures the difference in populations between the different spin energy states are usually in the order of ppm (10^{-6}).

2.4: Chemical shift.

The scale most commonly used to assign peaks in an NMR spectra is the ppm-scale. This scale is defined in terms of the difference in frequency between the frequency ν of the unknown and the frequency ν_{ref} of the reference.

$$ppm = \frac{\nu - \nu_{ref}}{\nu_{ref}} = \frac{\Delta\nu}{\nu_{ref}} \frac{[Hz]}{[MHz]} \qquad \text{Eq.2.9}$$

The Larmor frequency of each spin transition detected in a sample varies due to effects caused by the chemical environment of the nuclei being detected. This effect occurs due to varying electron density surrounding the detected nucleus. The shielding effect σ alters the magnetic field B_0 and the result is that every nucleus experiences a different field B_{eff} depending on its surroundings.

$$B_{eff} = (1 - \sigma)B_0 \qquad \text{Eq.2.10}$$

Inserting equation 2.11 into equation 2.8 gives the following expression for the Larmor frequency ν_L

$$\nu_L = \frac{\gamma}{2\pi}(1-\sigma)B_0 \qquad \text{Eq.2.11}$$

2.5: Acquiring a spectrum – the pulse method

In NMR Spectroscopy radio frequency (rf) pulses are used to excite all nuclei within the sample at the same time. There are soft pulses which only deliver one frequency, and there are hard pulses delivering a range of frequencies. This range is depending on the spectral width (range of ppm-values). It is in this thesis, and most commonly, used hard pulses.

To understand the pulse method, one should picture a Cartesian coordinate system consisting of a x-, y- and z-axis where the magnetization at equilibrium (before the pulse(s) start) is oriented along the z-axis. The xy-plane rotates around the z-axis. Pulses are then applied along either of the axis rotating the magnetization. A pulse along the axis of the magnetization has no effect on the magnetization.

When a pulse is applied, the magnetization flips with an angle Θ depending on the magnetogyic ratio γ of the nuclei being detected, the field strength B and the pulse duration τ_p.

$$\Theta = \gamma B \tau_p \qquad \text{Eq.2.12}$$

The signal intensity is the same as a sin-function, meaning the signal detected reaches a maximum when a 90°-pulse is applied, a minimum when a 270°-pulse is applied and no signal when a 180°-pulse or a 360° is applied.

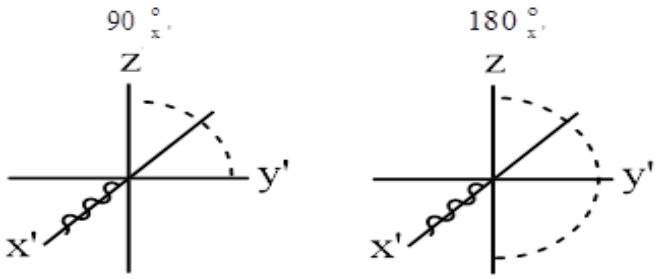

Figure 2.5.1: Vector representation of rotation of magnetization as a result of a 90°- and a 180° pulse along the x-axis. An apostrophe is added to the label for the x and y axis to emphasize that their positions are not fixed, but rotates around the z-axis.

2.6: The Fourier transform

As spectra are recorded as a function of time, the spectra must be transformed from a time domain to a frequency domain. This operation is called Fourier transform.

$$F(\omega) = \frac{1}{\sqrt{2\pi}} \int_{-\infty}^{\infty} e^{-i\omega t} dt \qquad \text{Eq.2.13}$$

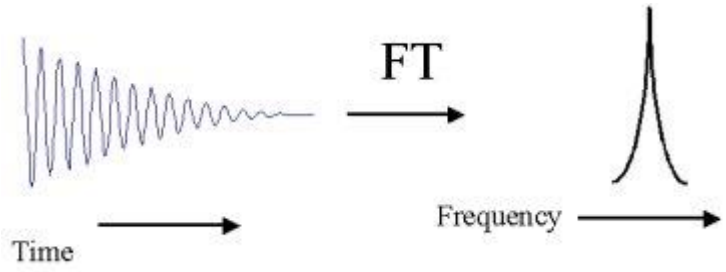

Figure 2.6.1: Visual representation of the Fourier transform of the time domain free induction decay (FID) into the frequency domain spectrum. [23]

2.7: Relaxation

In NMR, the spin system is returned to equilibrium in a process called relaxation. The relaxation of spins is possible due to the presence of local fields. These local fields are created by the spins themselves, and the local field from one spin is experienced by several nearby spins. A source to such a field is called a *relaxation mechanism* and for I=1/2 nuclei two mechanisms dominate; *dipole-dipole* mechanism and chemical shift anisotropy [24]. Due to the dipole-dipole mechanism's high dependence on distance between the spins, relaxation measurements are highly concentration dependant. In this thesis, paramagnetic species may also be contributing on a significant level, since bio-oils contain a substantial amount of oxygen. In addition to this, O_2 inevitably enters the sample during preparation and samples are not degassed. The effect of oxygen has been explored and results show the effect is large for slowly relaxing species while it is negligible for species with low relaxation times [19].

2.7.1: Correlation time

Due to the ever-changing local fields within the sample because of molecular motion, the relaxation process is best described by the correlation time τ_c. The correlation time τ_c is the time it takes an arbitrary molecule to rotate one radian. $\overline{B_{loc}^2}$ is the average local field strength across the sample and τ is the time.

$$G(\tau) = \overline{B_{loc}^2} \exp(-|\tau| / \tau_c) \qquad \text{Eq.2.14}$$

Fourier transform of this equation leads to the spectral density function J(ω)

$$G(\tau) \xrightarrow{FT} J(\omega) = \overline{B_{loc}^2} \frac{2\tau_c}{1+\omega^2\tau_c^2} \qquad \text{Eq.2.15}$$

The rotational correlation time depends on the viscosity η, the molecular radius r_g and the temperature T. k is the Boltzmann's constant.

$$\tau_c = \frac{4\pi\eta r_g^3}{3kT} \qquad \text{Eq.2.16}$$

2.7.2: Solomon equations and the spectral density function.

In weakly coupled homonuclear AX spin systems there are four energy eigenstates, depending on the spin state of each of the coupled spins.

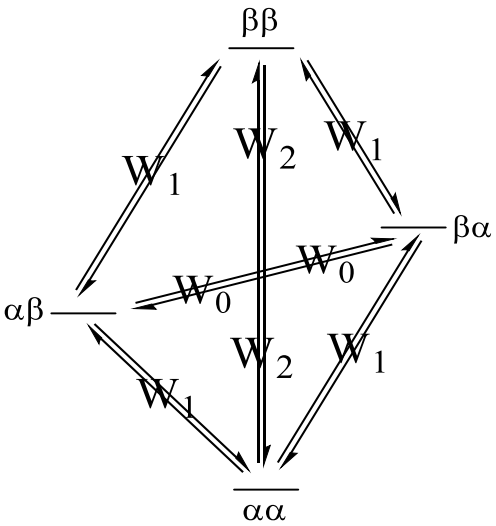

Figure 2.7.1: Possible spin eigenstates and spin transitions in a homonuclear AX spin system.

This results in 12 possible transitions; eight single-quantum transitions (W_1), two double-quantum transitions (W_2) and two zero-quantum transitions (W_0). The transition probabilities depend on the spectral density at the different transitions and the dipole-dipole coupling constant b, when internal molecular motions are ignored.

$$W_1 = \frac{3}{20} b^2 J(\omega_0) \qquad \text{Eq.2.17}$$

$$W_2 = \frac{3}{5} b^2 J(2\omega_0) \qquad \text{Eq.2.18}$$

$$W_0 = \frac{1}{10} b^2 J(0) \qquad \text{Eq.2.19}$$

Basing relaxation on the rotational correlation time τ_c and their corresponding spectral density J(ω) one obtains the current relationships between the two relaxation times and the spectral density.

$$T_1^{-1} \propto 2J(\omega_0) + 8J(2\omega_0) \qquad \text{Eq.2.20}$$

$$T_2^{-1} \propto 3J(0) + 5J(\omega_0) + 2J(2\omega_0) \qquad \text{Eq.2.21}$$

Transverse relaxation is strongly affected by field inhomogeneities and reduced relaxation times are observed. This reduced relaxation time is labelled T_2^* and is a function of the transverse relaxation time T_2, the magnetogyric ratio γ and the field inhomogeneity ΔB_0

$$\frac{1}{T_2^*} = \frac{1}{T_2} + \gamma \Delta B_0 \qquad \text{Eq.2.22}$$

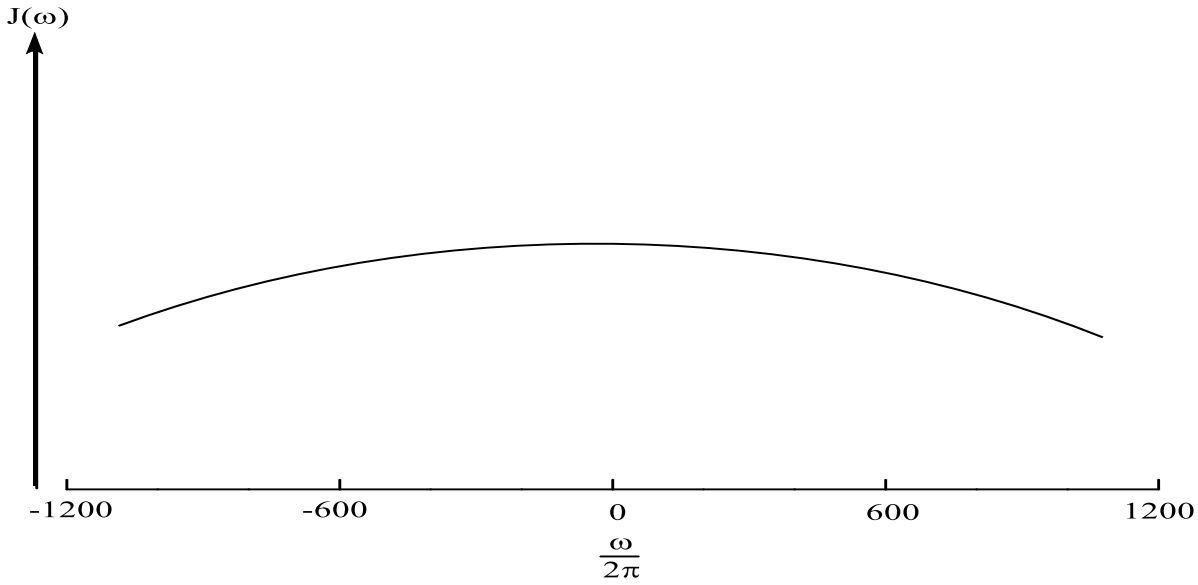

Figure 2.7.2: Spectral density as a function of frequency.

As shown in eq.2.21 and eq.2.22 T_2 depends on the spectral density J(0), while T_1 does not. This implies that $T_1 > T_2$ unless the spectral density function (figure 2.7.2) is flat, which is only the case when $J(0) = J(\omega_0) = J(2\omega_0)$. When the spectral density function of a spin is flat, the spin is said to be within the extreme narrowing range and $T_1=T_2$. At high magnetic fields (11,7 and 14,1T used in this thesis) only small molecules with a short rotational correlation time will be within this range. However, at lower magnetic fields the extreme narrowing range will be broader and cover a larger number of rotational correlation times.

2.7.3: T_1-measurement

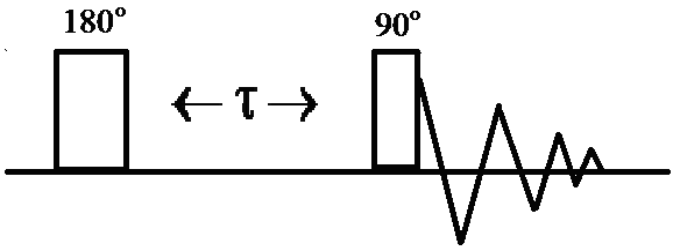

Figure 2.7.3: Pulse sequence used to measure T_1 using inversion recovery (T1ir).

Measurements are done varying the value from τ using the vd-lists in appendix B. The value for T_1 is determined with the help of TopSpin 3.5.pl5 and Dynamic Center,version 2.4.4 using the fitting function $f(t) = I_0 \cdot [1 - 2\exp(-t/T_1)]$

2.7.4: T_2-measurement

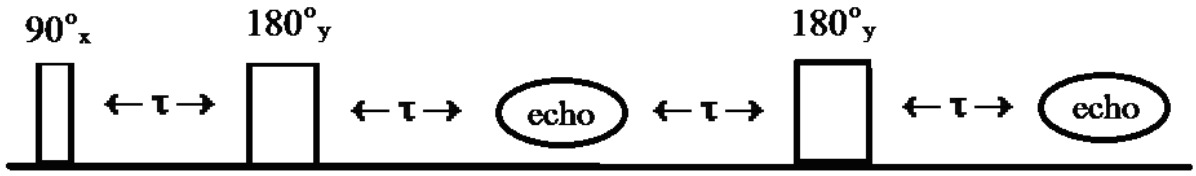

Figure 2.7.4: Carr-Purcell-Maiboom-Gill sequence (cpmg) used in T_2-analysis.

The interval between the echoes are determined by the time values from the vc-lists in appendix C. The T_2 value is determined using the same software as in the determination of T_1, but with the fitting function $f(t) = I_0 \cdot \exp(-t/T_2)$

2.8: Diffusion

The concepts behind pulsed gradient spin-echo techniques used in diffusion experiments are more than 60 years old [25]. However, in the era of continuous wave instrumentation there was minor use of diffusion oriented NMR spectroscopy [26]. With the introduction of Fourier-transform pulse instrumentation [27] in the 1980s and an addition of better software and hardware both for performing experiments [28] and processing diffusion studies are now performed at much larger scale with improved accuracy and resolution. Progress within gradient stability and gradient strengths allow for slowly diffusing (larger molecules) to be detected accurately [2].

Diffusion is the random motion of molecules in the sample. The type of diffusion measured in NMR is called self-diffusion [29]. The diffusion coefficient depends on the temperature T, the viscosity η and the radius of the solvated molecule r. For a molecule with a perfect sphere shape the diffusion coefficient D at infinite dilution is given by the Stoke-Einstein equation

$$D^0 = \frac{k_B T}{6\pi\eta r} \qquad \text{Eq.2.23}$$

Since the molecular radius r is proportional to the molecular mass MW the diffusion coefficient is also proportional to molecular mass MW [30].

$$D \propto \frac{1}{\sqrt[3]{MW}} \qquad \text{Eq.2.24}$$

And for a sample containing multiple species

$$\frac{D_1}{D_2} \propto \sqrt[3]{\frac{MW_2}{MW_1}} \qquad \text{Eq.2.25}$$

To better compare different samples with each other, an internal standard can be added to each sample. This standard must be chemically inert and have a constant radius. A logical and practical standard in terms of NMR measurements is tetrametylsilane (TMS). With such a standard present, it is possible to eliminate potential differences in viscosity and temperature between two sample one wishes to compare [31].

$$\frac{D_{TMS}}{D_X} = \frac{\frac{k_B T}{6\pi\eta r_{TMS}}}{\frac{k_B T}{6\pi\eta r_X}} = \frac{r_X}{r_{TMS}} \qquad \text{Eq.2.26}$$

This relationship between the radius of TMS r_{TMS} and the radius of another molecule in the sample r_X can then be used to look at differences between different samples, independent of differences in viscosity and temperature.

2.8.1: Measuring diffusion

In general, the signal S acquired at a time t in a NMR experiment is given by the magnetization M at position r modified by a phase factor

$$S(t) = \int M(\boldsymbol{r}) e^{i\phi(r,t)} dV \qquad \text{Eq.2.27}$$

In diffusion experiments gradients are used to induce a phase change. Using rectangular gradient pulses with a duration δ and strength g on a sample containing spins with coherence order p and magnetogyric ratio γ the phase change induced by the gradient pulse at a position **r** in the sample is

$$\phi(\boldsymbol{r}) = p\gamma\delta\boldsymbol{g}\cdot\boldsymbol{r} \qquad \text{Eq.2.28}$$

When diffusion experiments are performed, transverse magnetization are twined into a helix by a gradient pulse, before it is untwined by a second gradient pulse [32]. The jerk Λ of the helix is defined by the magnetogyric ratio γ of the nuclei in question, the gradient pulse duration δ and the gradient strength g

$$\Lambda = \frac{2\pi}{\gamma\delta g} = q^{-1} \qquad \text{Eq.2.29}$$

2.8.2: Using the attenuated signal to determine the diffusion coefficient.

The Bloch-Torrey equation is used to determine the signal attenuation resulting from the pulse sequences run in the determination of the diffusion coefficient D in freely diffusing samples. The flow term of the Bloch-Torrey equation is ignored, as there is no flow present in the samples.

$$\frac{\partial \boldsymbol{M}(\boldsymbol{r},t)}{\partial t} = \gamma \boldsymbol{M}\times\boldsymbol{B}(\boldsymbol{r},t) - \frac{M_x i + M_y j}{T_2} - \frac{(M_z - M_0)k}{T_1} + \nabla\cdot\boldsymbol{D}\cdot\nabla\boldsymbol{M} \qquad \text{Eq.2.30}$$

The Bloch-Torrey equation is then solved and the solution achieved is different for each pulse sequence. However, for the purpose this thesis the most important thing is that the signal strength can be described as a function of the original signal strength I_0 multiplied by an exponential factor b and the self-diffusion coefficient D that causes the signal attenuation.

$$I = I_0 e^{-bD} \qquad \text{Eq.2.31}$$

Rewriting this equation with respect to the exponential factor b leads to

$$\ln\left(\frac{I}{I_0}\right) = -bD \qquad \text{Eq.2.32}$$

The factor b is the signal attenuation factor caused by the gradient strength g and duration δ, as well as the magnetogyric ratio γ of the nuclei in question and the diffusion time Δ. For a normal stimulated echo (STE) and a double stimulated echo (DSTE) sequence the attenuation factor b is

$$b(STE) = \gamma^2\delta^2 g^2\left(\Delta - \frac{\delta}{3}\right), \qquad b(DSTE) = 2\gamma^2\delta^2 g^2\left(\Delta - \frac{\delta}{3}\right) \qquad \text{Eq.2.33}$$

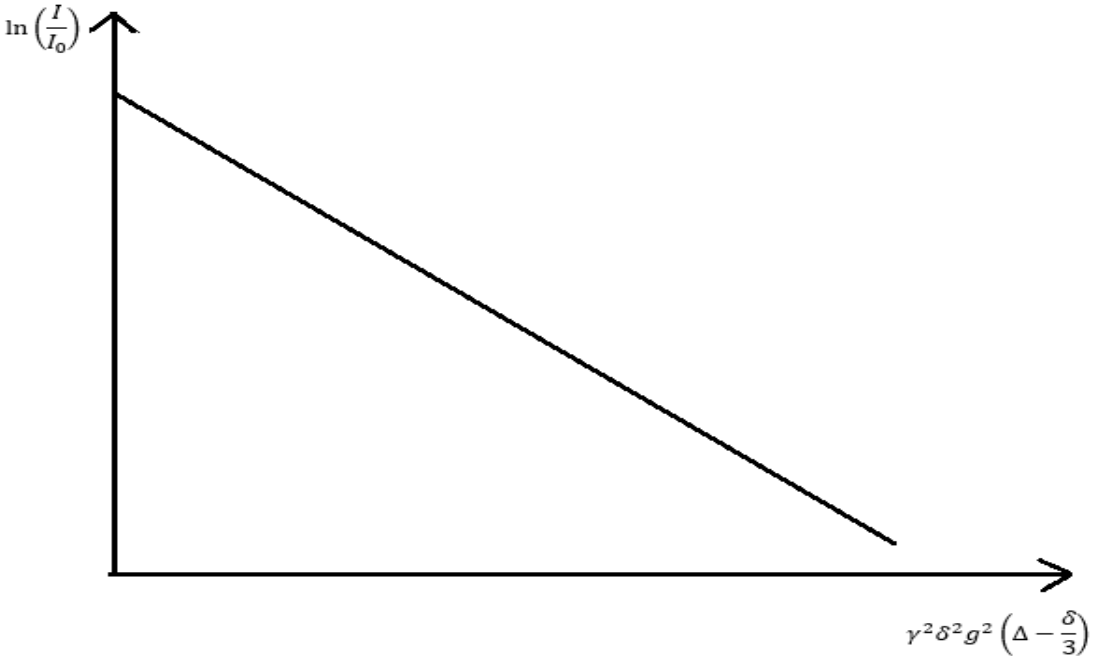

Figure 2.8.1: Example plot of b plotted against $\ln\left(\frac{I}{I_0}\right)$*. The slope of the line is -D.*

Chapter 3

Experimental

3.1: Sample preparation.

The oils were weighed in using an analytical weight (Δm=±0,0005) then solved using 790µL Toluene-d8. The sample was then shaken vigorously for one minute before 690µL sample was transferred to a NMR-tube. 10µL TMS was added as reference before the top of the NMR-tube were melted off in order to keep the sample volume constant. Samples were stored in a refrigerator (4-7°C) in a beaker covered in Al-foil.

The concentration series of the bio-oil Exp_35 were made using DMSO-d6 instead of Toluene-d8 as a solvent. The preparation of these samples was the same, except the weighed-in oil was dissolved in 690µL solvent. 590µL were then transferred to the NMR-tube before 10µL TMS was added as reference. The tops of these sample tubes were not immediately melted.

The standard samples containing hydrocarbons were made to a concentration of approximately 150mM total (i.e. when a sample containing two different hydrocarbons, 75mM of each was added) based on densities of pure components.

Table 3.3.1: Sample overview – standard samples.

	V heptane [µL]	V hexadecane [µL]	Total volume [µL]	C heptane [mM]	C hexadecane [mM]
Standard 1	13,3		600	150,3	
Standard 2		26,5	600		150,2
Standard 3	6,6	13,2	600	74,6	74,8

Table 3.3.2: Sample overview – oil samples.

Sample name	Mass oil [mg] Δm=±0.5mg	Sample concentration [g/mL]
Ekofisk 20mg	22,3	0,03
Ekofisk 200mg	200,1	0,25
Grane 20mg	26,8	0,03
Grane 190mg	190,0	0,24
Stockton 40mg	40,0	0,05
Stockton 200mg	200,7	0,25
35LC	27,1	0,04
35MCminus	59,9	0,09
35MC	82,5	0,12
35MCplus	102,2	0,15
35HC	130,9	0,19

3.2: Analysis on the 600MHz.

In this section commands in TopSpin are written in **bold** while configurations in TopSpin not done using the command line (i.e. processing) are written in *italics*. All pulse sequence figures are drawn using TopSpin, unless otherwise is mentioned.

3.2.1: Shimming.

After the sample had been inserted tuning and matching were performed using **atma** followed by **atmm** only if the automatic tuning and matching was insufficient. Locking were performed using **lock** before the solvent were selected. Then the phase was corrected using **autophase** before the field were manually corrected if necessary. **autogain** was typed followed by **topshim gui** which was started using the configurations shown in figure 3.1.

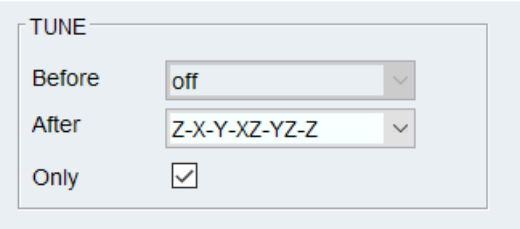

*Figure 3.1: Configurations for **topshim gui.***

Autogain was run again after the topshim, before the phase was automatically corrected using **autophase** again. Then **tune.sx** were performed before finally **loopadj** were used to do the final phase- and lockgain-configurations.

3.2.2: Calibrating pulse length and ^{1}H-spectrum (zg)

The receiver gain was acquired using **rga**. The 360°-method was used to calibrate the 90°-pulselength. This was done by setting **o1p** to a selected peak before varying **p1** until the signal from this signal was as close to zero as possible. **p1** was then divided by four to obtain the 90°-pulselength. In the calibration **p1** was increased by 0,4µs every step, meaning that the used pulse length for a 90° pulse should be within ±0,1µs of the actual pulse length. Pulse lengths acquired were in the interval 6.7-7.5µs.

^{1}H-spectrum was then obtained using the 90°-pulselength found using the 360°-method with o1p=4,7 and sw=10,0131. Four scans were done (**ns 4**) with zero dummy scans (**ds 0**). The delay between scans were 10s (**d1 = 10**) and the number of points were 65k (**td = 65k**). This experiment took 1 minute. The spectrum was processed using **efp** (efp = em + ft + apk). Manual phasing was performed if **apk** was insufficient and the baseline was corrected using **bas ->** *autocorrect baseline using polynomial*.

3.2.3: ^{1}H-T_1 (T1ir)

For the T_1 measurement the inverse recovery sequence was used. D1 was set to 15s with d11 set to 30ms. The gap between the pulses are values from the vd-list in appendix B. Spectrum was acquired with 65k points in the F2-dimension, **ns 8** and **ds 4**.

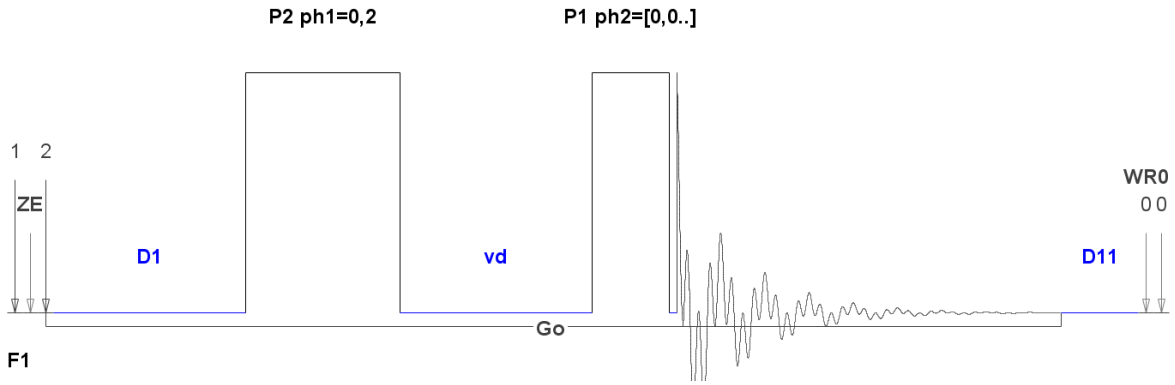

Figure 3.2: T1ir-sequence used to measure spin-lattice relaxation.

The spectrum was processed using **xf2** and manually phased by manually phasing the last row (FID 32) to pure absorption.

3.2.3.1: Processing in TopSpin

To calculate values for T_1 using TopSpin the following procedure was followed: *Analyze -> Dynamics -> T1T2*. Peak picking was done manually, using spectrum #32 and integrating the peaks. In the Relaxation parameter window the number of components were changed in order to achieve the best possible fit for each peak. Fitting were performed based on peak intensities.

3.2.3.2: Processing in Dynamics Center

The procedure in Dynamics Center was followed using manual threshold peak picking on the 32th spectrum. The threshold was placed as close as possible to the baseline without including the baseline. Since the baseline in Dynamics Center were not necessarily the same as in TopSpin and varied between the different datasets the reproducibility of the peak selection is low. The number of components were set to 3 for the oils and the first fit value are used in the plots due to great uncertainty in the values for the second and third component.

3.2.4: ^{1}H-T2 (cpmg)

For the T_2-measurement the Carr-Purcell-Meiboom-Gill (cpmg) sequence was used. D1 was set to 10s, d20 to 2ms and d11 to 30ms. The times vc are given in the vc-list in appendix B. Spectrum was acquired with 65k points in the F2-dimension, **ns 8** and **ds 16**.

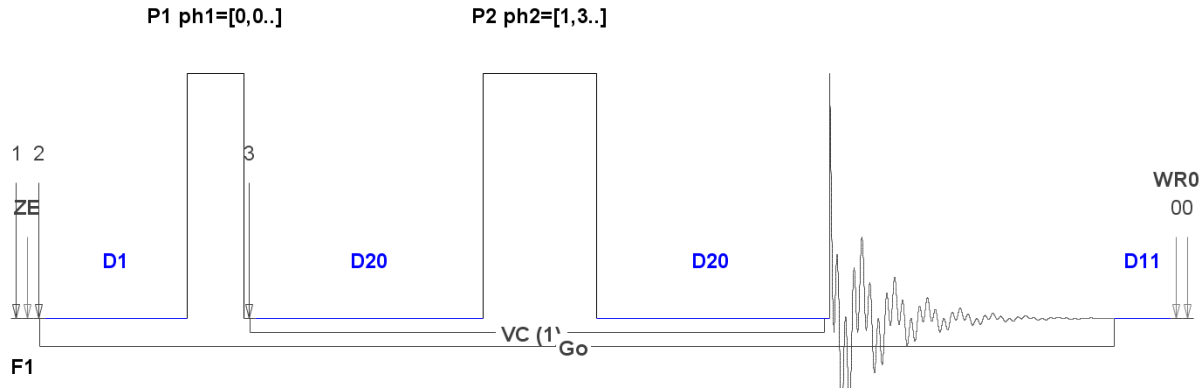

Figure 3.3: cpmg-sequence used to measure spin-spin relaxation.

The spectrum was processed using **xf2** and manually phased by manually phasing the first row (FID 1) to pure absorption.

The T_2-analysis in TopSpin and Dynamics Center was done the same way as the one for T_1, except peak picking/manual threshold were done in the first spectrum (FID 1).

3.2.5: T_1-T_2 correlation measurement (t1sr_cpmg_all_echoes)

T_1-T_2 measurements on the AV600 were performed using the t1sr_cpmg_all_echoes sequence with **d1=1s**, **ns=8**, **ds=2**, **td(F2)=8192** and **d20=2ms**.

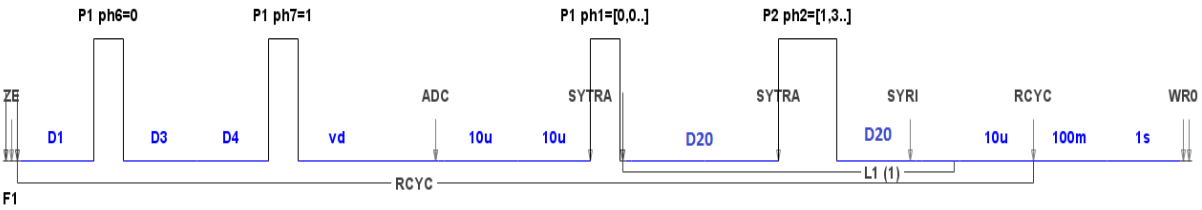

Figure 3.4: T1sr_cpmg_all_echoes sequence used in the T_1-T_2 correlation measurements on the 600MHz.

3.2.5.1: Processing in MatLab

MATLAB version R2016b was used in the processing of the T_1-T_2 correlation (figure 3.4 and figure 3.8) data. Scripts used are found in appendix C. Firstly, the script T1_T2_500_sr.m was used with the value for the echo spacing in the CPMG train set to 2ms. Secondly, the inverse Laplace software was opened typing “TwoDLaplaceInverse” in the command window.

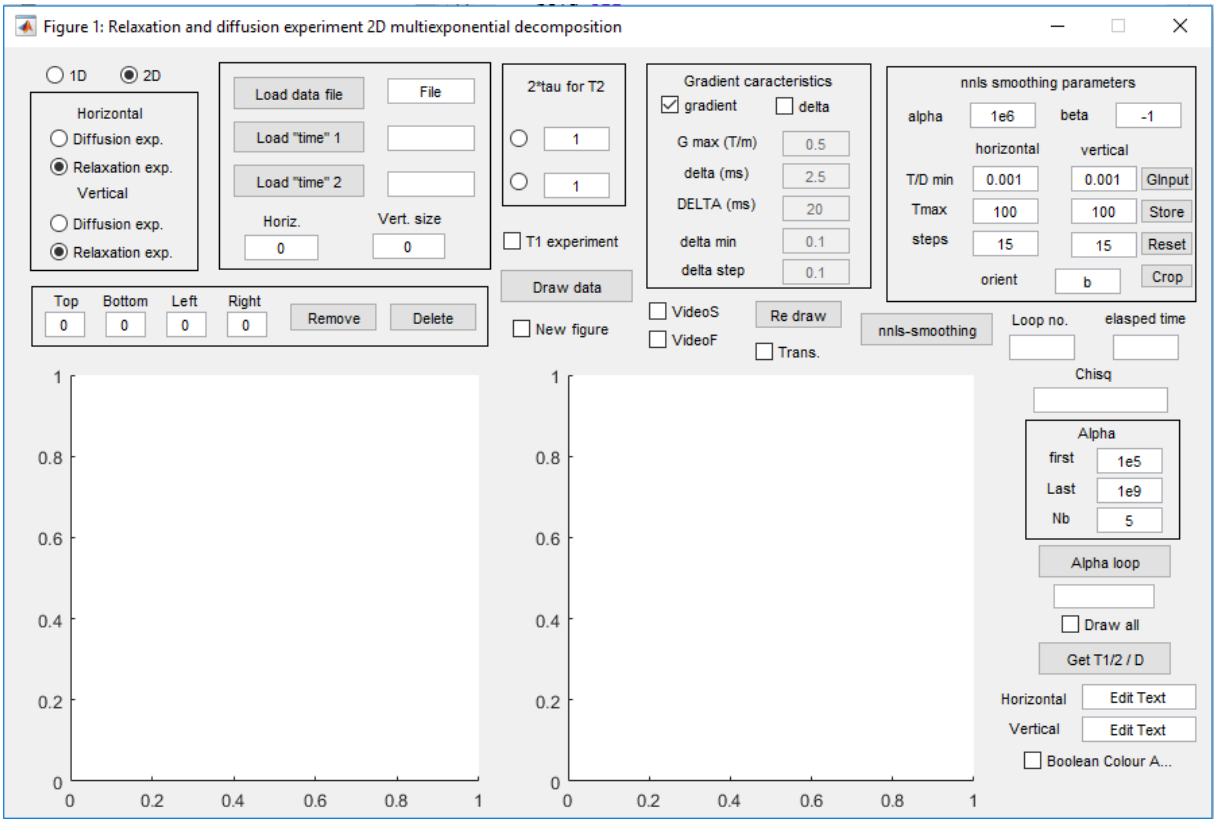

Figure 3.5: The Inverse Laplace window.

The script previously run creates three files of interest inside the original data folder: T1_T2_data_inv, t_ir and t_cpmg. To further process and plot the data the following sequence is followed;

1. Load data file – T1_T2_data_inv
2. Load “time” 1 – t_ir
3. Load “time” 2 – t_cpmg
4. Draw data
5. Change both horizontal and vertical steps in the nnls smoothing parameters to 32
6. Nnls-smoothing
7. From the figure achieved in the right-hand window T/Dmin and Tmax can now be readjusted to more appropriate values.
8. Nnls-smoothing
9. Change alpha values to adjust the look of the plot until it looks satisfactory
10. Repeat for another dataset or close the window

The plotted figures presented in this thesis are created by selecting the folder with the processed data and using the plotfig_T1T2_500.m script.

3.3: Analysis on the 500WB magnet using diffprobe

Shimming and 90°-pulse calibrated was done the same way for the 500WB as it was for the 600MHz. The non-diluted oils were shimmed using **gs** with **d1=1s** if necessary.

3.3.1: Diffusion measurements

Diffusion was measured using the double stimulated echo sequence with LED (leddste). Leddste experiments were done using the **diff5** program within TopSpin (version 3.5pl6). The protocol "DSTEWATER" was selected and the expected diffusion constant was set to 5,00E-10 for the crude oils dissolved in Toluene-d8 and 5,00E-11 for the biooil concentration series dissolved in DMSO-d6. LED-delay was set to 5ms, number of scans set to 8 and number of dummy scans set to 4. The number of gradient steps was changed between 16, 32 and 64 to find the most efficient value. DELTA was also changed between 11,23ms, 50ms, 100ms and 200ms to check the time dependence of the diffusion coefficient. Gradient pulse duration δ was set to 5,00ms and the pre-scan delay (d1+aq) was set to 10s.

3.3.1: ^{1}H-DOSY

For the non-diluted samples the ledbpg2s sequence was used in order to counteract internal gradients. Experiments were run with td(F1)=32k, **d20=11,23ms**, **ns=8**, **ds=4**, **d1=8s** and **d21=5ms** This sequence was not run using **diff5**, it was set up normally and executed using **DOSY**. 32 linear gradient steps were used, with maximum and minimum values used for the different samples shown in table 3.3.2.

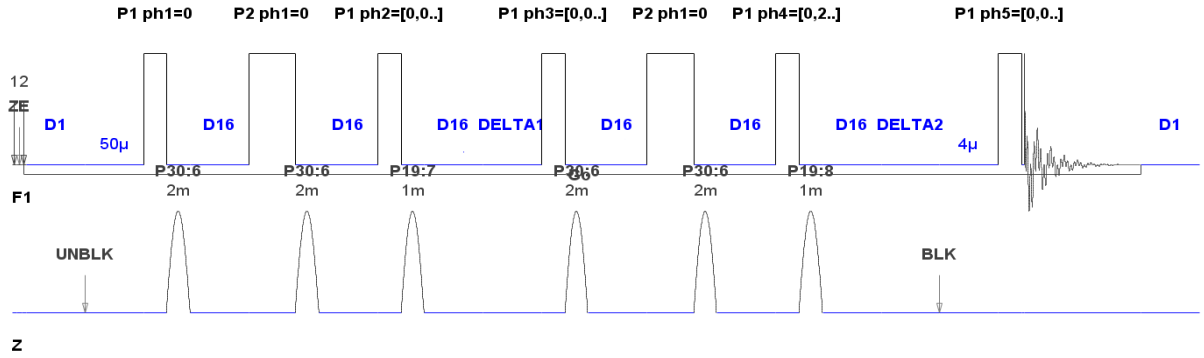

Figure 3.6: Ledbpgp2s-sequence used in diffusion measurements.

Table 3.3.3: Minimum and maximum gradient strenghts used for the non-diluted samples.

Oil sample	g_{min} [gauss/cm]	g_{max} [gauss/cm]
Grane crude	1,082	1060,521
EXP35 biooil	1,082	1060,521
Ekofisk crude	1,082	541,082
Stockton crude	1,082	541,082

Data was processed using **xf2** and manually phasing the first spectra. Baseline was corrected using **bas**. -> *Auto-correct baseline using polynomial.*

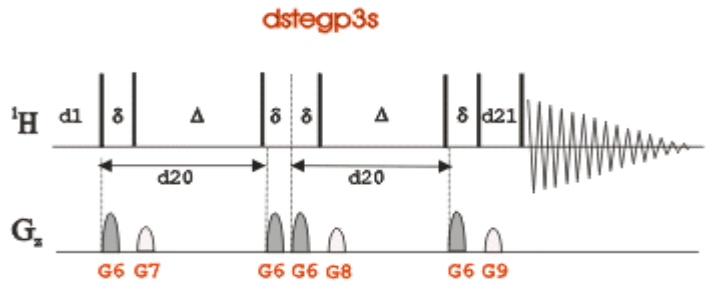

Figure 3.7: leddste-sequence used in diffusion measurements in order to compensate for convection. Figure from the TopSpin manual.

A change in DELTA (Δ) leads to a change in the gradient strength g necessary to achieve the same value for b (Eq.2.33). Values for Δ and corresponding gradient strengths are tabulated below.

Table 3.3.4: Values for g_{min} and g_{max} for each of the different Δ-values.

Δ [ms]	g_{min} [gauss/cm] crude oil sample	g_{max} [gauss/cm] crude oil sample	g_{min} [gauss/cm] biooil sample	g_{max} [gauss/cm] biooil sample
11,23	12	248	24	780
50	6	114		
100	3	81		
200	2	57		

Data was processed using **xf2** and phased manually. For the comparison between the spectra with different number of gradient steps (td(F1)) **dosy2d setup** and **dosy2d** was used before **.md** to compare the spectra.

3.3.1.2: Processing in Dynamics Center

The processed spectrum was uploaded to Dynamics Center version 2.4.8. Peaks were picked using manual threshold with "peak epsilon in F2" set to 50. Dynamics Center then fitted the data using the fitting formula $f(B) = I_0 \cdot e^{-BD}$. The results from the fitting was the exported to Excel.

3.3.2: T_1-T_2 correlation measurement (t1ir_cpmg_all_echoes)

T_1-T_2 correlation measurements on the 500WB were performed using the t1ir_cpmg_all_echoes sequence with **d1=4s**, **ns=8**, **ds=2**, **td(F2)=8192** and **d20=2ms**.

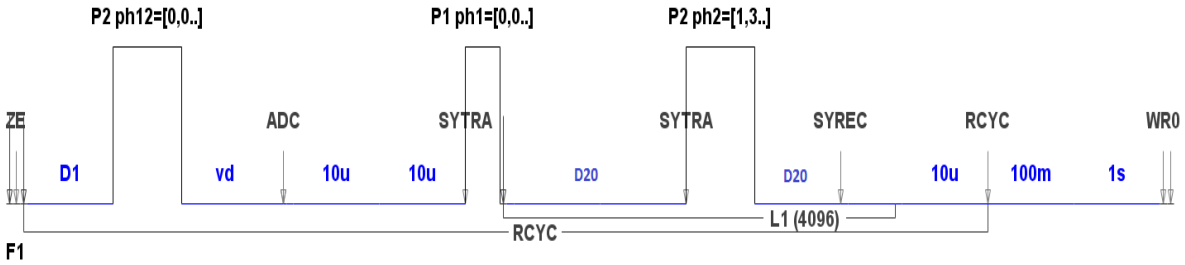

Figure 3.8: T1ir_cpmg_all_echoes sequence used to measure T_1-T_2 correlation of the non-diluted oils.

3.3.2.1: Processing in MatLab

The data achieved with the t1ir_cpmg_all_echoes sequence was processed the same way as the data achieved with t1sr_cpmg_all_echoes except the script named T1_T2_sr.m was used instead of the T1_T2_ir.m script.

Chapter 4

Results – Optimizing diffusion experiments and standard samples.

4.1: Instrumental variation measuring diffusion coefficients.

A series of six experiments were performed on the EXP35_MCplus sample to control the variation in fitted diffusion coefficients from the TopSpin fitting tool as well as potential instrumental instabilities. Experiments were done with Δ=11,23ms and td(F1)=32. The same peaks are picked for all the experiments and plotted in figure 4.1.

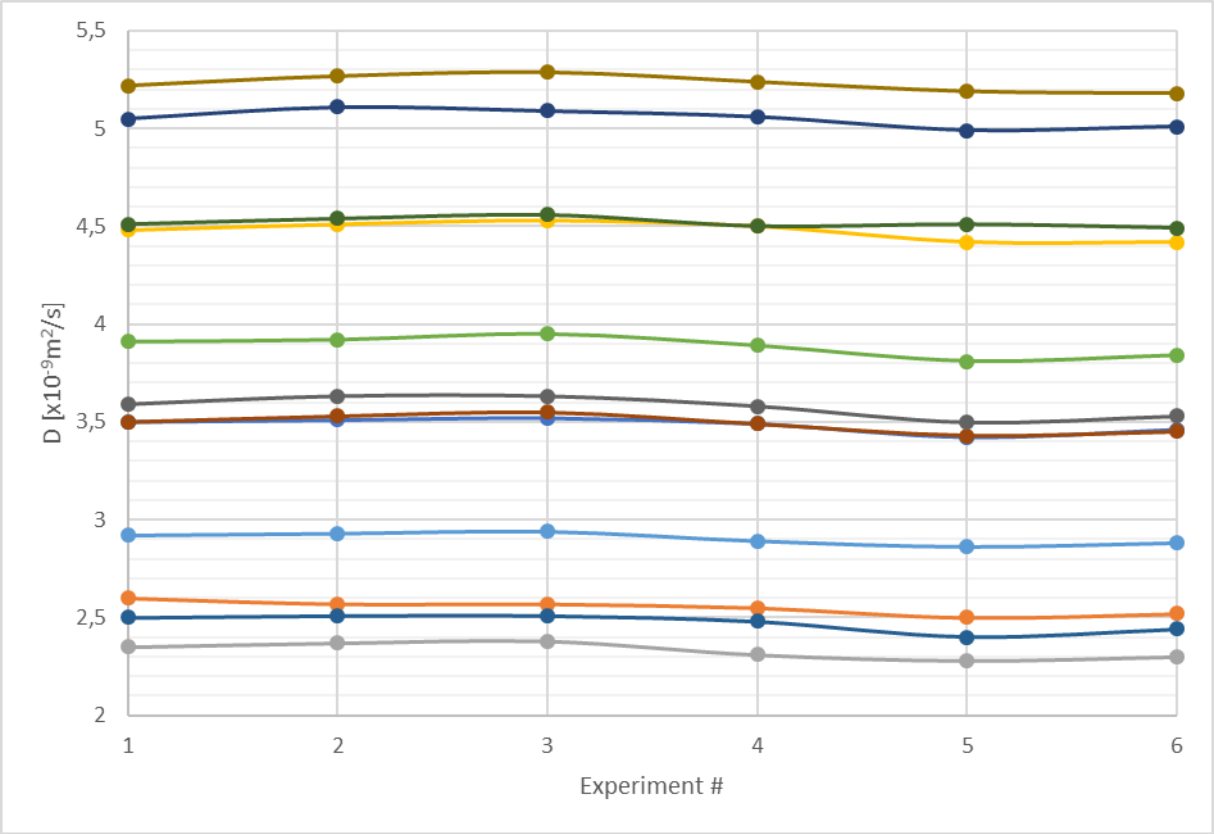

Figure 4.1.1: Plot instrumental variation for experiments performed on the EXP35_MCplus sample using the leddste sequence with Δ=11,23ms and td(F1)=32.

Variance caused by the TopSpin fitting tool and potential instrumental variations leads to uncertainty in the second decimal number. The largest observed standard deviation observed for the peaks plotted in figure 4.1.1 is 1,6% and the average standard deviation for all the peaks is 1,1%.

4.2: Diffusion measurement optimization

Using the ledbpg2s sequence, oil signals had an unrealistically high diffusion rate. A sample containing only the solvent (Toluene-d8) were analyzed using the ledbgp2s sequence in addition to a sequence designed to compensate for convection (leddste).

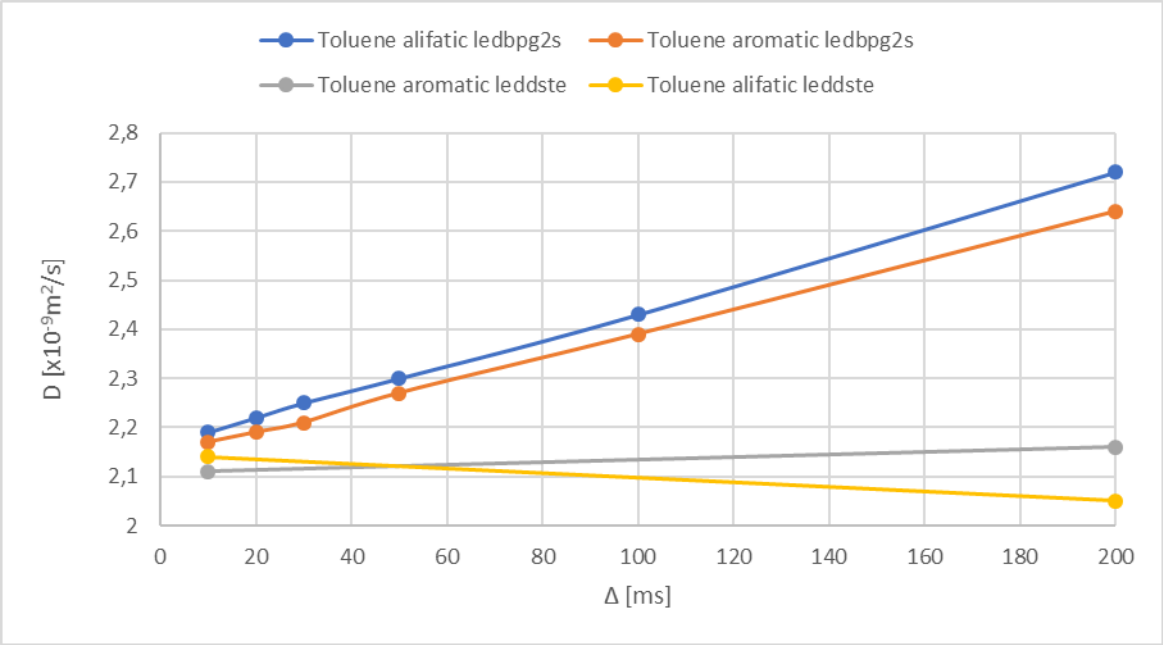

Figure 4.2.1: Plot time dependent diffusion coefficient using the ledbgp2s- and the leddste sequence.

Clearly convection is present in the samples with Toluene-d8 as a solvent. This is apparent since the diffusion coefficient calculated using ledbpg2s sequence increases with increasing diffusion time Δ. The diffusion coefficient also varies with time for the leddste sequence, but these variations are smaller (within the instrumental variation) and does not show a clear trend.

The Δ series was done for all the samples. There was no time dependent diffusion coefficient for the oil signals in either of the samples. However, most samples showed an increase in diffusion coefficient from Δ=11,23ms to Δ=50ms for the toluene and TMS signals.

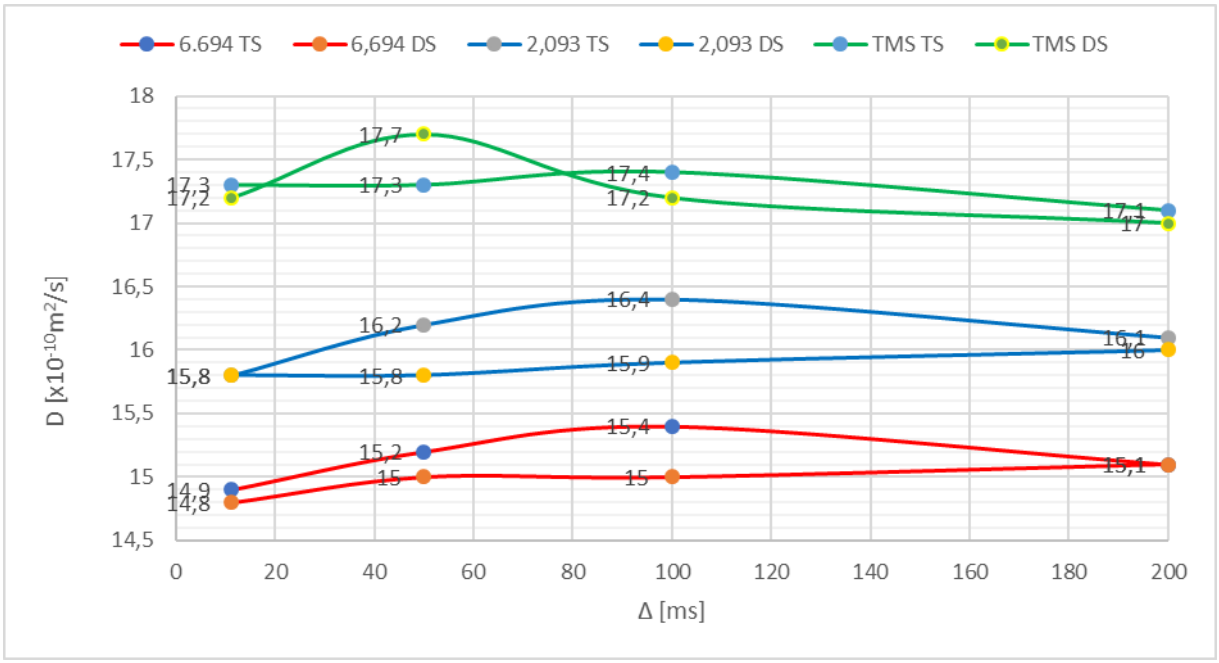

Figure 4.2.2: Plot diffusion coefficients of toluene and TMS peaks in the Stockton 200mg sample with the convection compensating leddste sequence. Diffusion coefficients are calculated using both Dynamics Center (DS) and TopSpin (TS).

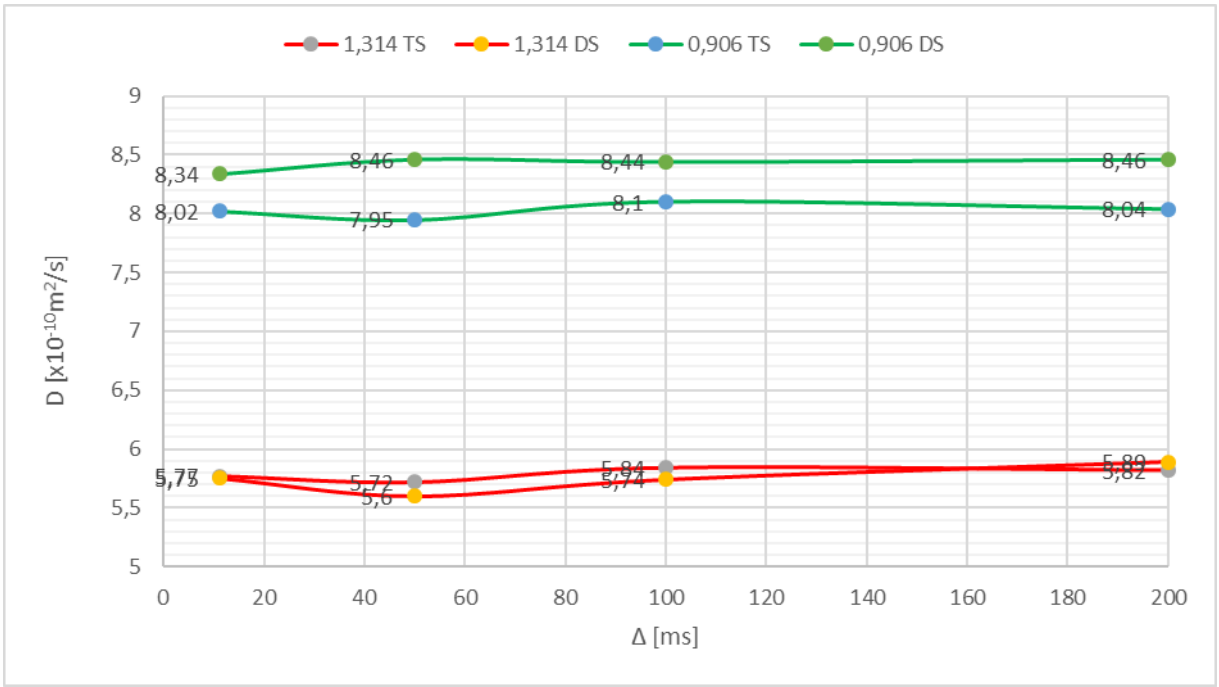

Figure 4.2.3: Plot diffusion coefficients of the aliphatic oil peaks in the Stockton 200mg sample with the convection compensating leddste sequence. Diffusion coefficients are calculated using both Dynamics Center (DS) and TopSpin (TS).

For the five biooil concentrations and two of each crude oil concentration a series with varying amount of gradient steps (td(F1)) were obtained with Δ=11,23ms. In addition to the delay between scans (d1), this is the main factor determining the time the experiments take.

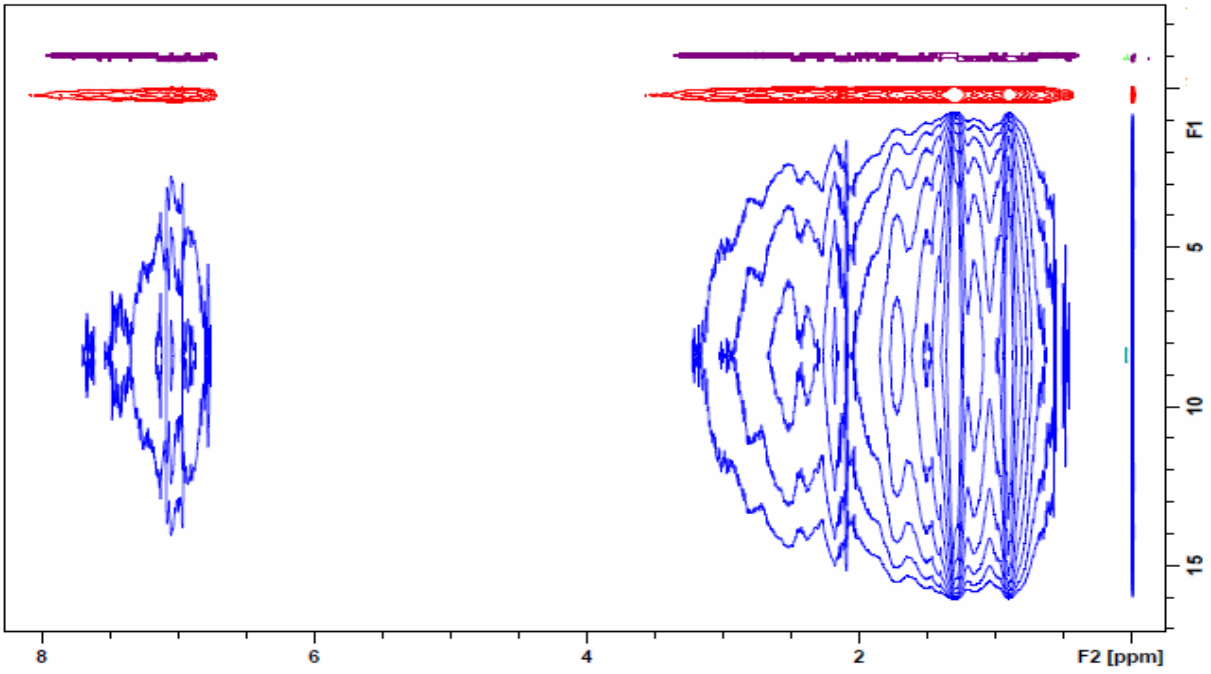

Figure 4.2.4: Stacked plot of Stockton 200mg diffusion measurements with 16 (blue), 32 (red) and 64 (purple) gradient steps.

Although the median value for each ppm-value is the same, the resolution of the diffusion spectra becomes 16 times better by using 32 gradient steps instead of 16 gradient steps, while only doubling the time of the experiment. However, the resolution is only three times better by using 64 gradient steps instead of 32 while doubling the time of the experiment.

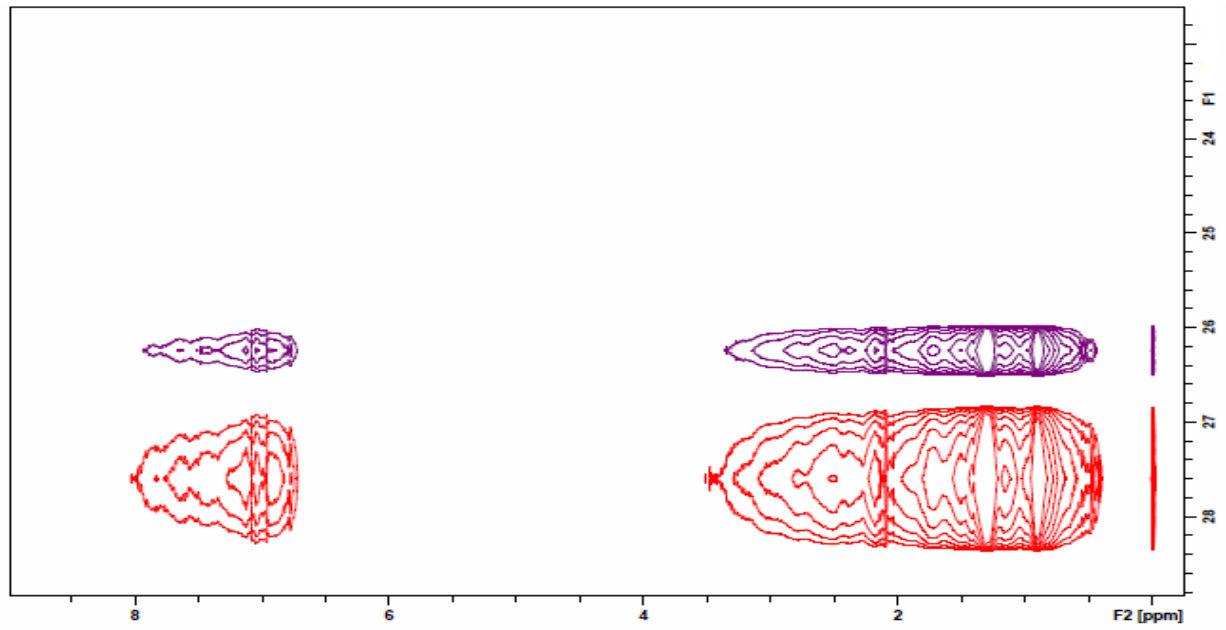

Figure 4.2.5: A closer look at the diffusion spectra with 32 gradient steps (red) and 64 gradient steps (purple).

4.3: Relaxation – standard samples.

Both spectral T_1 and T_2 measurements were performed on standard samples containing known concentrations of small hydrocarbons. Standard relaxation experiments were performed to control whether small hydrocarbons had an appropriate T_1/T_2 ratio or not. T_1-T_2 correlation measurements were also performed on the standards to see how it coincides with the spectral T_1 and T_2 relaxation measurements. The methods of TopSpin fitting and Dynamics Center fitting are also compared.

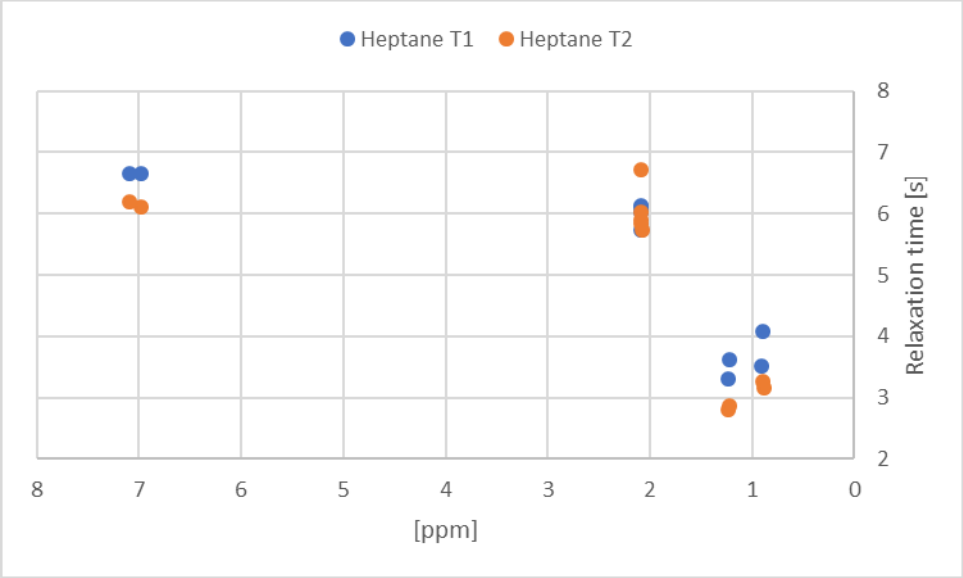

Figure 4.3.1: Relaxation times of the 150mM heptane standard sample.

The figure above shows that the T_1/T_2 ratio of the solvent (toluene) is very close to 1 as the T_1 and T_2 relaxation times are overlapping. However, the T_1/T_2 ratio of heptane (1,3ppm and 0,9ppm) are slightly higher, and the ratio is also higher for the CH_2 groups (1,3ppm) than for the CH_3 groups (0,9ppm).

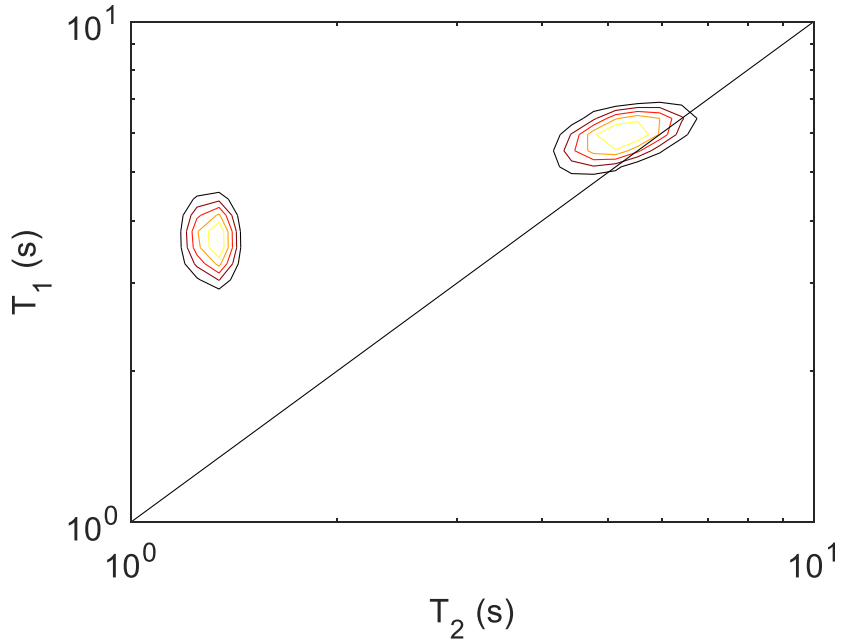

Figure 4.3.2: T_1-T_2 correlation plot of heptane dissolved in toluene-d8 with TMS as a reference.

Table 4.3.1: Relaxation data calculated with TopSpin and Dynamics Center for the 150mM heptane standard sample.

	T_1 [s]	T_2 [s]	T_1/T_2		T_1 [s]	T_2 [s]	T_1/T_2
	TopSpin				Dynamics Center		
7,0 ppm – toluene aromatic	7,16	6,05	1,18		6,54	6,05	1,08
2,2 ppm – toluene methyl	6,75	5,83	1,16		5,85	6,05	0,97
1,4 ppm – heptane CH_2	3,74	2,78	1,35		3,37	2,83	1,19
0,9 ppm – heptane CH_3	3,84	3,23	1,19		3,65	3,28	1,11
0,0 ppm - TMS	7,17	6,58	1,09		4,21	7,05	0,60

Table 4.3.2: Relaxation data from the T_1-T_2 correlation measurement for the 150mM heptane standard sample.

	T_1 [s]	T_2 [s]	T_1/T_2
T_1-T_2 correlation plot – heptane distribution	3,69	1,32	2,80
T_1-T_2 correlation plot – toluene/TMS distribution	5,92	5,16	1,15

From the table and figure above the value for T_2 from the T_1-T_2 correlation measurement is too low for the heptane peak, resulting in a very high T_1/T_2 ratio for such a small molecule. As heptane, the solvent (toluene-d8) and TMS are relatively small molecules and therefore within the extreme narrowing limit the T_1/T_2 ratio is expected to be 1 or very close to 1. Furthermore, there is great variation of the T_2 relaxation time of the functional groups of heptane compared to the variation in T_1 relaxation time both for the TopSpin and the Dynamics Center fitting calculations.

The T_1 fitting of Dynamics Center appears to be more potent for slightly broader peak. Here the T_1 relaxation time calculated from the narrow TMS peak is very low compared to the value calculated with TopSpin, resulting in $T_1/T_2 << 1$. The T_1/T_2 ratios calculated with Dynamics Center fitting is closer to the expected value, mainly due to lower T_1 relaxation times.

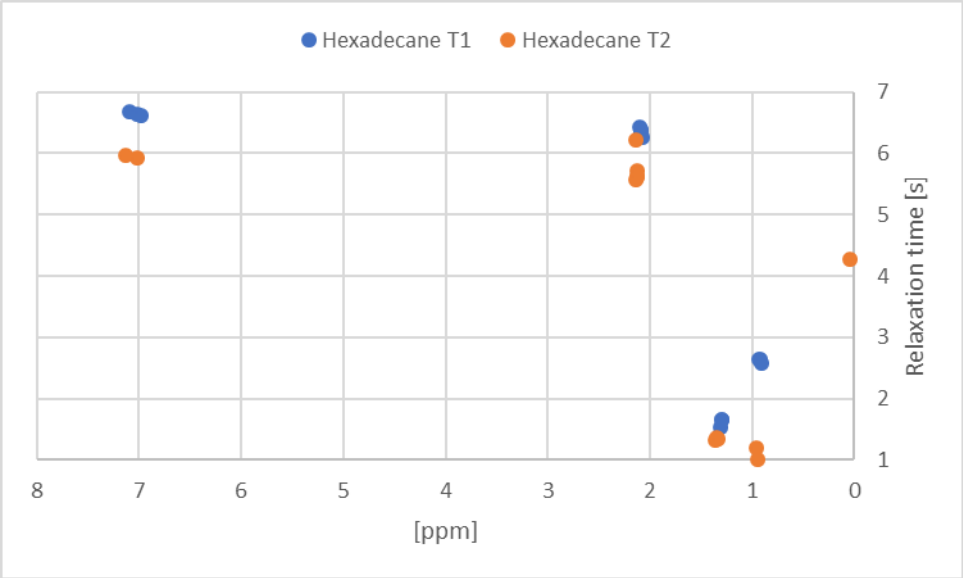

Figure 4.3.3: Relaxation times of the 150mM hexadecane standard sample.

As was seen for the heptane standard (figure 4.3.1), the T_1/T_2 ratio of the solvent is very close to 1. However, there is a greater deviation between the T_1 relaxation times fitted to the CH_2 and the CH_3

groups for hexadecane than was seen for heptane. Additionally, the T_1/T_2 ratios of the CH_2 and CH_3 groups are vastly different for hexadecane.

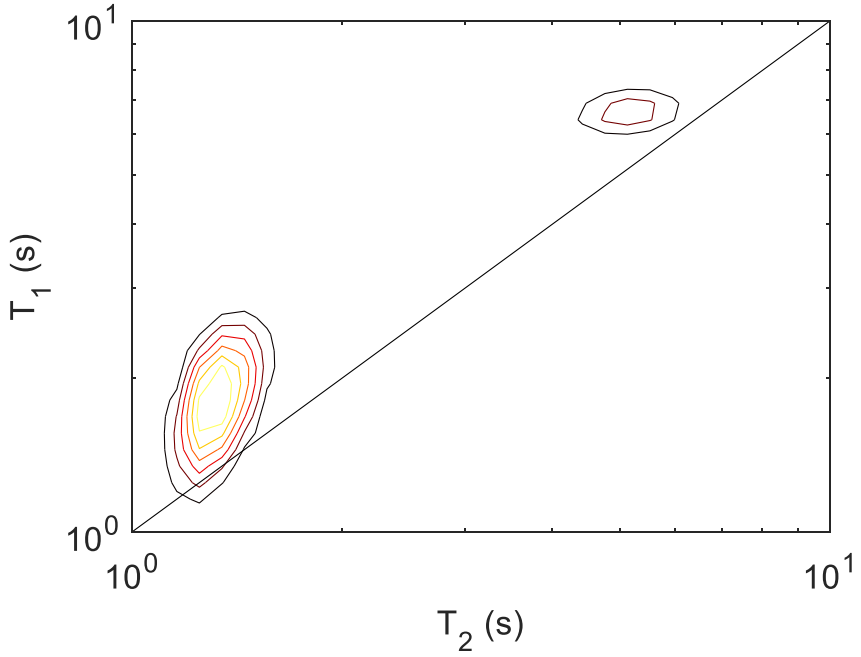

Figure 4.3.4: T_1-T_2 correlation plot of hexadecane dissolved in toluene-d8 with TMS as a reference.

Table 4.3.3: Relaxation data calculated from the 150mM hexadecane standard sample.

	T_1 [s]	T_2 [s]	T_1/T_2		T_1 [s]	T_2 [s]	T_1/T_2
	TopSpin				Dynamics Center		
7,0 ppm – toluene aromatic	7,26	5,85	1,24		6,43	5,82	1,10
2,2 ppm – toluene methyl	6,63	5,55	1,19		6,43	5,82	1,10
1,4 ppm – hexadecane CH_2	1,56	1,32	1,18		1,71	1,35	1,27
0,9 ppm – hexadecane CH_3	2,61	1,19	2,19		2,70	1,16	2,33
0,0 ppm - TMS	5,26	4,24	1,24		4,70	4,23	1,11

Table 4.3.4: Relaxation data from the T_1-T_2 correlation measurement for the 150mM hexadecane standard sample.

	T_1 [s]	T_2 [s]	T_1/T_2
T_1-T_2 correlation plot – hexadecane distribution	1,78	1,34	1,33
T_1-T_2 correlation plot – toluene/TMS distribution	6,69	5,20	1,29

The hexadecane distribution in the T_1-T_2 correlation plot is here closer to the expected T_1/T_2 ratio than what was the case for the heptane standard. The same differences between the fitting from the different software seen for heptane is also seen for the hexadecane standard. However, the variation of T_1 relaxation time of the functional groups of hexadecane calculated with both software are greater than what was seen for heptane.

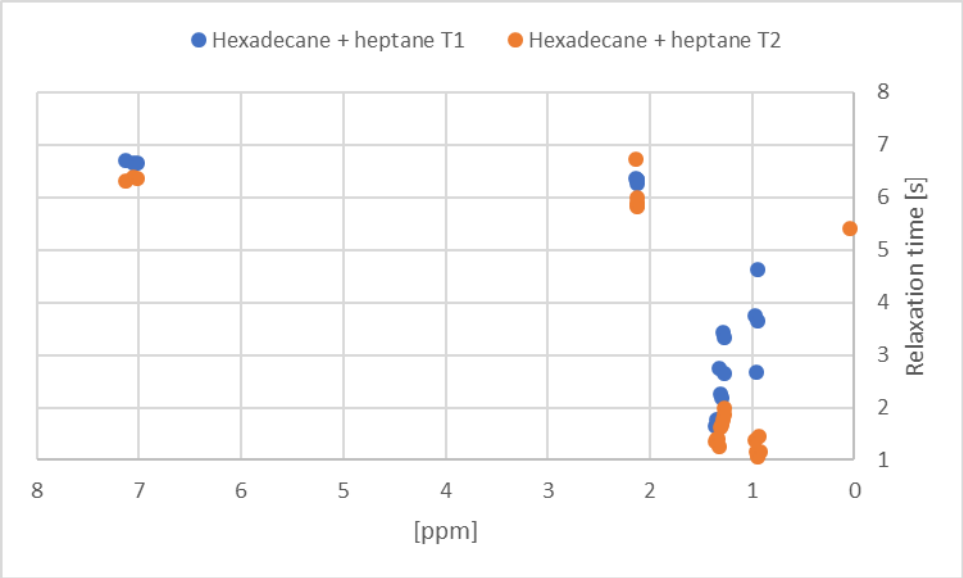

Figure 4.3.5: Relaxation times of the 75mM hexadecane and heptane standard sample.

The relaxation times of the heptane and hexadecane mixture again show a T_1/T_2 ratio of close to 1 for the solvent. The peaks from the hydrocarbons at 1,3ppm and 0,9ppm show that the fitting of the CH_2 groups at 1,3ppm has contribution from both hydrocarbons, with a wide range of T_1 and T_2 relaxation times. However, the T_2 relaxation times of the CH_3 groups are predominately influenced by hexadecane. This is the opposite of what is expected, since both molecules have equal amount of methyl groups. One would rather expect the fitting of the CH_2 groups to be influenced more by hexadecane since hexadecane has 14 CH_2 groups, while heptane has 5.

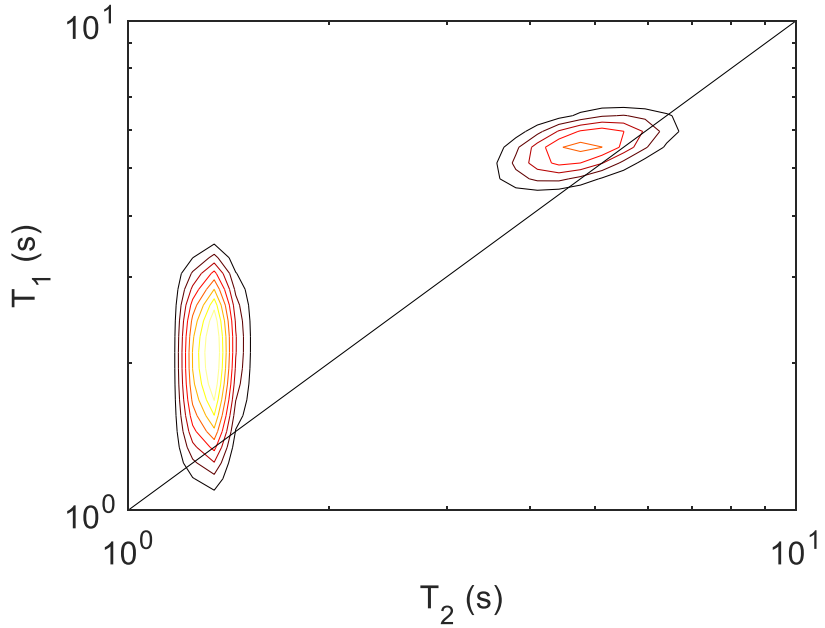

Figure 4.3.6: T_1-T_2 correlation plot of hexadecane + heptane dissolved in toluene-d8 with TMS as a reference.

Table 4.3.5: Relaxation data calculated from the 75mM hexadecane + heptane standard sample using TopSpin.

	T_1 [s]	T_2 [s]	T_1/T_2
7,0 ppm – toluene aromatic	7,26	6,31	1,15
2,2 ppm – toluene methyl	6,78	5,81	1,17
1,4 ppm – hexadecane + heptane CH_2	1,55	1,34	1,16
0,9 ppm – hexadecane + heptane CH_3	3,74	1,48	2,53
0,0 ppm - TMS	5,52	5,35	1,03

As seen previously the variation in T_1 between the two functional groups is large. However, the CH_2 peak will be mostly weighed towards the hexadecane values for a single component fit using TopSpin while the CH_3 peak has equal contribution from both hydrocarbons. When comparing with the table 4.3.1 and 4.3.3 it appears that the T_2 relaxation time of the methyl peak has much more contribution from hexadecane than heptane.

Table 4.3.6: Relaxation data calculated from the hydrocarbon peaks of the 75mM hexadecane + heptane standard sample using Dynamics Center.

	T_1 [s]	T_2 [s]	T_1/T_2
CH_2 hexadecane	1,57	1,38	1,14
CH_3 hexadecane	2,66	1,14	2,33
CH_2 heptane	3,48	1,72	2,02
CH_3 heptane	3,72	1,42	2,62

From table 4.3.6 it is clear that Dynamics Center has no problem separating heptane and hexadecane when it comes to T_1 fitting. However, the T_2 relaxation times calculated for heptane is much lower than what was seen in table 4.3.1.

Table 4.3.4: Relaxation data from the T_1-T_2 correlation measurement for the 75mM heptane + hexadecane standard sample.

	T_1 [s]	T_2 [s]	T_1/T_2
T_1-T_2 correlation plot – hydrocarbon distribution	2,04	1,33	1,53
T_1-T_2 correlation plot – toluene/TMS distribution	5,61	4,85	1,16

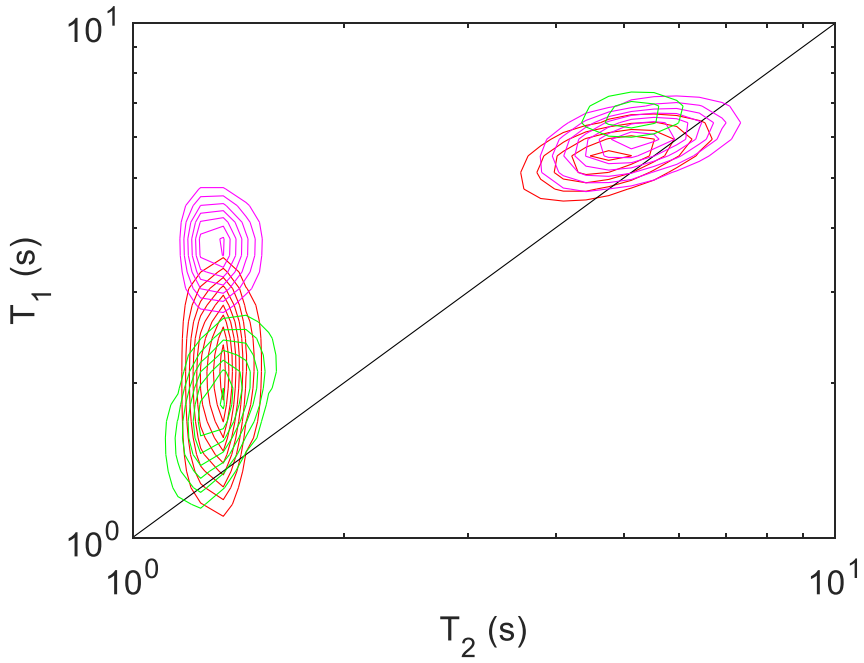

Figure 4.3.7: Overlapping T_1-T_2 correlation plot of hexadecane (green), heptane (pink) and hexadecane + heptane (red).

The figure above shows that the T_1-T_2 correlation measurement of hexadecane + heptane averages out the distribution calculated from the samples with only one hydrocarbon present.

Chapter 5

Results – Concentration series of the oils.

In the concentration series of the oils the normalized diffusion results are presented (Eq. 2.26). The TMS signal is therefore not included, as this is always $r_x/r_{TMS}=1{,}00$.

5.1: Concentration series of the Stockton crude.

Table 5.1.1: Sample information with respect to concentrations used.

Name	Mass [mg] Δm=±0.5mg	Concentration [g/mL]
Stockton 40mg	40,0	0,05
Stockton 200mg	200,7	0,25

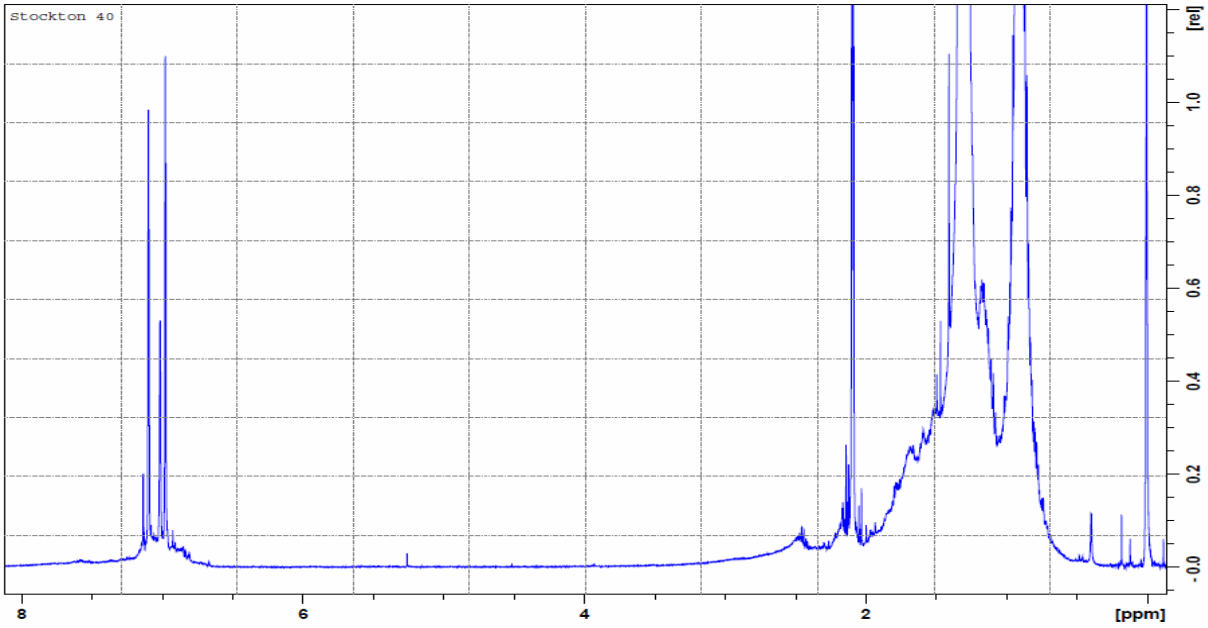

Figure 5.1.1: ^{1}H-spectrum of 40,0mg Stockton crude dissolved in Toluene-d8 with TMS as a reference.

The three signals from toluene are dominating in the aromatic region, although low intensity signals from the oils are present. The methyl group of toluene is located at 2,1ppm. The main signals from the oil is found at 0,95ppm and 1,35ppm, corresponding to CH_3 and CH_2 groups respectively.

5.1.1: Diffusion measurements.

Diffusion measurements were performed using the leddste sequence with td(F1)=64, d20=11.23ms and d1+aq=10s.

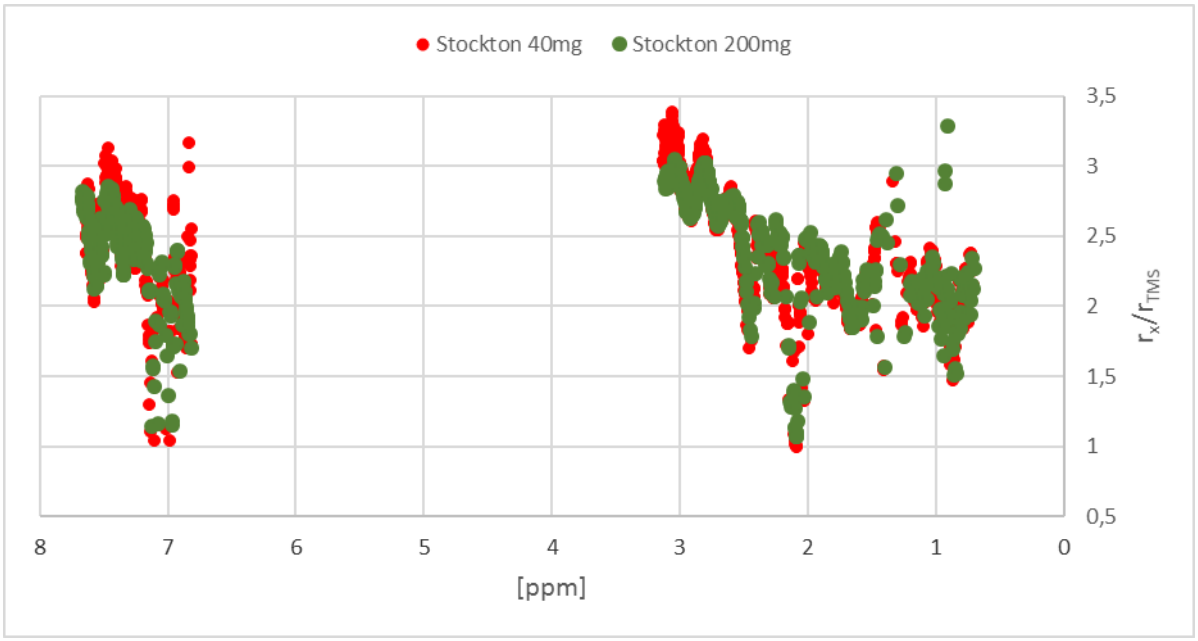

Figure 5.1.2: Comparison of r_x/r_{TMS} of the two concentrations of the Stockton crude oil.

The molecular radiuses in both aromatic and aliphatic region appear to be overlapping. In the range 2,8-3,1 and 7,2-7,5ppm there appears to be slightly larger molecular radiuses for the lowest concentration, however this is due to fitting problems occurring when using a threshold close to the baseline in Dynamics Center.

5.1.2: Relaxation measurements – T_1

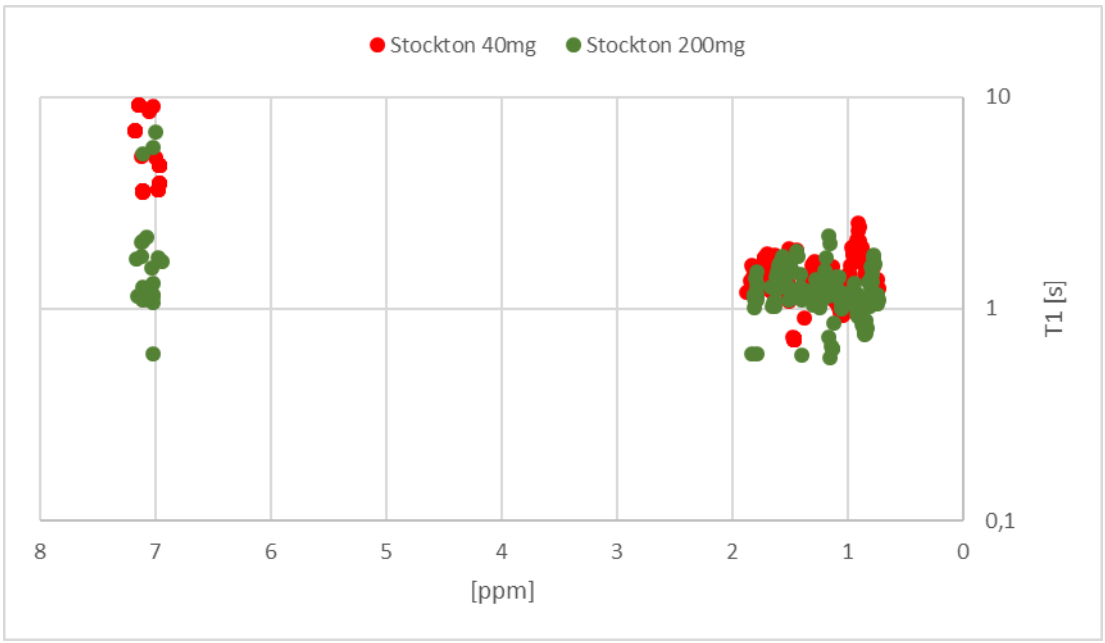

Figure 5.1.3: Comparison of T_1 relaxation times of Stockton 40mg and Stockton 200mg.

The relaxation times in the aliphatic region are overlapping due to no aggregation. The viscosity of the Stockton crude is low resulting in only a low shift to shorter relaxation times, unlike the change in relaxation times in aliphatic region seen for the biooil later (figure 5.2.3).

The relaxation times of the lowest concentration are higher in the aromatic region. This is due to the low signal from the oil in this region compared to the solvent signal. When the oil concentration is increased, the oil signal contributes more to the fitting in the aromatic region. This causes the fitted value to decrease due to oil component generally having lower relaxation times than the solvent since they are larger molecules.

5.1.3: Relaxation measurements – T_2

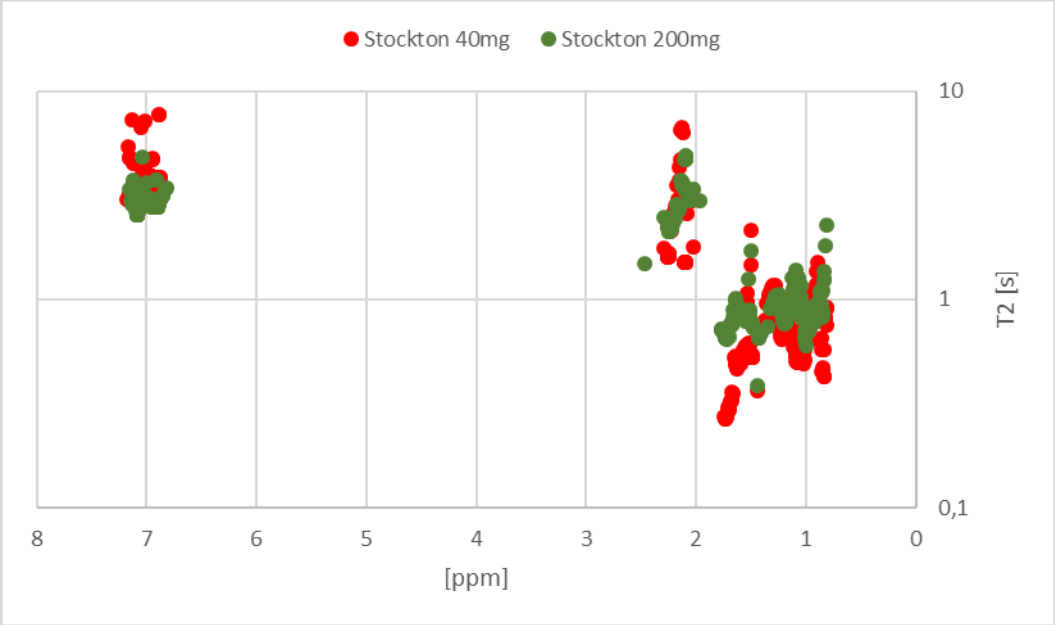

Figure 5.1.4: Comparison of T_2 relaxation times of Stockton 40mg and Stockton 200mg.

For T_2 as for T_1 there is almost complete overlap of relaxation times in the aliphatic region. However, in aromatic region neither the concentrations are high enough to cause any notable contribution to the fitting of the T_2 relaxation times.

Table 5.1.2: Average relaxation times in specific regions of Stockton 40mg and Stockton 200mg.

[ppm]	T_1 [s]	T_2 [s]	T_1/T_2		T_1 [s]	T_2 [s]	T_1/T_2
	Stockton 40mg				Stockton 200mg		
Aromatic	5,17	3,52	1,47		1,88	2,92	0,64
1,9-2,5	*	2,52			*	2,47	
0,8-1,7	1,46	0,69	2,11		1,21	0,95	1,27

** no fit available*

As mentioned above the T_1 relaxation times in the aromatic region of the high concentration sample has contribution from both the oil and the solvent, while the T_2 relaxation times are predominately solvent. This results in a T_1/T_2 ratio of less than 1 in the aromatic region of this sample.

5.1.4: T_1-T_2 correlation measurements.

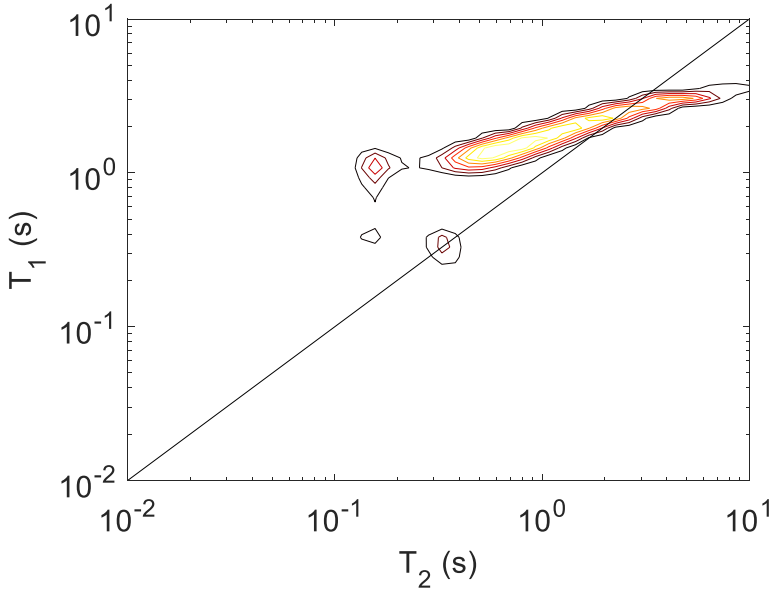

Figure 5.1.5: T_1-T_2 correlation plot of Stockton 40mg.

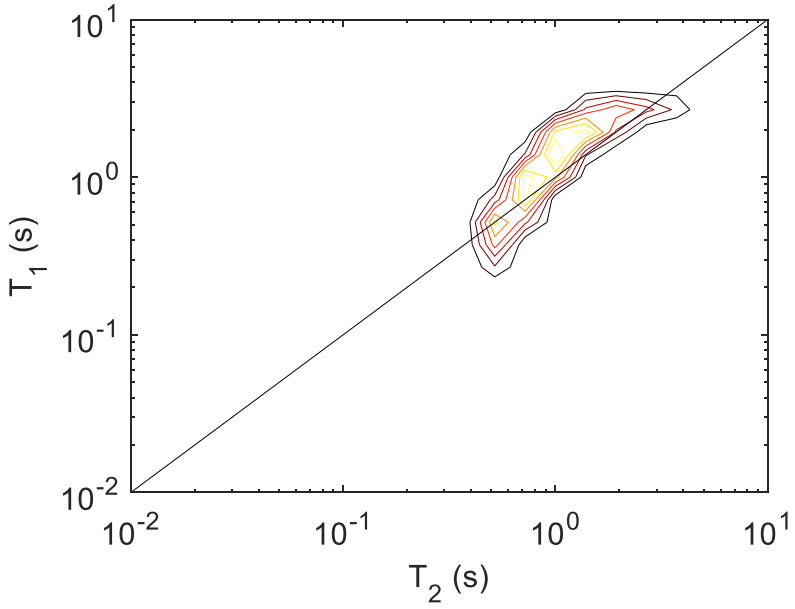

Figure 5.1.6: T_1-T_2 correlation plot of Stockton 200mg.

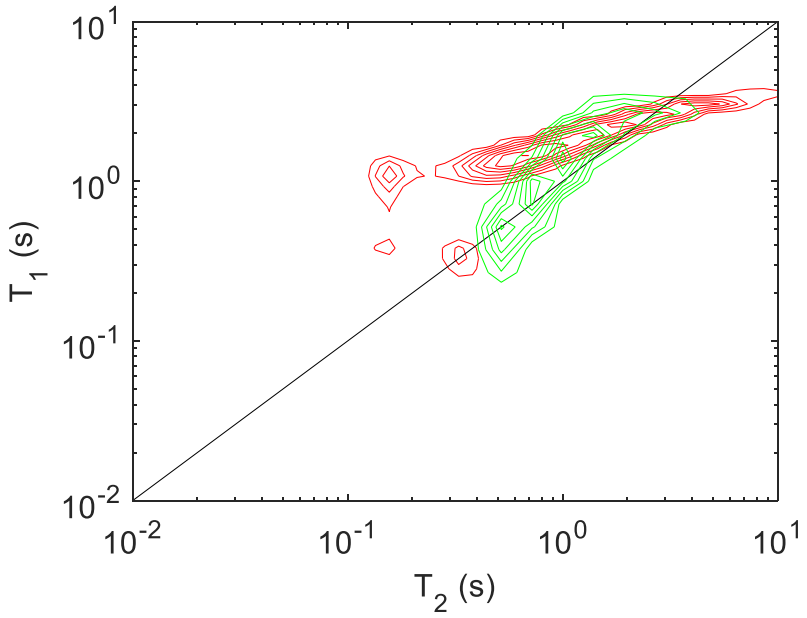

Figure 5.1.7: Overlapping T_1-T_2 correlation plot of Stockton 40mg (red) and Stockton 200mg (green).

The T_1-T_2 correlation plot comparison show overlapping values over most the range. However, the components with the lowest T_2 relaxation time appear to have slightly higher T_1 relaxation time in the low concentration sample.

5.2: Concentration series of the biooil EXP35.

Table 5.2.1: Sample information with respect to concentrations used.

Name	Mass [mg] Δm=±0.5mg	Concentration [g/mL]
35LC	27,1	0,04
35MCminus	59,9	0,09
35MC	82,5	0,12
35MCplus	102,2	0,15
35HC	130,9	0,19

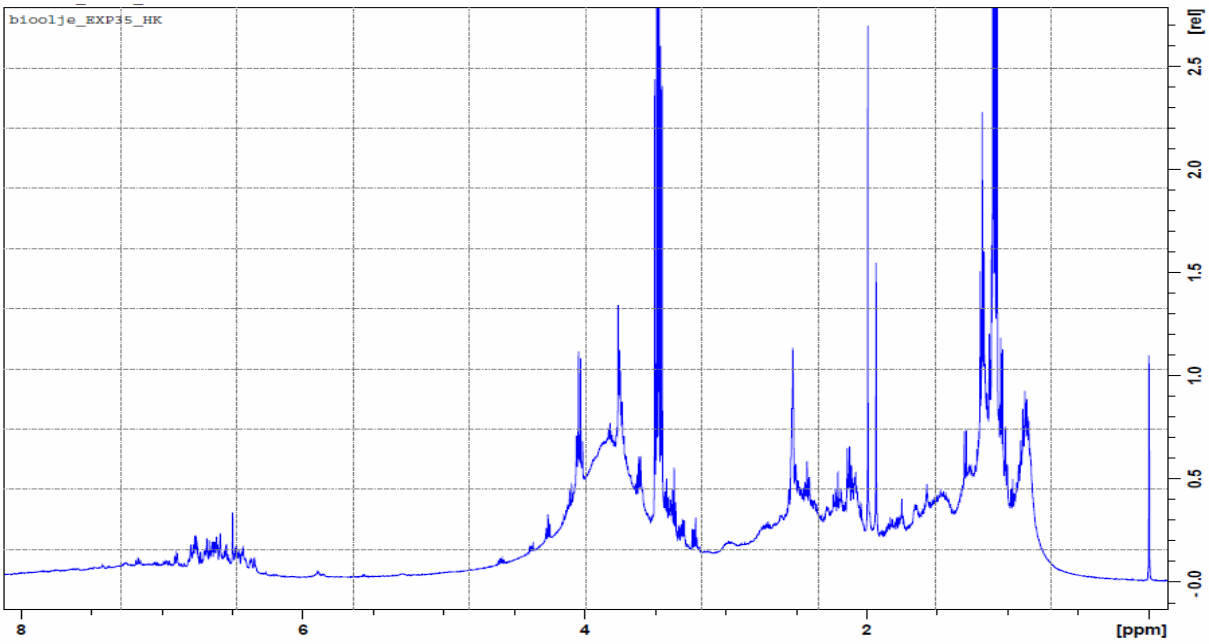

Figure 5.2.1: ^{1}H-spectrum of the bio-oil Exp_35 dissolved in DMSO-d6 with TMS as reference.

The DMSO-d6 HOD signal at 3,4ppm is rather broad causing overlap in the fitting of both relaxation times and diffusion coefficients. The result of this is a wide distribution of relaxation times and diffusion coefficients for the near lying ppm-range (3,3 – 3,5ppm).

5.2.1: Diffusion measurements.

Diffusion measurements were performed using the leddste sequence with td(F1)=64, d20=11.23ms and d1+aq=10s.

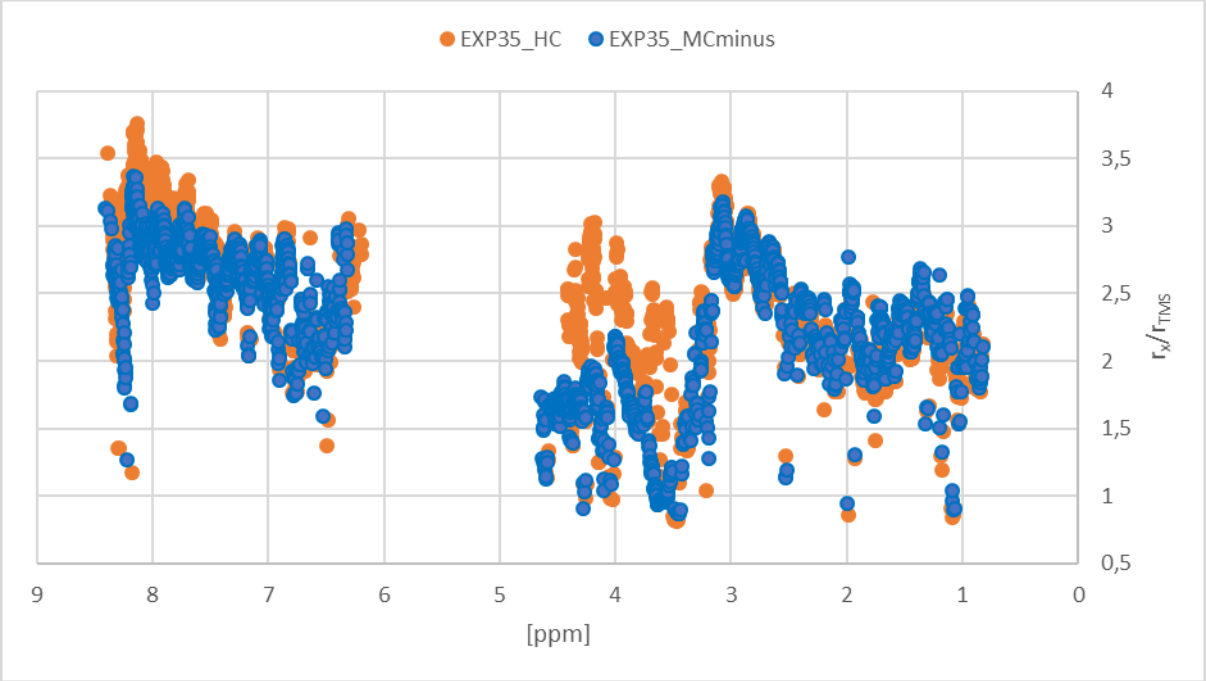

Figure 5.2.2: Comparison of r_x/r_{TMS} of the concentrations MCminus and HC.

The molecules in the range 3,7- 4,2ppm shows higher molecular radius in the most concentrated sample. The region corresponds to proton neighboring oxygen (i.e. ethers) and conjugated systems. This is also the case in the aromatic region 7,5-8,2ppm, which corresponds to conjugated aromatics. This coincides nicely with aggregation caused by increased hydrogen bonding for the most electronegative components of the samples.

5.2.2: Relaxation measurements – T_1

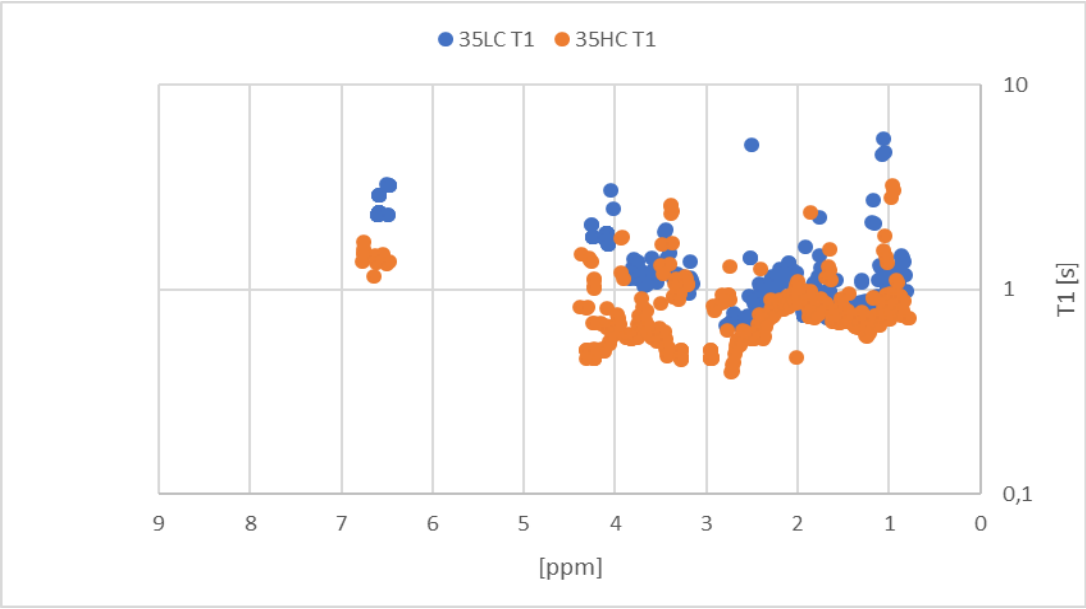

Figure 5.2.3: Comparison of T_1 relaxation times of 35LC and 35HC.

As viscosity is not compensated for this comparison shows a decrease in relaxation times over all the ppm-values. However, the reduction of relaxation times is greater in the regions there were shown an increase in molecular size in the diffusion comparison.

5.2.3: Relaxation measurements – T_2

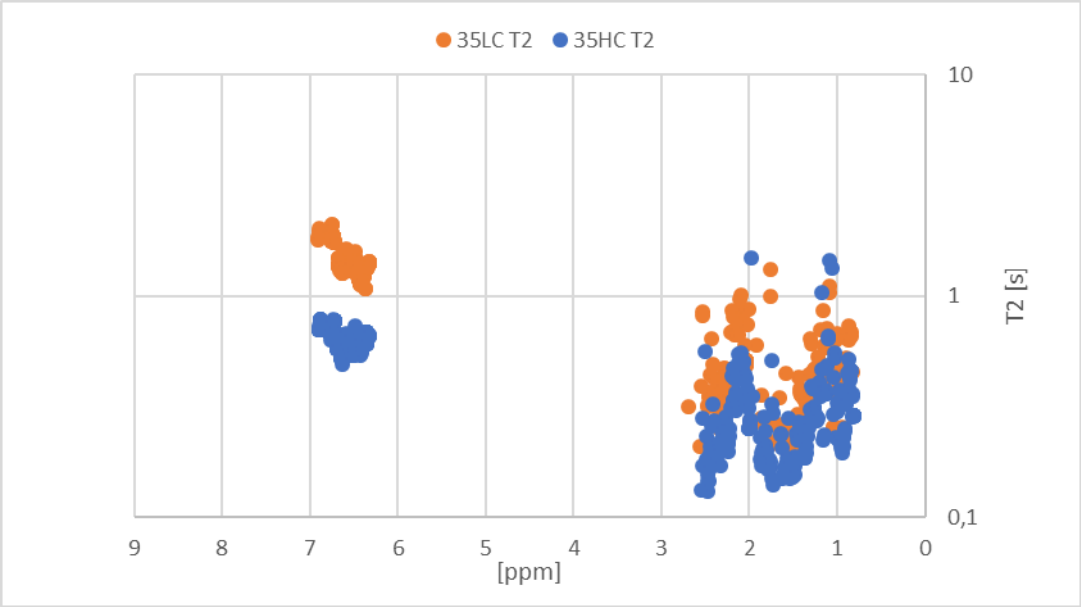

Figure 5.2.4: Comparison of T_2 relaxation times of 35LC and 35HC.

No good fitting was obtained in the region 3-4,4ppm for the low concentration sample. This region is therefore not included in the plot. Again, as viscosity is not compensated for, T_2 decreases with increasing concentration over the entire sample. However, as T_2 is more susceptible to increase in molecular size due to its dependency on the spectral density at the zero frequency (J(0)), it is clear that the decrease in T_2 relaxation times is greater in the aromatic region.

Table 5.2.2: $\overline{T_1}/\overline{T_2}$ aromatic region EXP35_LC and EXP35_HC.

Concentration	Average T_1 [s]	Average T_2 [s]	$\overline{T_1}/\overline{T_2}$
LC	2,513	1,480	1,698
HC	1,431	0,665	2,152

5.2.4: T_1-T_2 correlation measurements.

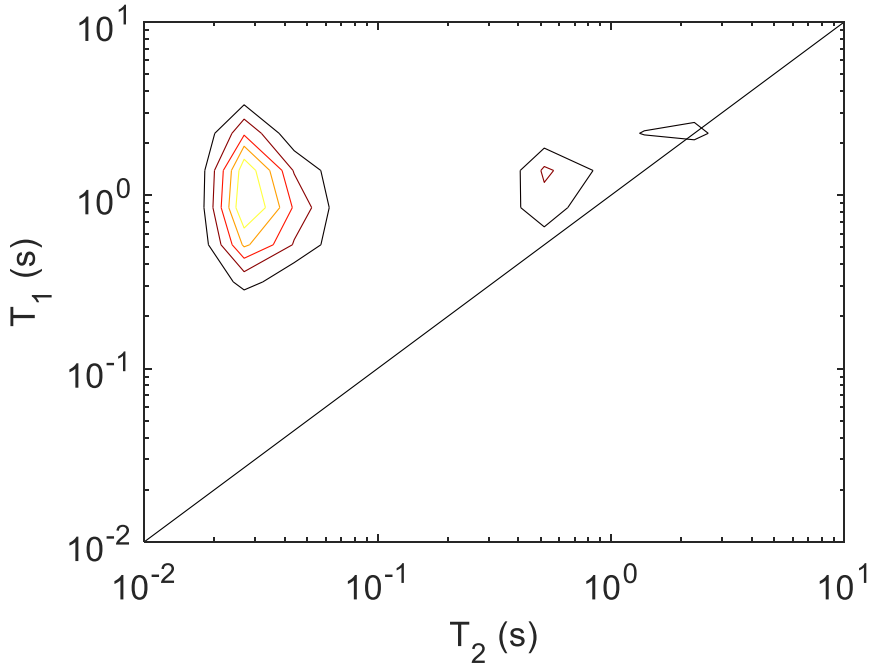

Figure 5.2.5: T_1-T_2 correlation plot of EXP35_LC.

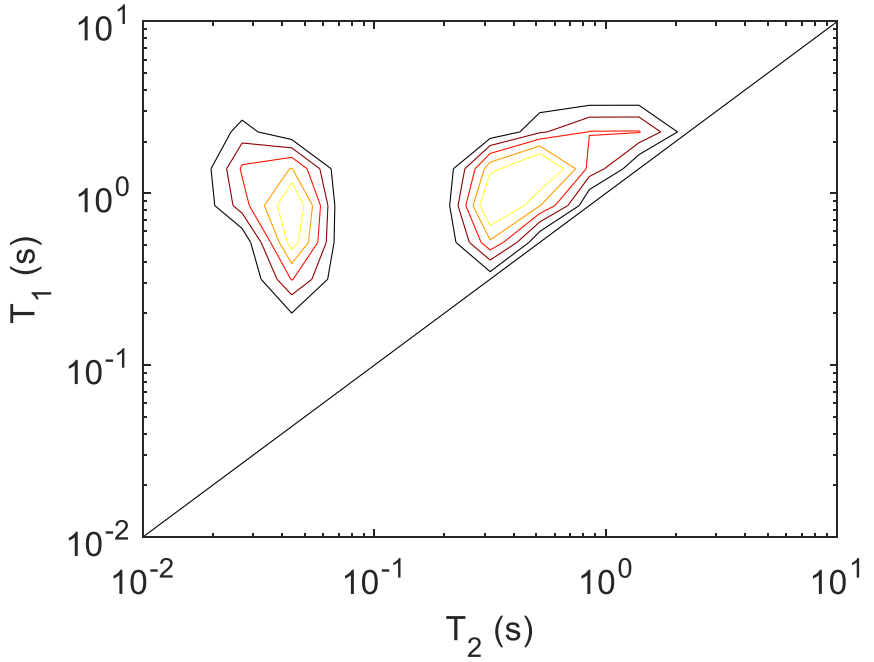

Figure 5.2.6: T_1-T_2 correlation plot of EXP35_HC.

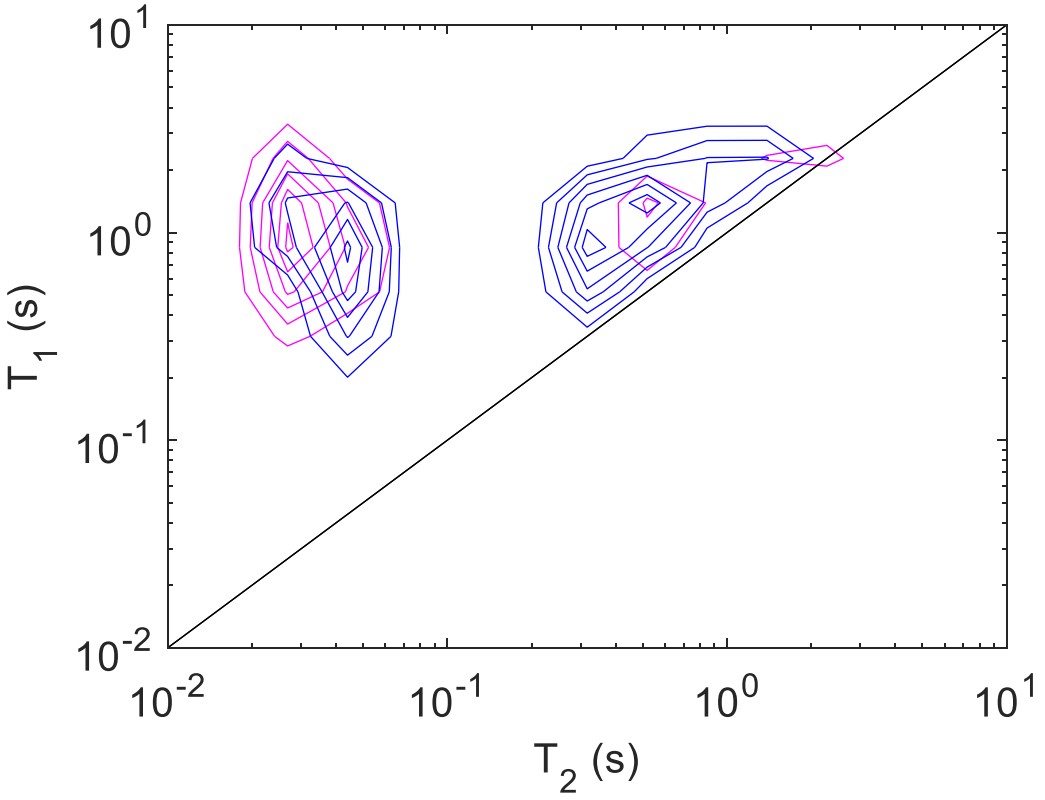

Figure 5.2.7: Overlapping T_1-T_2 correlation plot of EXP35_LC (pink) and EXP35_HC (blue).

The T_1-T_2 correlation plots show the distribution close to the T_1=T_2 being moved diagonally towards lower values for both T_1 and T_2 with increasing concentration. This distribution also becomes broader in both the T_1 and the T_2 dimension. Both concentrations show a region with T_2<<T_1 corresponding to aggregating and large molecules. This region is relatively equal for both the concentration, although the lower concentration appears to have slightly lower T_2 values compared to the higher concentration.

5.3: Concentration series of the Grane crude.

Table 5.3.1: Sample information with respect to concentrations used.

Name	Mass [mg] Δm=±0.5mg	Concentration [g/mL]
Grane 20mg	26,8	0,03
Grane 190mg	190,0	0,24

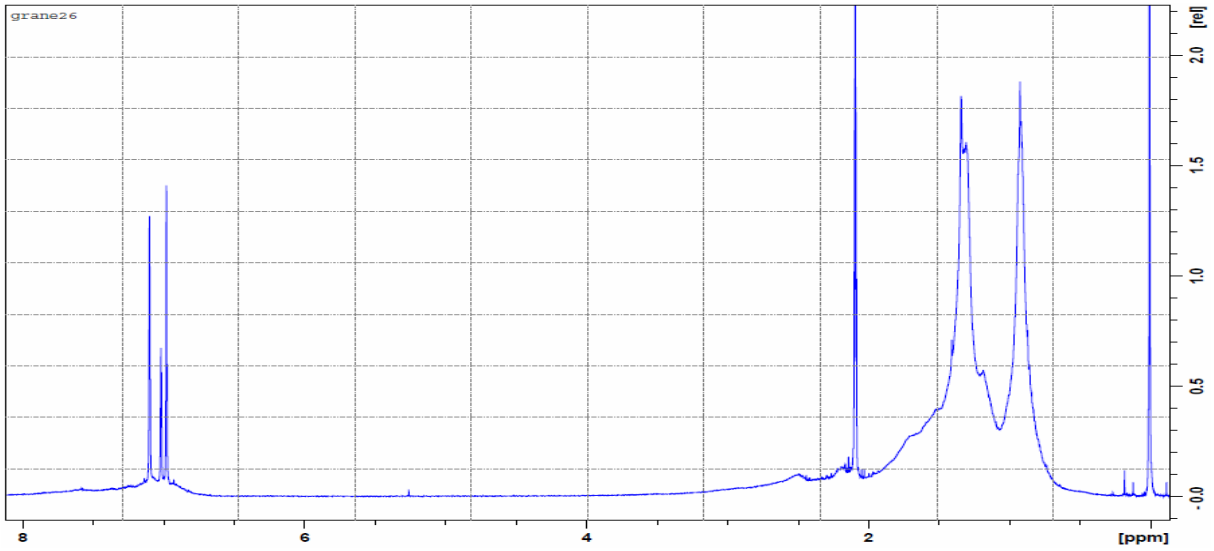

Figure 5.3.1: ^{1}H-spectrum of 26,8mg Grane crude dissolved in Toluene-d8 with TMS as a reference.

The ^{1}H-spectrum of the Grane crude oil shows more intensity than the other oils around 2,5ppm, and also in the aromatic region. However, the aromatic region is also for this crude oil dominated by the three signals of toluene.

5.3.1: Diffusion measurements

The diffusion measurements were performed using the leddste sequence with td(F1)=64, d20=11.23ms and d1+aq=10s.

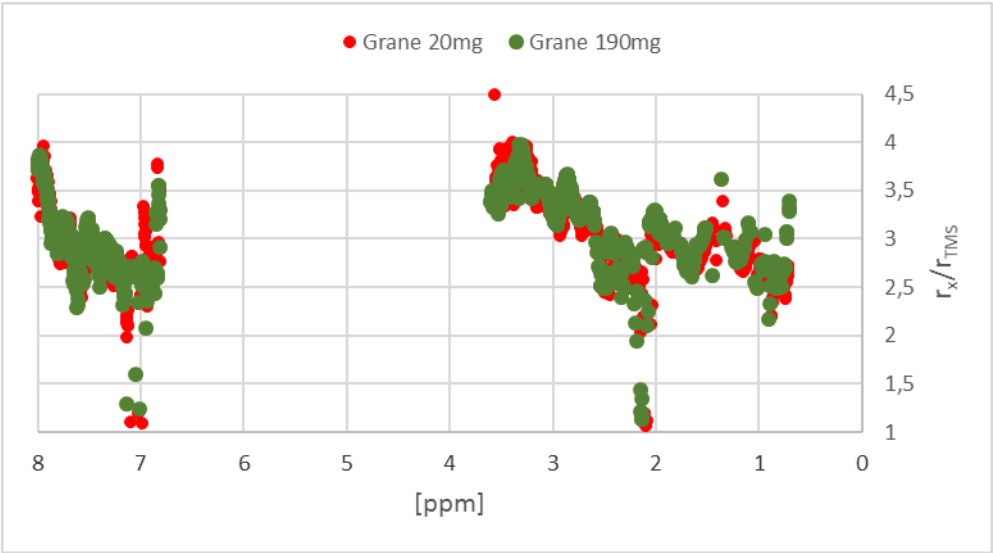

Figure 5.3.2: Comparison of r_x/r_{TMS} of the two concentrations of the Grane crude oil.

The molecular radiuses in both aromatic and aliphatic region are overlapping. In the aliphatic region, the most electronegative molecules (2,5-3,5ppm) appear to have noticeable larger molecular radiuses than the rest of the region. This is also the case in the aromatic region (7,9-8,1ppm).

5.3.2: Relaxation measurements – T_1

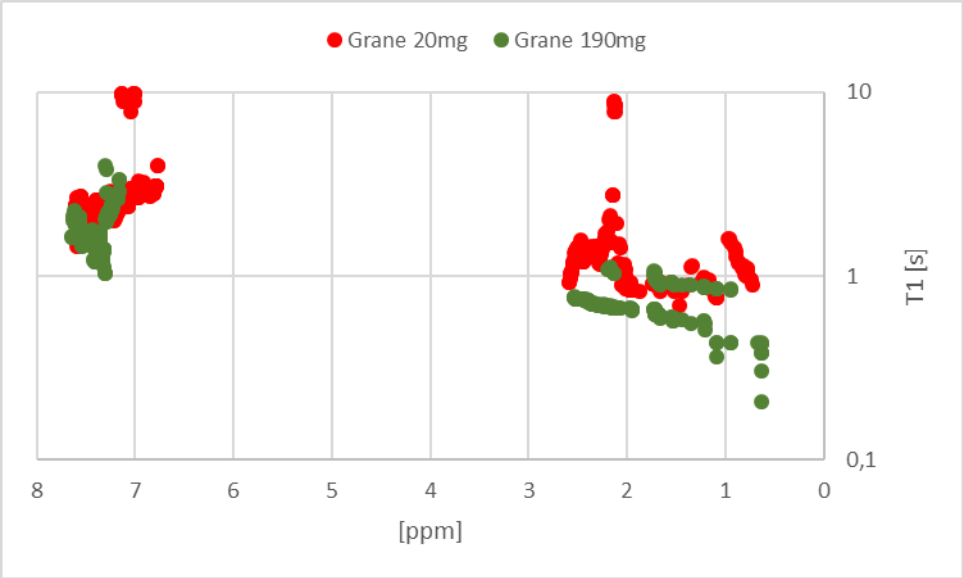

Figure 5.3.3: Comparison of T_1 relaxation times of Grane 20mg and Grane 190mg.

The T_1 relaxation comparison show that Dynamics Center is not able to fit the entire aromatic region for the sample with the highest concentration, however the relaxation times calculated are overlapping elsewhere in this region. In the aliphatic region, the highest concentration has two bands of relaxation times. One of those bands show relaxation times in the interval 0,51-0,75s in the region 1,2-2,5ppm while the other band has relaxation times in the interval 0,8-1,0s. The band with the highest relaxation times overlaps with the relaxation times calculated for the low concentration sample in the aliphatic region, while the band with the lowest relaxation times show lower relaxation times than the low concentration sample.

The sample with the lowest concentration has relaxation times in the range 1,0-1,5s in the aliphatic region and 1,5-2,6s in the aromatic region. Only the lowest concentration show relaxation times purely fitted to the solvent, with distributions with relaxation times in the range of 8,0-10,0s at 2,1ppm and in the interval 7,0-7,1ppm.

5.3.3: Relaxation measurements – T_2

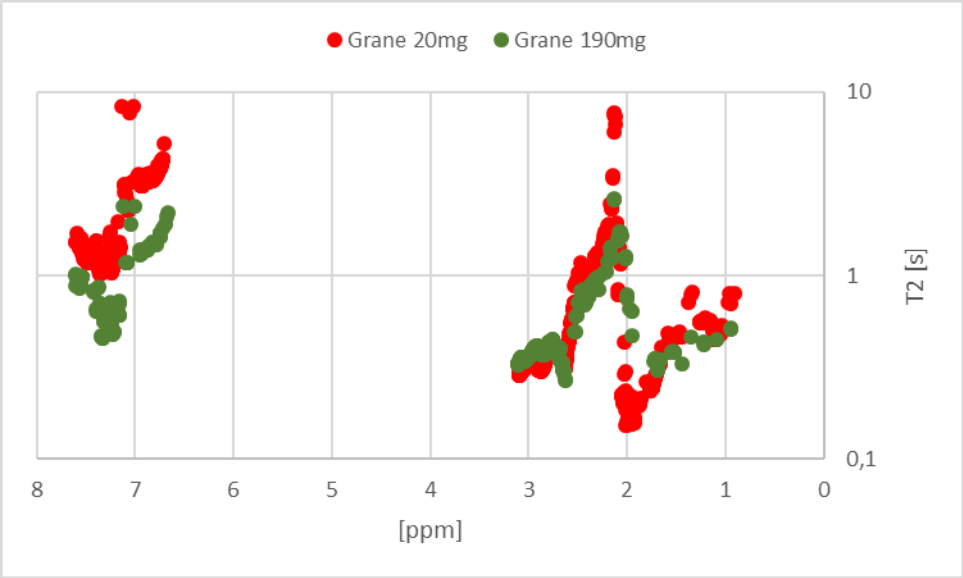

Figure 5.3.4: Comparison of T_2 relaxation times of Grane 20mg and Grane 190mg.

The T_2 comparison show overlapping values in the aliphatic region with a rather broad interval of T_2 relaxation times due to problems with T_2 fitting at the edge of broad peaks. The T_2 relaxation times are generally slightly higher for the lowest concentration in the aliphatic region. In the aromatic region, the lowest concentration shows higher T_2 relaxation times by a good margin.

5.3.4: T_1-T_2 correlation measurements.

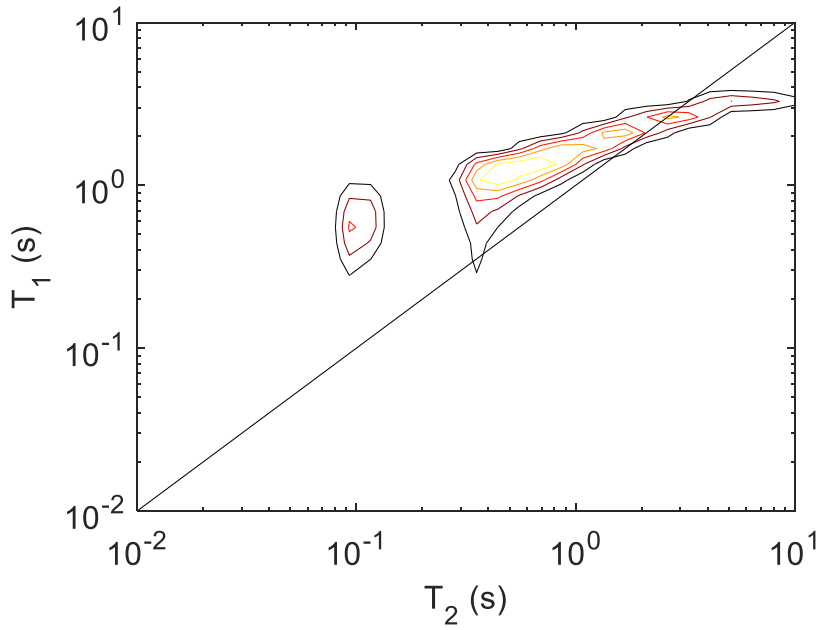

Figure 5.3.5: T_1-T_2 correlation plot of Grane 20mg.

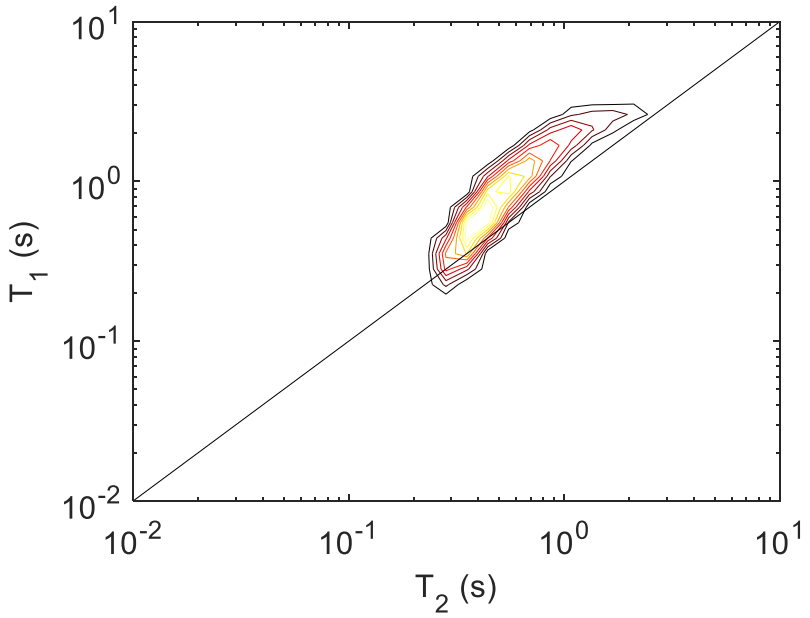

Figure 5.3.6: T_1-T_2 correlation plot of Grane 190mg.

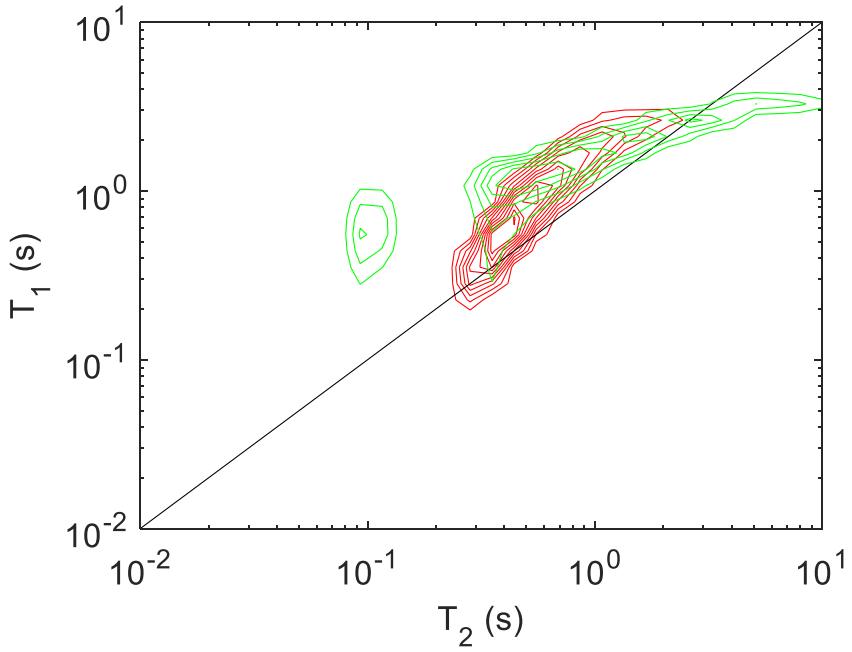

Figure 5.3.7: Overlapping T_1-T_2 correlation plot of Grane 20mg (green) and Grane 190mg (red).

The overlapping T_1-T_2 correlation plot show overlapping T_1-T_2 correlation close to the T_1=T_2 diagonal line. The lowest concentration also shows a distribution with T_2<<T_1 while the highest concentration does not. This is the opposite of what the spectral relaxation measurements show, where the highest concentration shows an increase in the T_1/T_2 ratio in the aromatic region.

5.4: Concentration series of the Ekofisk crude.

Table 5.4.1: Sample information with respect to concentrations used.

Name	Mass [mg] Δm=±0.5mg	Concentration [g/mL]
Ekofisk 20mg	22,3	0,03
Ekofisk 200mg	200,1	0,25

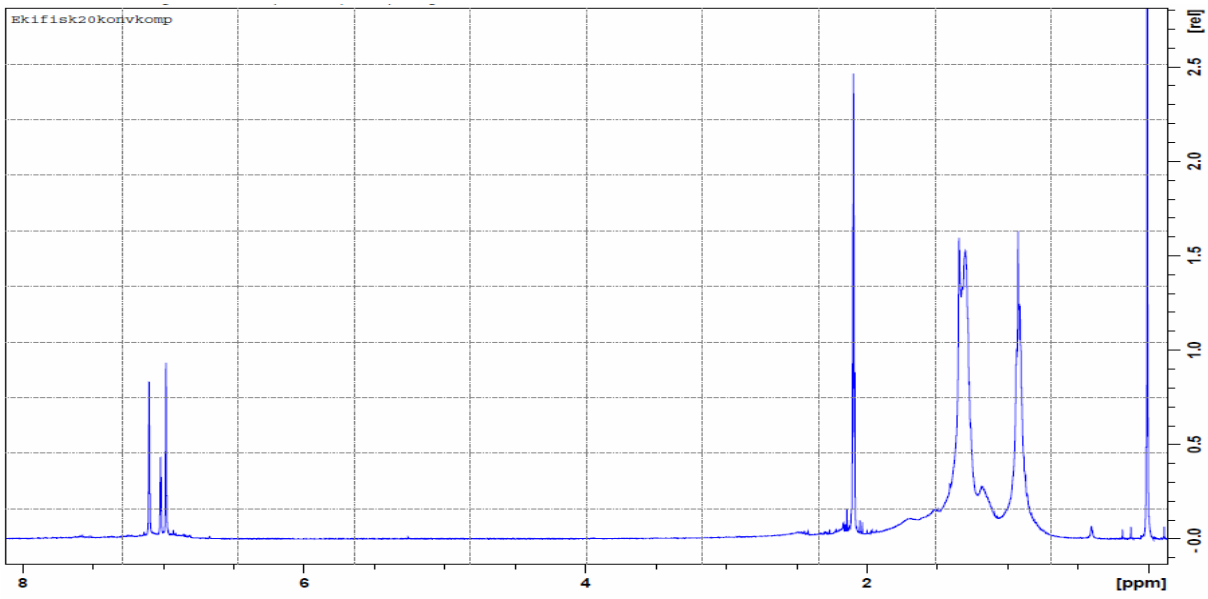

Figure 5.4.1: ^{1}H-spectrum of 22,3mg Ekofisk crude dissolved in Toluene-d8 with TMS as reference.

5.4.1: Diffusion measurements.

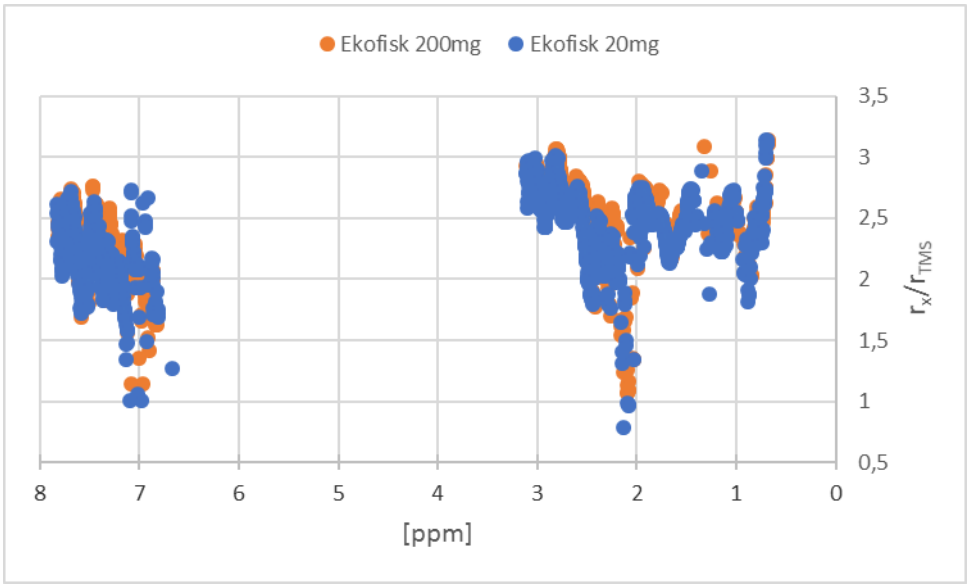

Figure 5.4.2: Comparison of r_x/r_{TMS} of the two concentrations of the Ekofisk crude oil.

There are no signs of aggregation as the molecular radiuses in both regions are overlapping.

5.4.2: Relaxation measurements – T_1

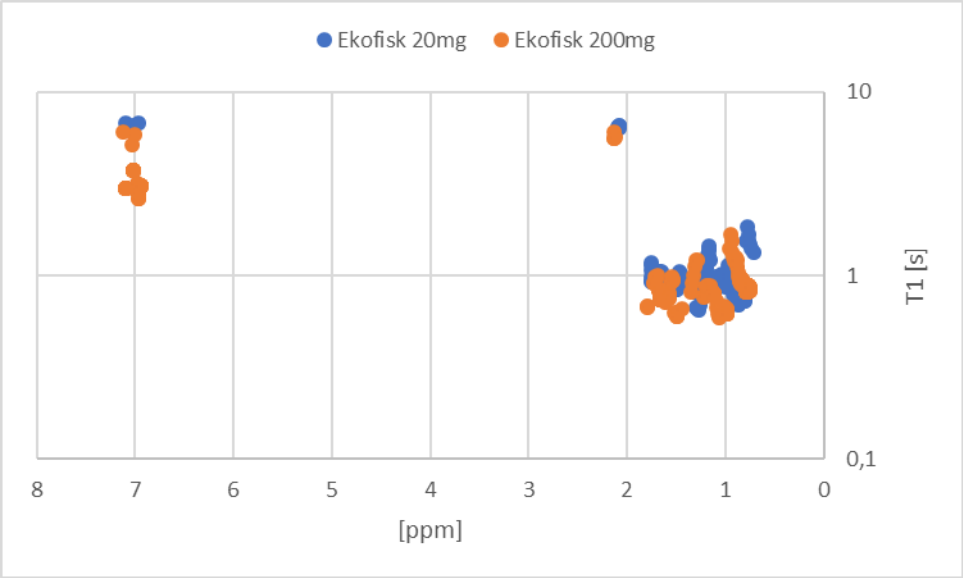

Figure 5.4.3: Comparison of T_1 relaxation times of Ekofisk 20mg and Ekofisk 200mg.

The relaxation times in the aliphatic region are mainly overlapping, although the highest concentration shows slightly lower T_1 values due to the increased viscosity. This can also be seen for the toluene methyl peak at 2,1ppm, where the highest concentration has a slightly lower relaxation time.

The lowest concentration shows only one distribution of relaxation times in the aromatic region. The relaxation times are high, meaning the lowest concentration causes insufficient signal intensity from the oil to have any effect on the fitting function. The highest concentration shows two distributions; one only fitted to the toluene peaks (5,1 seconds) and one fitted to the toluene peaks in addition to some contribution from the oil (2,6-3,1 seconds).

5.4.3: Relaxation measurements – T_2

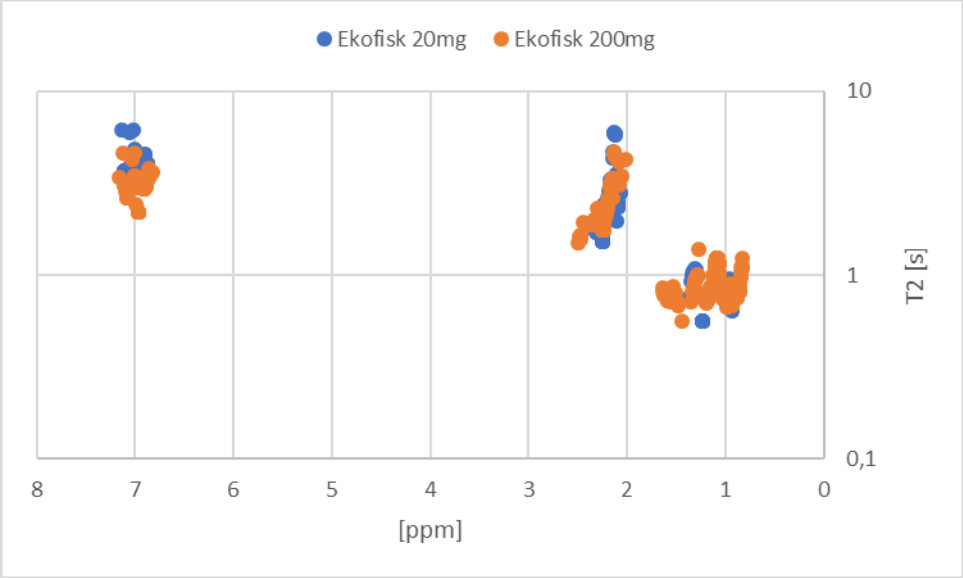

Figure 5.4.4: Comparison of T_2 relaxation times of Ekofisk 20mg and Ekofisk 200mg.

As for T_1 there are mostly overlapping values for T_2 in both regions. Unlike the T_1 plot (figure 4.4.3), the lowest concentration shows two distributions in the aromatic region; one fitted purely to toluene (6,1s), and another one having some contribution from the oil signals (3,2-3,7s).

5.4.4: T_1-T_2 correlation measurements.

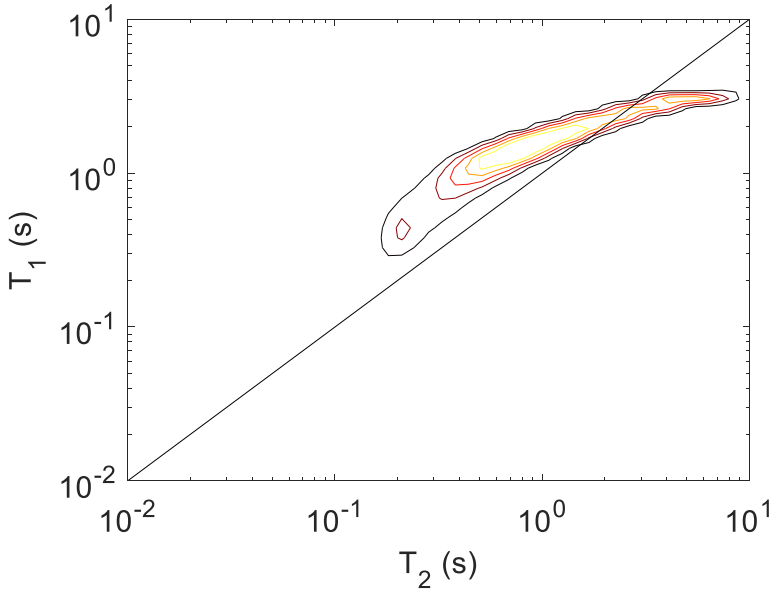

Figure 5.4.5: T_1-T_2 correlation plot of Ekofisk 20mg.

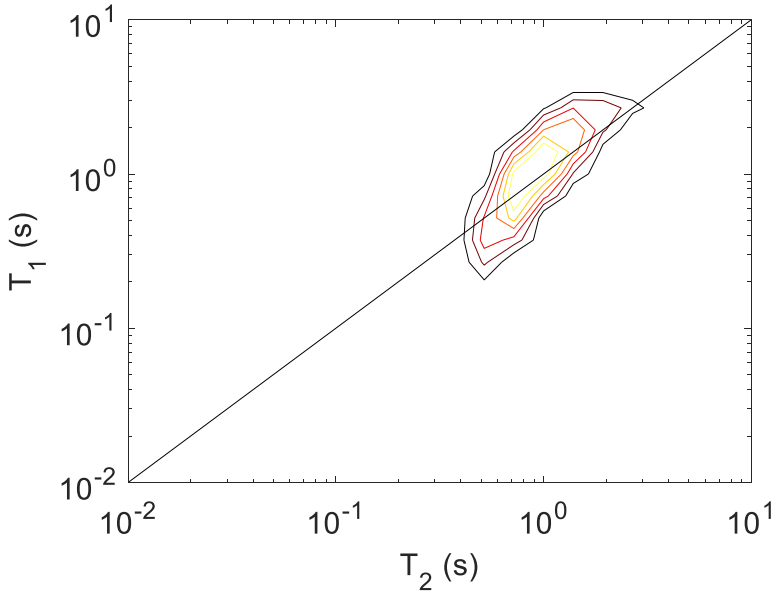

Figure 5.4.6: T_1-T_2 correlation plot of Ekofisk 200mg.

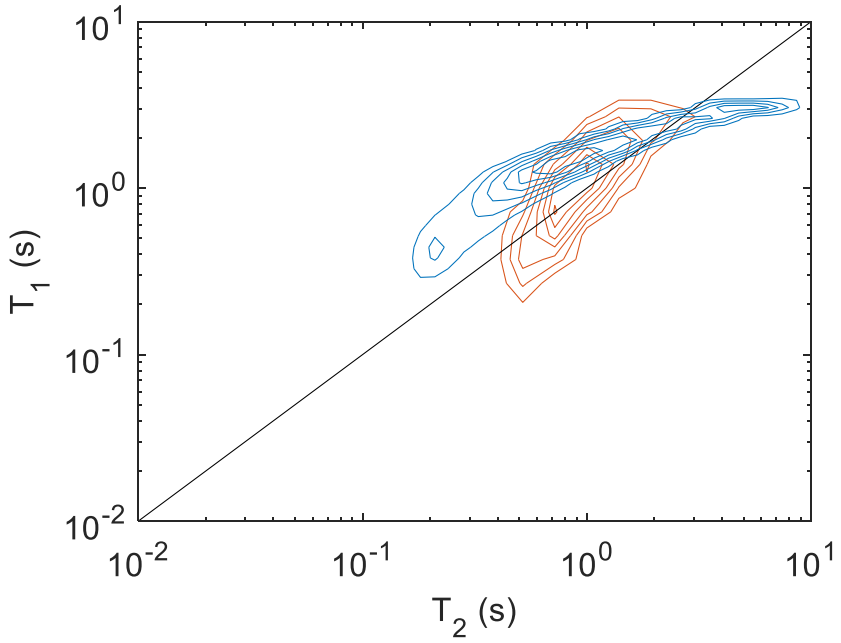

Figure 5.4.7: Overlapping T_1-T_2 correlation plot of Ekofisk 20mg (blue) and Ekofisk 200mg (orange).

The T_1-T_2 correlation plot comparison show a broader range for the lowest concentration. The majority of the distribution for both concentrations are close to or at the T_1=T_2 line, and overlapping. The lowest concentration appears to have slightly higher T_1 values for the components with the lowest T_2 value.

5.5: Comparison of the diluted oils.

In the comparison of the oils the lowest concentrations are used, since the biooil diffusion measurements showed an increase of molecular size with increased concentration.

5.5.1: Diffusion measurements

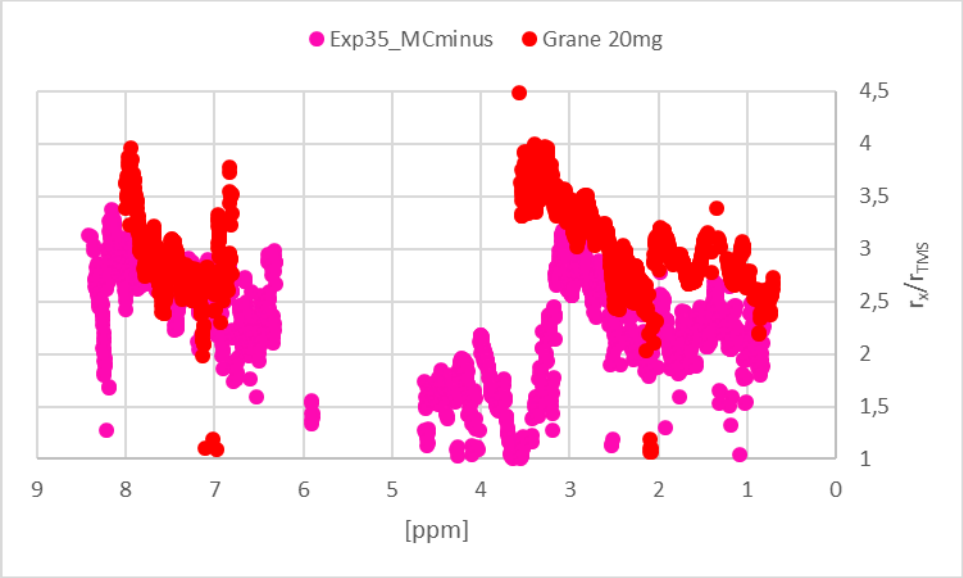

Figure 5.5.1: Comparison of r_x/r_{TMS} of Grane 20mg and EXP35_MCminus.

In the aliphatic region, the molecules in the Grane crude oil have larger molecular radiuses than the EXP35 biooil. As mentioned before the HOD-signal from the solvent (DMSO-d6) used for the biooil is broad and has high intensity and this causes the fitted diffusion coefficients in the region 3,4-3,7ppm to be highly weighed towards the diffusion coefficient of HOD. There is no basis for comparison of the diffusion coefficients of the biooil in the region 3,5-4,6ppm as neither of the crude oils have functional groups of significant intensities to compare with.

In the aromatic region, the ppm-range from where there is signal is broader for the biooil than for the Grane crude oil, causing a broader distribution for the biooil than for the crude oil. However, the molecular radiuses are overlapping in the region where both samples show peaks are overlapping.

Table 5.5.1: Diffusion data from the comparison of EXP35_MCminus (D_{TMS}=4,95x10^{-10}m^s/s) and Grane 20mg (D_{TMS}=2,06x10^{-9}).

Region	r_x/r_{TMS} EXP35	r_x/r_{TMS} Grane
Average 0,70-2,05ppm	2,20	2,86
Average 2,05-3,3ppm	2,60	3,18
Average aromatic region	2,67	2,9

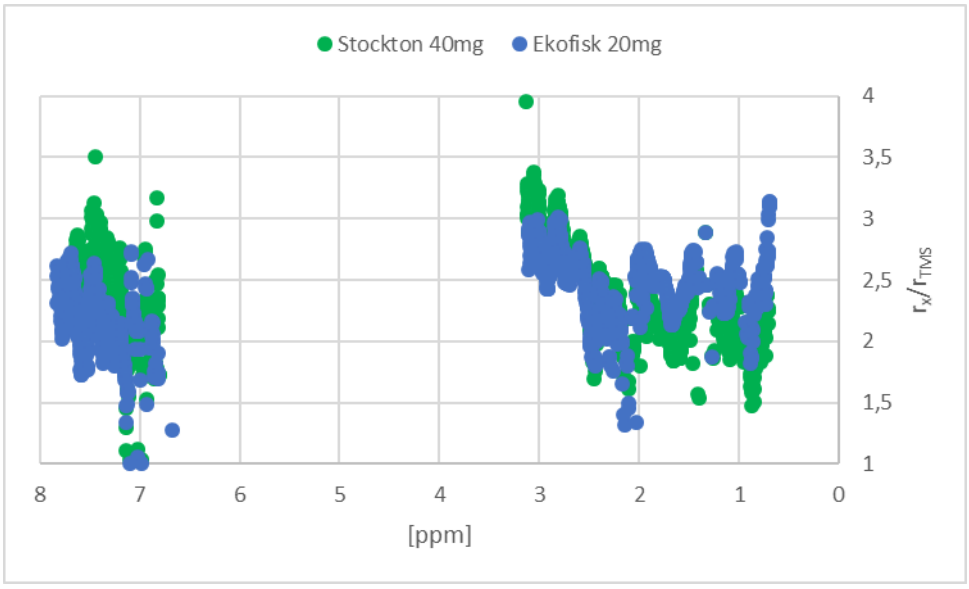

Figure 5.5.2: Comparison of r_x/r_{TMS} of Stockton 40mg and Ekofisk 20mg.

In the aliphatic region, ranging from 0,7-2,0ppm the Ekofisk crude solution has larger molecular radiuses then the Stockton crude solution. However, above 2,0ppm the molecular radiuses are overlapping in the aliphatic region. In the aromatic region, the Stockton crude have generally higher molecular radiuses than the Ekofisk crude.

Figure 5.5.2: Diffusion data from the comparison of Stockton 40mg (D_{TMS}=2,05x10^{-9}m^s/s) and Ekofisk 20mg (D_{TMS}=2,06x10^{-9}).

Region	r_x/r_{TMS} Stockton	r_x/r_{TMS} Ekofisk
Average 0,70-2,0ppm	2,13	2,45
Average 2,0-3,1ppm	2,68	2,52
Average aromatic region	2,40	2,17

5.5.2: T_1 relaxation measurements

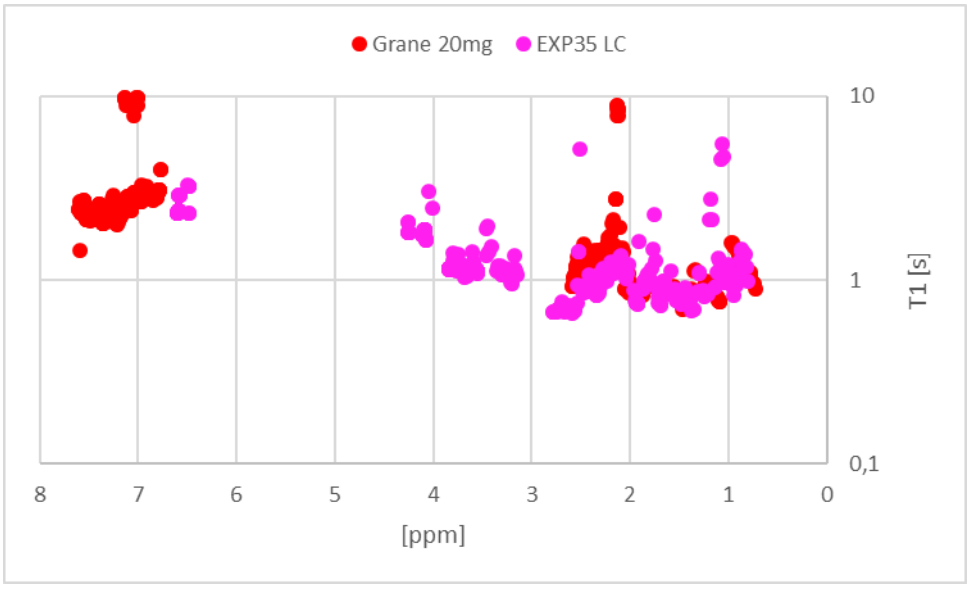

Figure 5.5.3: Comparison of T_1 relaxation times of Grane 20mg and EXP35_LC.

In the aliphatic region, from 0,7ppm to 2,0ppm the T_1 relaxation values of the biooil and the crude oil are overlapping. However, the Grane crude show higher T_1 relaxation times above 2,0ppm likely due to contribution from the methyl group of toluene. As seen in the diffusion comparison, the EXP35 biooil have functional groups occurring at higher frequencies than those of the Grane crude, meaning there is no basis for comparing these relaxation times with either of the crude oils.

Both the Grane crude and the EXP35 biooil have narrower ppm-ranges in the aliphatic region compared with the results from the diffusion measurement. This is due to Dynamics Center's inability to fit relaxation times for broad and relatively low intensity peaks.

In the aromatic region, there is a lack of fitted T_1 relaxation for the same reason as in the aliphatic region. However, the few relaxation times that are fitted are in the same order as the Grane crude.

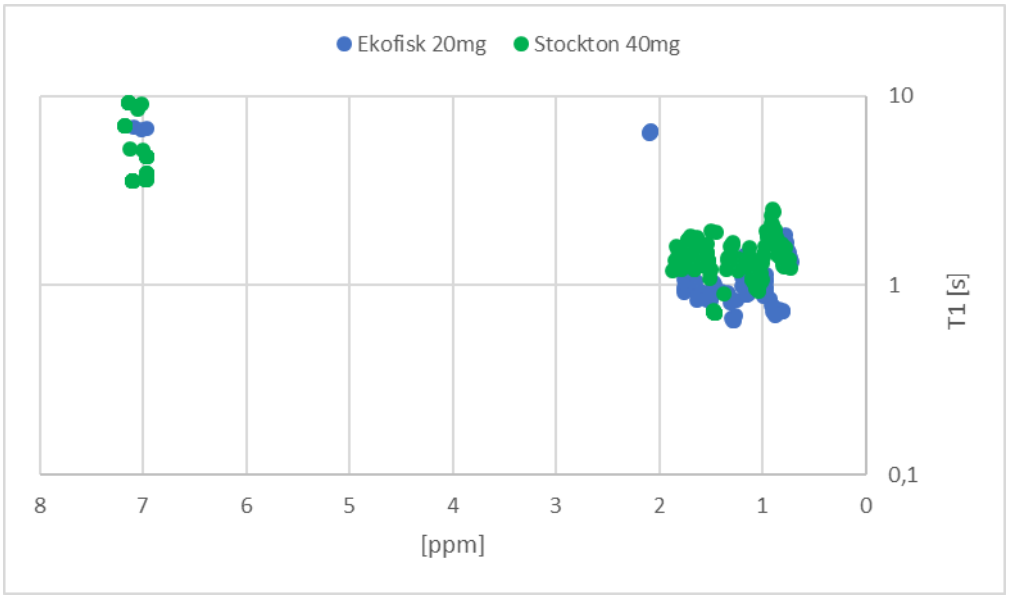

Figure 5.5.4: Comparison of T_1 relaxation times of Ekofisk 20mg and Stockton 40mg.

Again, the lacking fitting of low intensity broad peaks are apparent in the comparison of T_1 relaxation times of the Ekofisk and Stockton crude. In the aliphatic region, there are no peaks above 2,0ppm. The relaxation times that are fitted in the aliphatic region show slightly higher T_1 relaxation times for the Stockton crude compared to the Ekofisk crude.

In the aromatic region, the peaks from the oil are of too low intensity compared to the toluene peaks. This results in high T_1 relaxation times since most of the contribution to the fitting function are from toluene.

5.5.3: T_2 relaxation measurements

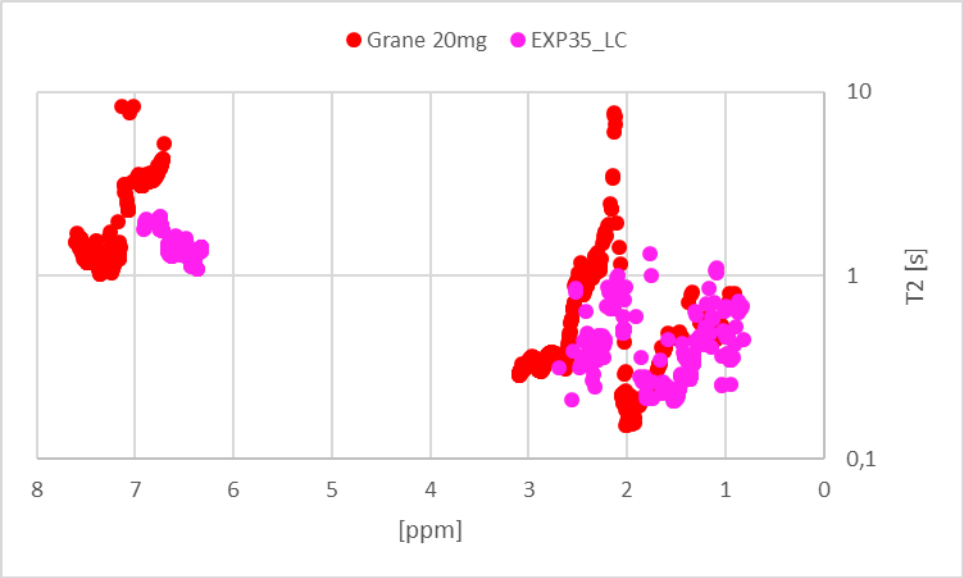

Figure 5.5.5: Comparison of T_2 relaxation times of Grane 20mg and EXP35_LC.

Both oils show large variance in the aliphatic region. Here no fitting was available by Dynamics Center above 2,6ppm for the EXP35 biooil. The Grane crude show a distribution of high T_2 relaxation times in the region 2,1-2,2ppm due to contribution from the toluene methyl peak.

In the aromatic region, the biooil again has a narrower interval from where there are fitted relaxation times than was seen in the diffusion measurement. The fitted T_2 relaxation times of the biooil are however in the same order as the T_2 relaxation times fitted from the Grane crude, with exception of the relaxation times having contribution from the aromatic signal of toluene.

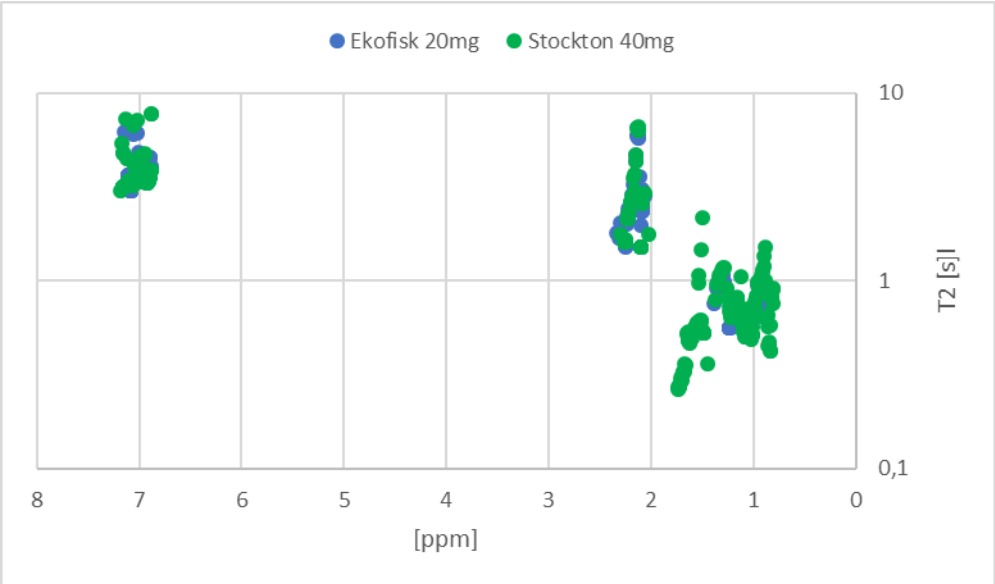

Figure 5.5.6: Comparison of T_2 relaxation times of Ekofisk 20mg and Stockton 40mg.

In the T_2 relaxation time comparison of Ekofisk 20mg and Stockton 40mg above the relaxation times are overlapping in both regions.

5.5.4: T_1-T_2 correlation measurements

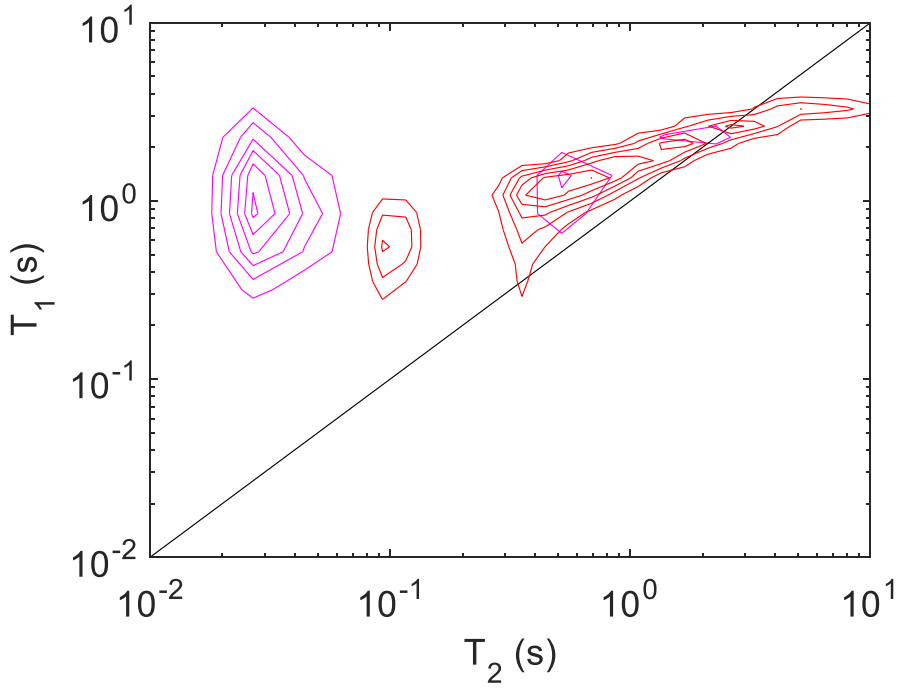

Figure 5.5.7: Overlapping T_1-T_2 correlation plot of Grane 20mg (red) and EXP35_LC (pink).

The overlapping T_1-T_2 correlation plot of Grane 20mg and EXP35_LC show that the distribution with T_1<<T_2 of EXP35_LC have a higher T_1/T_2 ratio than that of Grane 20mg. These low T_2 relaxation times were not found in the 2D T_2 measurement with spectral information of the oil. The recorded correlations of EXP35_LC close to the T_1=T_2 diagonal line overlaps with the distribution of Grane 20mg.

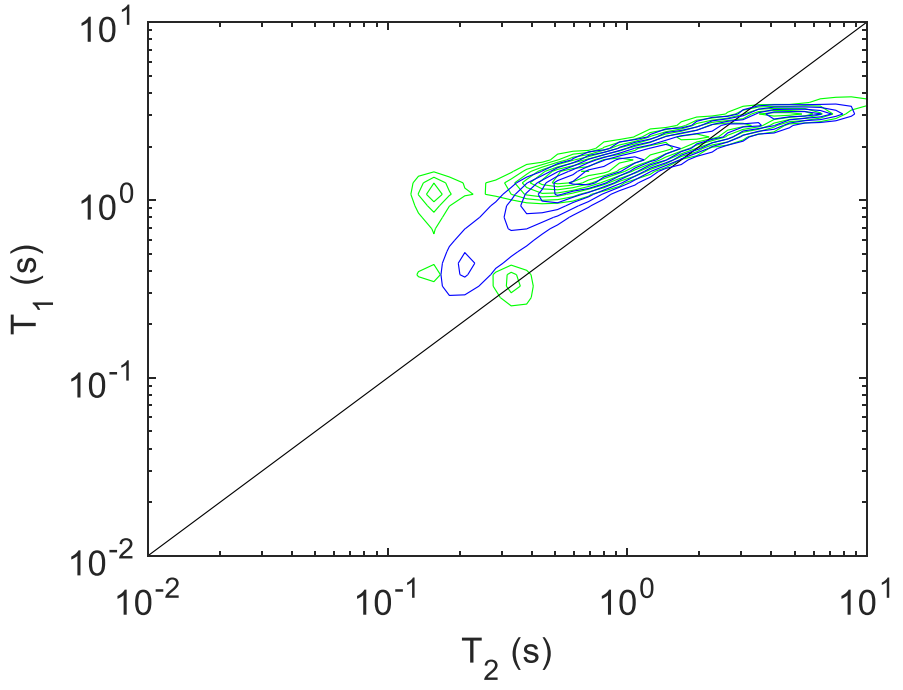

Figure 5.5.8: Overlapping T_1-T_2 correlation plot of Ekofisk 20mg (blue) and Stockton 40mg (green).

The T_1-T_2 correlation distribution of Ekofisk 20mg and Stockton 40mg are almost exclusively overlapping. For the lowest recorded T_2 relaxation times T_1 appear to be higher for the Stockton sample, resulting in a higher T_1/T_2 ratio than that of the Ekofisk sample.

Table 5.5.3: Compiled relaxation data achieved from Ekofisk 20mg and Stockton 40mg.

	Ekofisk 20mg			Stockton 40mg		
	T_1 [s]	T_2 [s]	T_1/T_2	T_1 [s]	T_2 [s]	T_1/T_2
Average aliphatic region	0,98	0,80	1,2	1,38	1,09	1,3
Average aromatic region	6,72	3,60	1,9	5,22	3,53	1,5
CH_2 peak using TopSpin fitting	1,39	0,73	1,9	0,95	0,78	1,2
CH_3 peak using TopSpin fitting	1,87	0,96	1,9	1,75	1,00	1,8
T_1-T_2 correlation lowest distribution with $T_1 \approx T_2$	1,05	0,45	2,3	1,24	0,42	3,0
T_1-T_2 correlation highest distribution with $T_1 \approx T_2$	5,87	3,03	1,9	5,17	3,06	1,7

Table 5.5.4: Compiled relaxation data achieved from Grane 20mg and EXP35_LC.

	Grane 20mg			EXP35_LC		
	T_1 [s]	T_2 [s]	T_1/T_2	T_1 [s]	T_2 [s]	T_1/T_2
Average 0,9-2,0ppm	0,97	0,36	2,7	1,09	0,41	2,7
Average 2.3-2,7ppm	1,34	0,30	4,5	0,94	0,40	2,4
Average aromatic region	2,88	2,24	1,3	2,42	1,50	1,6
CH_2 peak using TopSpin fitting	0,98	0,68	1,4	4,04	3,04	1,3
CH_3 peak using TopSpin fitting	1,64	0,82	2,0	4,74	3,86	1,2
T_1-T_2 correlation lowest distribution with $T_1 \approx T_2$	1,09	0,36	3,0	0,95	0,49	1,9
T_1-T_2 correlation highest distribution with $T_1 \approx T_2$	2,68	2,44	1,1	2,63	2,05	1,3
Center of T_1-T_2 correlation distribution with $T_1 << T_2$	0,57	0,10	5,7	0,94	0,03	31,3

Chapter 6

Results – non-diluted oils.

6.1: Measurements of the non-diluted Ekofisk crude.

6.1.1: Diffusion measurement of the non-diluted Ekofisk crude.

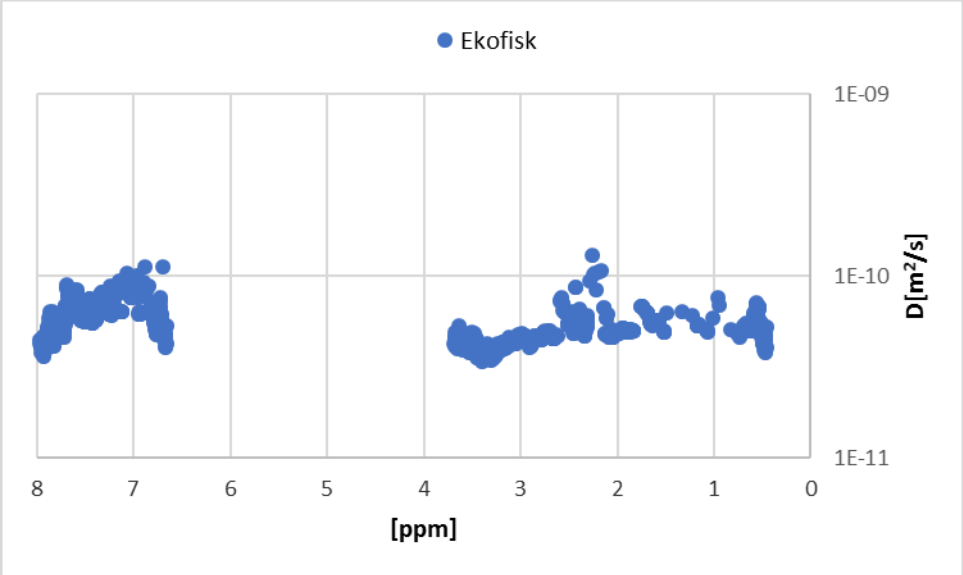

Figure 6.1.1: Diffusion measurement of the non-diluted Ekofisk crude.

All the diffusion coefficients of the Ekofisk crude are found in the interval $3{,}4x10^{-11}$-$1{,}0x10^{-10}m^2/s$. The differences seen in the T_2 plot (figure 6.1.3) are not shown in the diffusion plot and diffusion coefficient are relatively equal over all the functional groups.

6.1.2: T_1 measurement of the non-diluted Ekofisk crude.

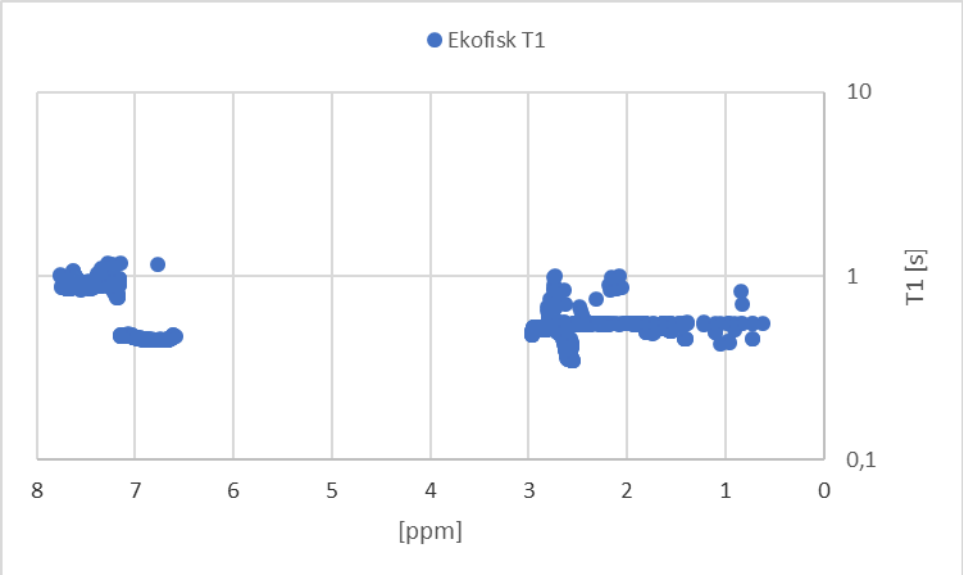

Figure 6.1.2: T_1 measurement of the non-diluted Ekofisk crude.

The T_1 relaxation times are ranging from 0,3-1,0s for the Ekofisk crude oil. This is a slightly narrower interval than what is seen in the T_1-T_2 correlation plot.

6.1.3: T_2 measurement of the non-diluted Ekofisk crude.

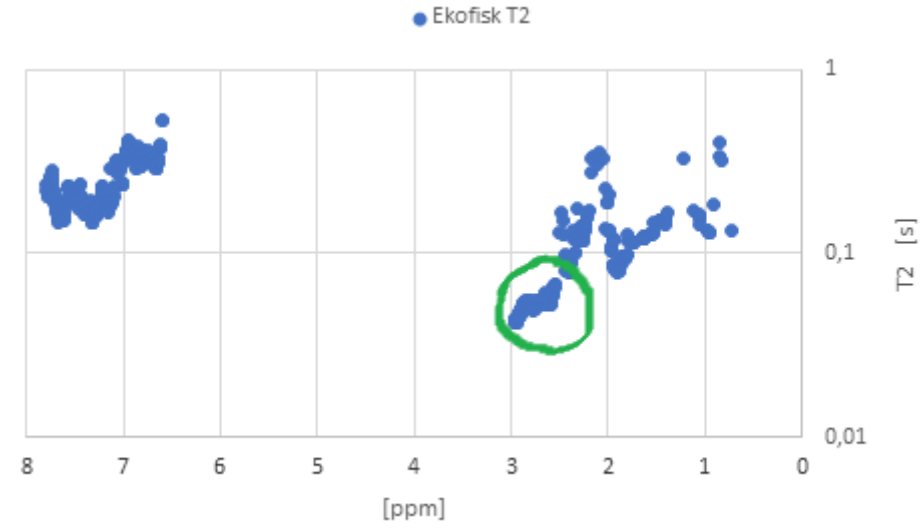

Figure 6.1.3: T_2 measurement of the non-diluted Ekofisk crude.

The main distribution of T_2 values is found in the interval 0,1-0,4s coinciding with the T_1-T_2 correlation plot of the Ekofisk crude. There is also a distribution with T_2 values ranging from 0,04-0,07s corresponding to the distribution with T_2<<T_1 in the T_1-T_2 correlation plot.

6.1.4: T_1-T_2 correlation measurement of the non-diluted Ekofisk crude.

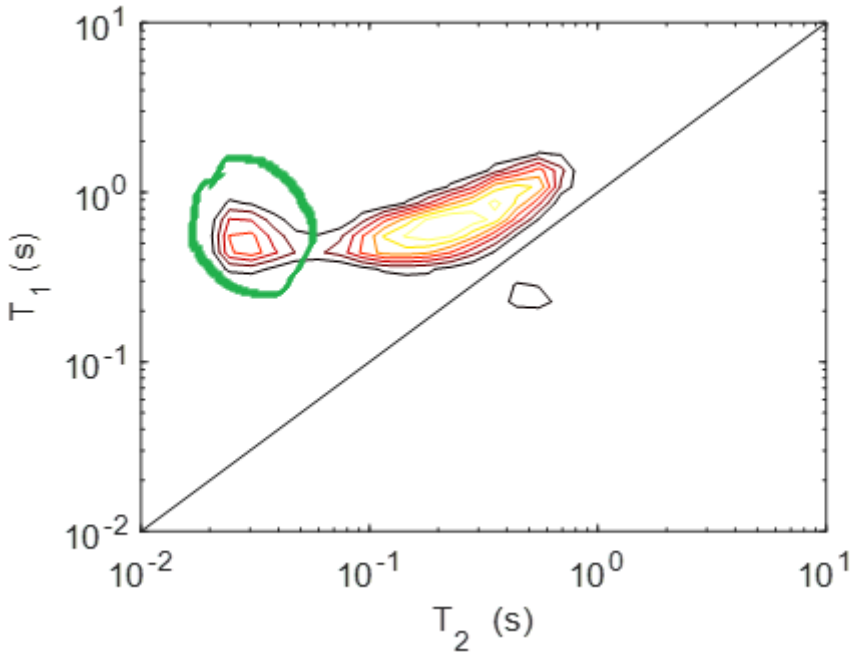

Figure 6.1.4: T_1-T_2 correlation plot of the Ekofisk crude oil.

The correlation plot shows two main distributions. The distribution close to the T_1=T_2 is also seen in the plots for the diluted samples (figure 5.4.5 and figure 5.4.6) and corresponds to the non-aggregating components of the oils. This distribution is found at a higher T_1/T_2 ratio since the viscosity of the diluted sample is lower due to the solvent having a lower viscosity than the crude oil. The distribution with T_2<<T_1 correspond to the aggregating components of the crude oil.

Table 6.1.1: Compiled information from the Ekofisk crude measurements.

	T_1 [s]	T_2 [s]	T_1/T_2	D [x10^{-11} m^2/s]
T_1-T_2 correlation plot highest distribution close to T_1=T_2	1,14	0,54	2,1	
T_1-T_2 correlation plot lowest distribution close to T_1=T_2	0,50	0,11	4,5	
T_1-T_2 correlation plot distribution with T_2<<T_1	0,50	0,03	16,7	
Average 0,72-2,50ppm using Dynamics Center fitting	0,54	0,13	4,2	5,44
Average 2,50-3,00ppm using Dynamics Center fitting	0,52	0,05	10,4	4,73
Average aromatic region using Dynamics Center fitting	0,77	0,23	3,3	6,24
CH_2 peak using TopSpin fitting	0,56	0,16	3,5	6,61
CH_3 peak using TopSpin fitting	0,90	0,20	4,5	7,24

6.2: Measurements of the non-diluted Grane crude.

6.2.1: Diffusion measurement of the non-diluted Grane crude.

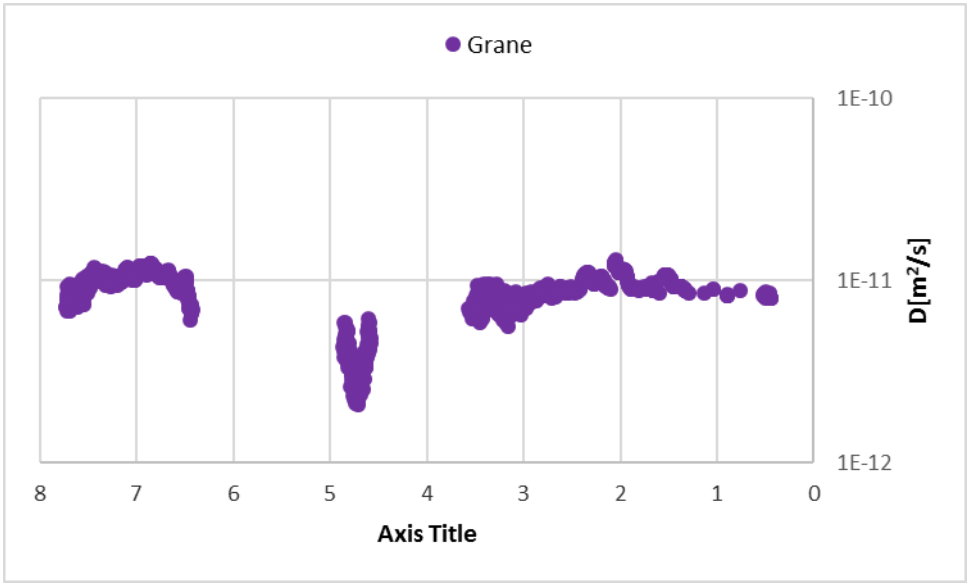

Figure 6.2.1: Diffusion measurement of the non-diluted Grane crude.

The Grane crude has diffusion coefficients ranging from $5{,}6x10^{-12}$ to $1{,}3x10^{-11}m^2/s$ in the aromatic and aliphatic region, with a slightly broader distribution of diffusion coefficients in the interval 3,0-3,5ppm corresponding to electronegative aliphatic components of the oil. The peak centered at 4,7ppm also show a wide distribution due to fitting problems caused by the broadness of the peak.

6.2.2: T_1 measurement of the non-diluted Grane crude.

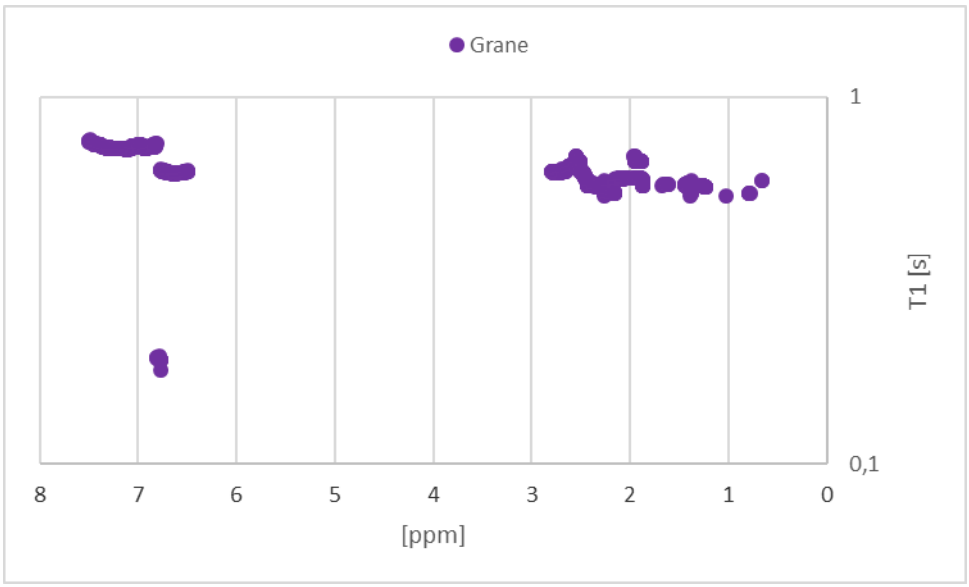

Figure 6.2.2: T_1 measurement of the non-diluted Grane crude.

The 2D T_1 measurement with spectral information show slightly lower T_1 values in the aliphatic region compared to the aromatic region. The distribution of T_1 relaxation times is rather narrow, ranging from 0,5-0,7s, which coincides with the narrow distribution seen in the T_1-T_2 correlation plot.

6.2.3: T_2 measurement of the non-diluted Grane crude.

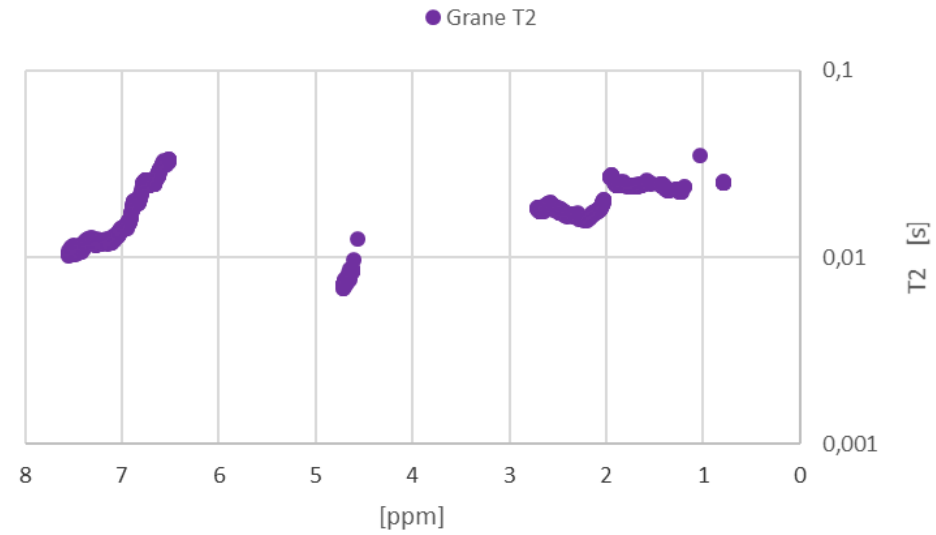

Figure 6.2.3: T_2 measurement of the non-diluted Grane crude.

The main T_2 distribution in the aliphatic region is between 0,02s and 0,03s, while the distribution in the aromatic region has slightly lower T_2 relaxation times. The correlation plot (figure 6.2.4) show a maximum value of T_2 at 0,07s, but relaxation times of this magnitude are not found from the 2D experiment maintaining spectral information.

6.2.4: T_1-T_2 correlation measurement of the non-diluted Grane crude.

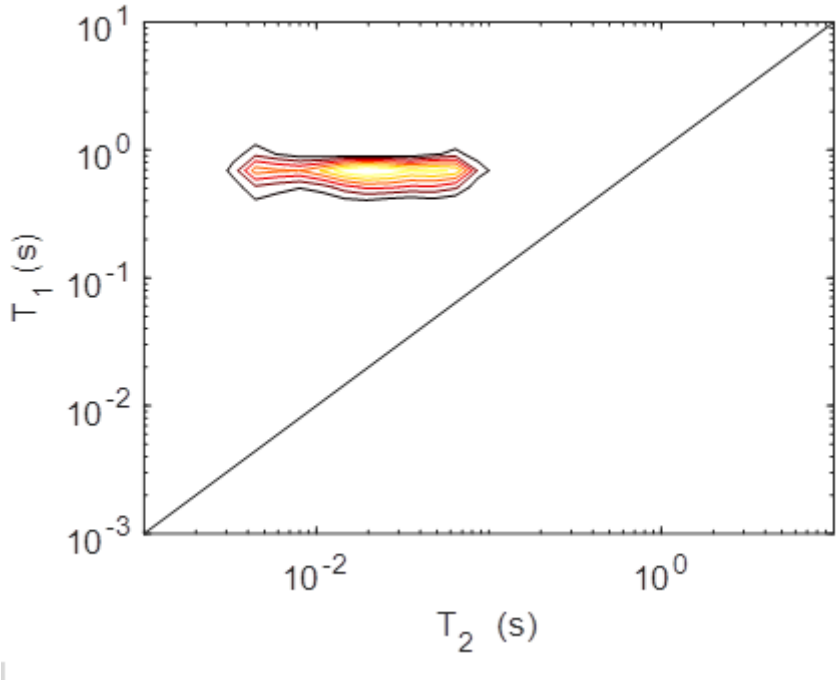

Figure 6.2.4: T_1-T_2 correlation plot of the Grane crude oil.

The correlation plot shows no distribution close to the T_1=T_2 diagonal line, but a wide distribution with T_2<<T_1. This may be due to field inhomogeneities caused by impurities in the sample in addition to aggregation.

Table 6.2.1: Compiled information from the Grane crude relaxation measurements.

	T_1 [s]	T_2 [s]	T_1/T_2	D [x$10^{-11}$$m^2$/s]
T_1-T_2 correlation plot lowest distribution with T_2<<T_1	0,69	0,010	69,0	
T_1-T_2 correlation plot highest distribution with T_2<<T_1	0,67	0,070	9,6	
Average aliphatic region using Dynamics Center fitting	0,60	0,020	30,0	0,88
Average aromatic region using Dynamics Center fitting	0,70	0,016	43,8	1,01
CH_2 peak using TopSpin fitting	0,59	**		0,98
CH_3 peak using TopSpin fitting	0,66	**		0,87

*** no fit available*

6.3: Measurements of the non-diluted EXP35 biooil.

6.3.1: Diffusion measurement of the non-diluted EXP35 biooil.

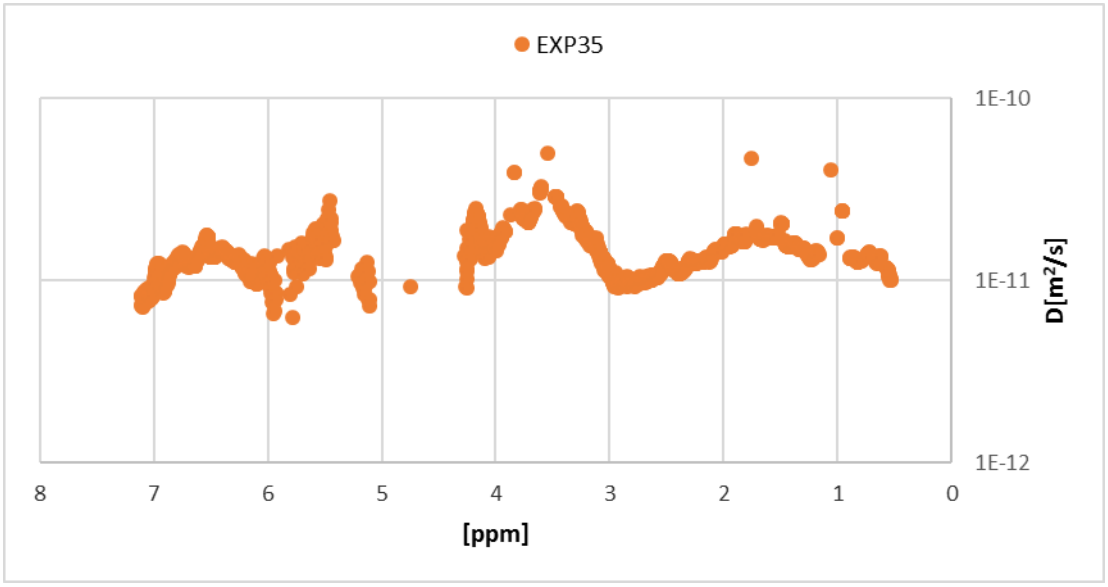

Figure 6.3.1: Diffusion measurement of the non-diluted EXP35 biooil.

The diffusion measurement of the biooil show greater variance in diffusion coefficients for different functional groups compared to the other crude oils. The diffusion coefficient calculated for the biooils are in the range of $6{,}6x10^{-12}$ to $3{,}0x10^{-11}m^2/s$.

6.3.2: T_1 measurement of the non-diluted EXP35 biooil.

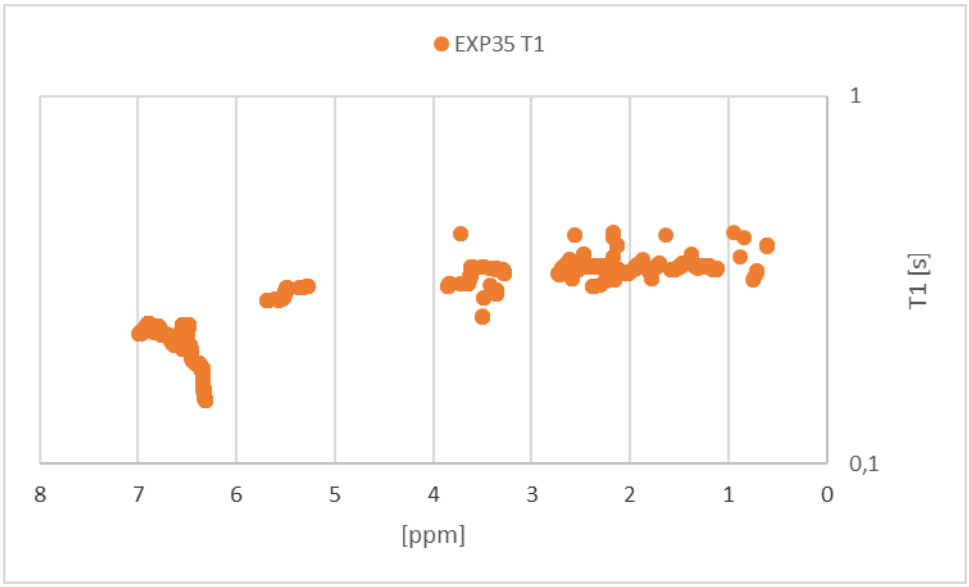

Figure 6.3.2: T_1 measurement of the non-diluted EXP35 biooil.

The aromatic region shows T_1 relaxation times in the range of 0,15-0,23s while the rest have relaxation times in the range 0,28-0,43s.

6.3.3: T_2 measurement of the non-diluted EXP35 biooil.

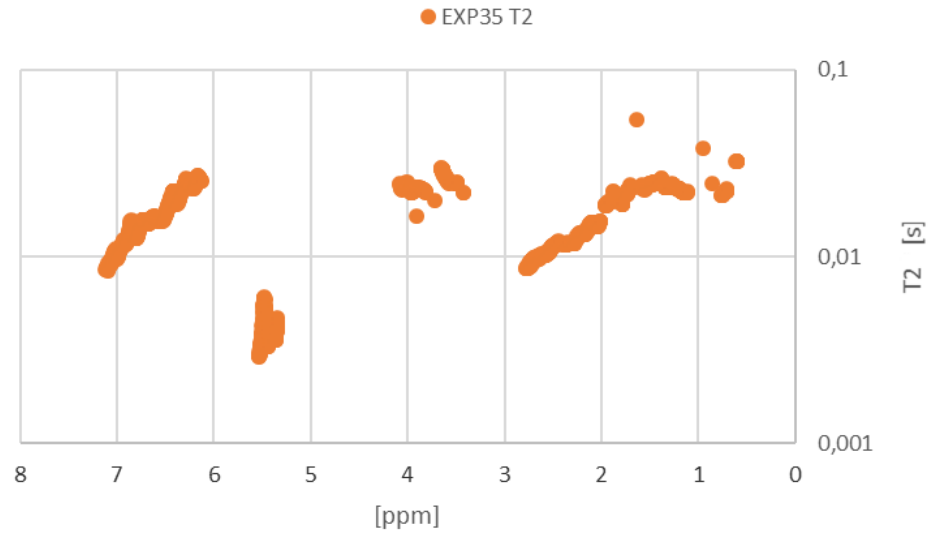

Figure 6.3.3: T_2 measurement of the non-diluted EXP35 biooil.

The aliphatic region ranging from 0,7-2,7ppm as well as the aromatic region from 6,0-7,1ppm has T_2 relaxation times in the interval of 0,009-0,025s. The distributions from 3,4-4,1ppm and 5,3-5,5ppm have T_2 relaxation times in the intervals 0,016-0,027s and 0,003-0,006s respectively.

6.3.4: T_1-T_2 correlation measurement of the non-diluted EXP35 biooil.

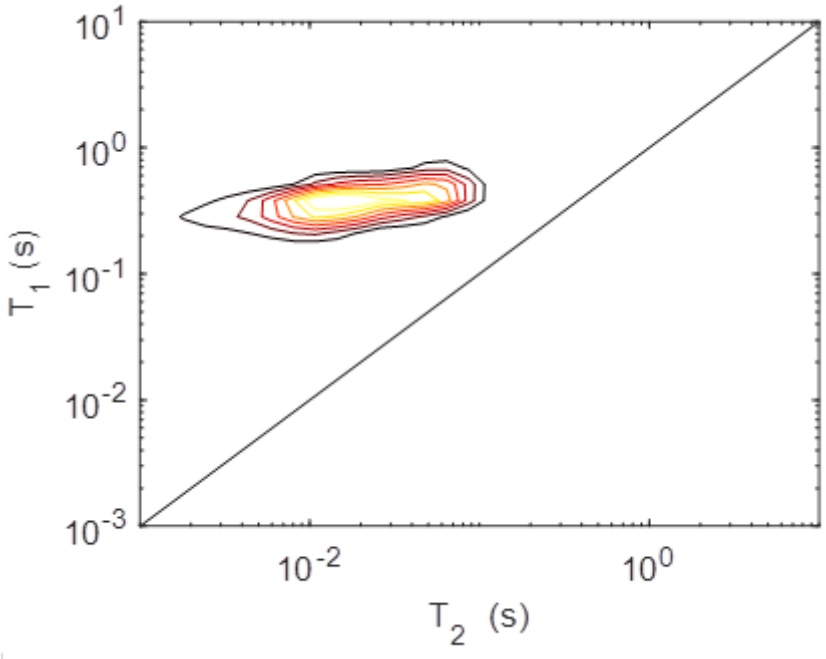

Figure 6.3.4: T_1-T_2 correlation plot of the EXP35 biooil.

The biooil only show a distribution with $T_2 << T_1$ with T_2 values in the range of approximately 0,01s and 0,1s. The components with the highest T_2 value might correspond to the distribution close to the $T_1=T_2$ in figure 5.2.6 due to the high viscosity of the biooil. However, the components with the lowest T_2 value in the non-diluted sample corresponds to the aggregating components of the biooil.

Table 6.3.1: Compiled information from the EXP35 biooil measurements.

	T_1 [s]	T_2 [s]	T_1/T_2	D [x10^{-11} m^2/s]
T_1-T_2 correlation plot lowest distribution with T_2<<T_1	0,33	0,0083	39,8	
T_1-T_2 correlation plot highest distribution with T_2<<T_1	0,43	0,061	7,0	
Average 0,6-2,7ppm using Dynamics Center fitting	0,34	0,016	21,3	1,29
Average 3,3-3,8ppm using Dynamics Center fitting	0,33	0,024	13,8	1,73
Average 5,3-5,6ppm using Dynamics Center fitting	0,30	0,004	75	2,38
Average 6,3-7,0ppm using Dynamics Center fitting	0,19	0,016	11,9	1,41
6,42ppm using TopSpin fitting	0,35	0,010	35,0	1,79
5,50ppm using TopSpin fitting	0,39	**	**	2,02
3,43ppm using TopSpin fitting	0,32	0,011	29,1	5,04
0,95ppm using TopSpin fitting	0,44	0,021	21,0	4,37
0,61ppm using TopSpin fitting	0,42	0,016	26,3	1,13

*** no fitting available*

6.4: Measurements of the non-diluted Stockton crude oil.

6.4.1: Diffusion measurement of the non-diluted Stockton crude oil.

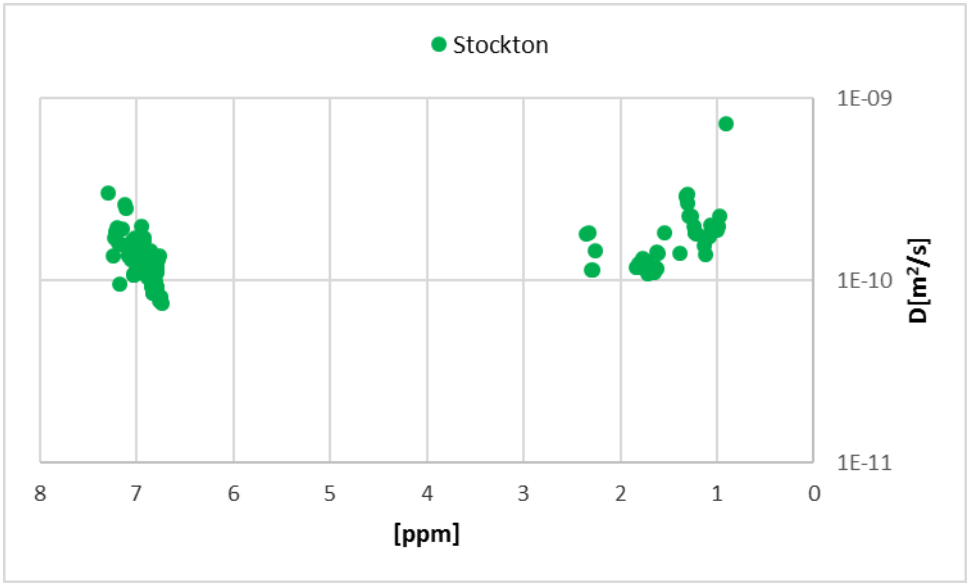

Figure 6.4.4: Diffusion measurement of the non-diluted Stockton crude.

The diffusion measurement of the Stockton crude show diffusion coefficients in the aliphatic region ranging from $1{,}1x10^{-10}$ to $2{,}6x10^{-10}m^2/s$. The aromatic region has diffusion coefficients ranging from $7{,}6x10^{-11}$ to $2{,}5x10^{-10}m^2/s$.

6.4.2: T_1 measurement of the non-diluted Stockton crude oil.

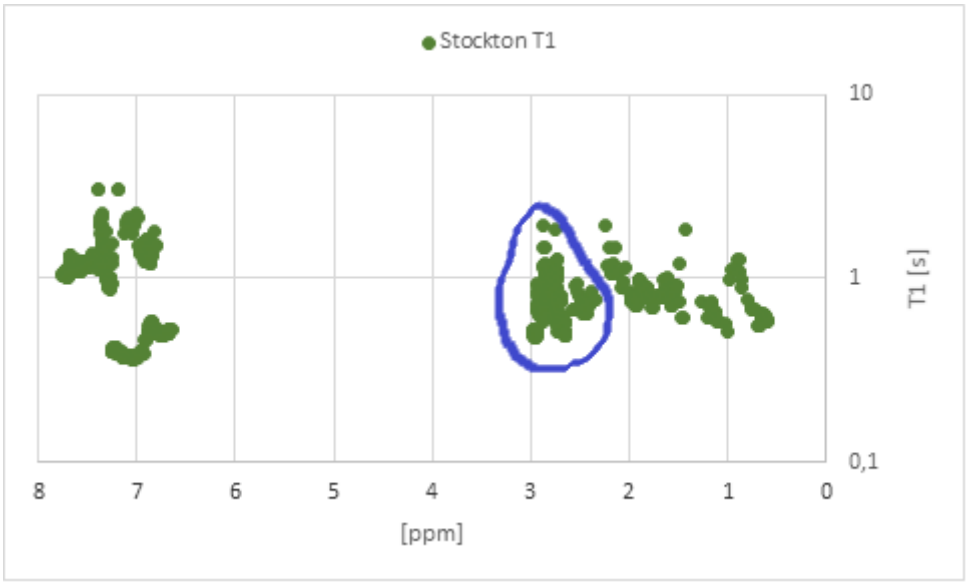

Figure 6.4.2: T_1 measurement of the non-diluted Stockton crude.

The aliphatic region has T_1 relaxation times between 0,5s and 1,9s. The aromatic region shows two distributions of T_1 relaxation times; one ranging from 0,36 to 0,60s and another one ranging from 0,86s to 2,03s.

6.4.3: T_2 measurement of the non-diluted Stockton crude oil.

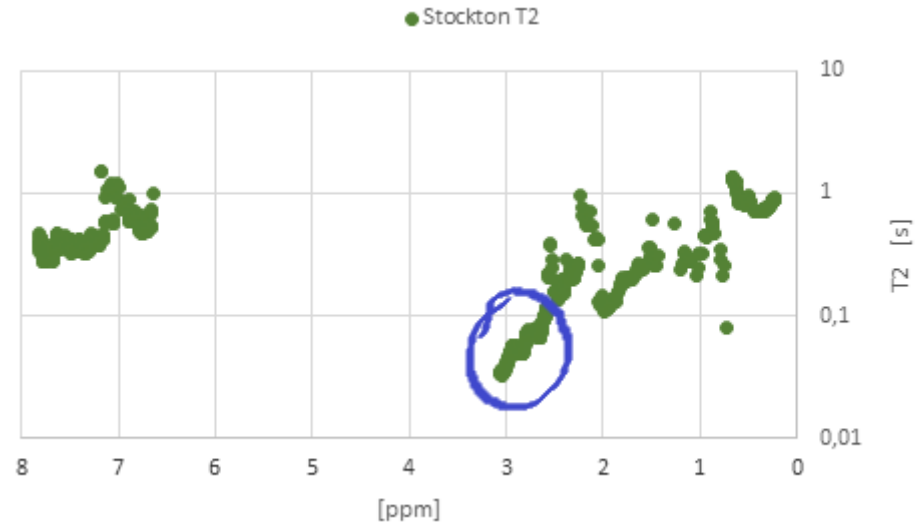

Figure 6.4.3: T_2 measurement of the non-diluted Stockton crude.

The aliphatic region shows T_2 relaxation times ranging from 0,03-1,36s, but with the majority of relaxation times between 0,15s and 0,44s. The lowest relaxation times are, as for the other crude oils, found in the most electronegative part of the aliphatic region – ranging from 2,5-3,0ppm. The relaxation times in the aromatic region are ranging from 0,28s to 1,1s.

6.4.4: T_1-T_2 correlation measurement of the non-diluted Stockton crude oil.

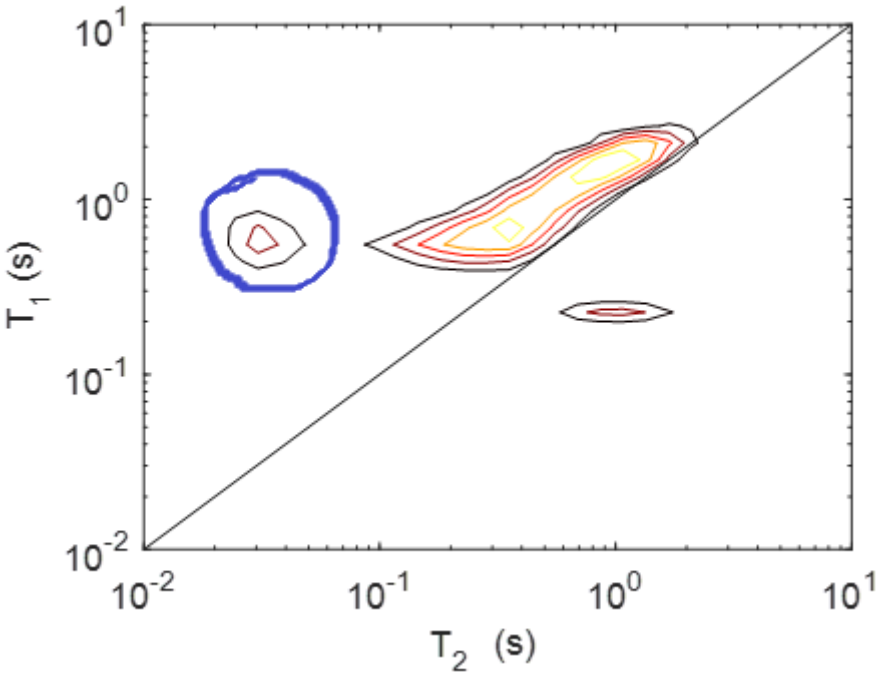

Figure 6.4.4: T_1-T_2 correlation plot of the Stockton crude oil.

The T_1-T_2 correlation plot show a distribution close to or at the T_1=T_2 diagonal line. It also shows a distribution with T_2<<T_1 with weak intensity.

Table 6.4.1: Compiled information from the EXP35 biooil measurements.

	T_1 [s]	T_2 [s]	T_1/T_2	D [x10^{-10} m^2/s]
T_1-T_2 correlation distribution with T_2<<T_1	0,62	0,032	19,4	
T_1-T_2 correlation plot highest distribution close to T_1=T_2	1,99	1,38	1,1	
T_1-T_2 correlation plot lowest distribution close to T_1=T_2	0,54	0,19	2,8	
Average 0,3-2,5ppm using Dynamics Center fitting	1,00	0,49	2,0	2,03
Average 2,5-3,0ppm using Dynamics Center fitting	0,72	0,06	12,0	**
Average aromatic region using Dynamics Center fitting	0,81	0,42	1,9	1,26
7,18ppm using TopSpin fitting	2,53	0,66	3,8	0,43
7,01ppm using TopSpin fitting	2,21	0,44	5,0	0,36
2,53ppm using TopSpin fitting	0,95	0,17	5,6	0,26
2,20ppm using TopSpin fitting	1,50	0,34	4,4	0,33
1,50ppm using TopSpin fitting	1,11	0,31	3,6	0,38
1,27ppm using TopSpin fitting	0,77	0,28	2,8	0,24
0,89ppm using TopSpin fitting	1,26	0,30	4,2	0,32

*** no fitting available*

6.5: Comparison of non-diluted oils.

Table 6.5.1: Viscosities of the oils.

Oil	Density @15°C [g/cc]	Kinematic Viscosity @20°C [cSt]	Dynamic Viscosity @20°C [cP]
Ekofisk	0,830	6	4,98
Grane	0,982	28	27,50
Stockton*	0,7297	3,4	2,5
EXP35	Not measured	Not measured	Not measured

**Viscosity estimated upon typical value for Permian basin crudes.*

6.5.1: Diffusion measurements

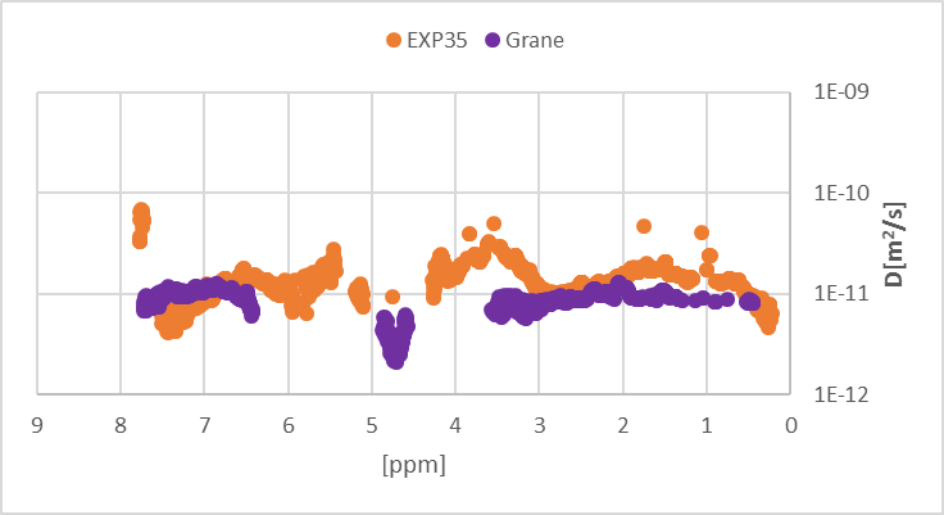

Figure 6.5.1: Comparison of diffusion coefficients of the non-diluted Grane and EXP35 samples.

The Grane crude oil have lower or equal diffusion coefficients in the aliphatic region compared to the EXP35 biooil. In the aromatic region, the diffusion coefficients of the Grane crude are equal or greater than those of the biooil. This coincides with the measurement done on the diluted samples, where the Grane crude showed larger molecular radiuses in the aliphatic region and mostly equal molecular radiuses in the aromatic region when compared with the biooil.

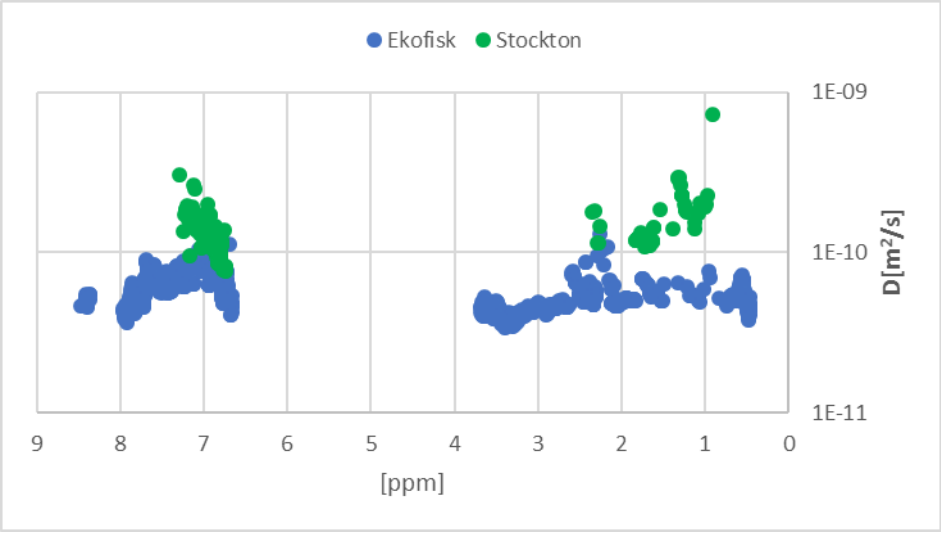

Figure 6.5.2: Comparison of diffusion coefficients of the non-diluted Stockton and Ekofisk samples.

The diffusion coefficients of Stockton are larger than those of the Ekofisk crude in the aliphatic region. The diluted Ekofisk sample also showed slightly larger molecular radiuses than the diluted Stockton sample, which coincides with what is observed for the comparison of the non-diluted samples.

In the aromatic region, the diffusion coefficients of the Stockton crude are equal or higher than those of the Ekofisk crude. Looking back at the diluted samples, Stockton had larger molecular radiuses than the Ekofisk sample in the aromatic region. This may be due to the increased viscosity of the Ekofisk crude compared to the Stockton crude or that the aromatic molecules of Ekofisk are more susceptible to aggregation at high concentration. It may also be a combination of both.

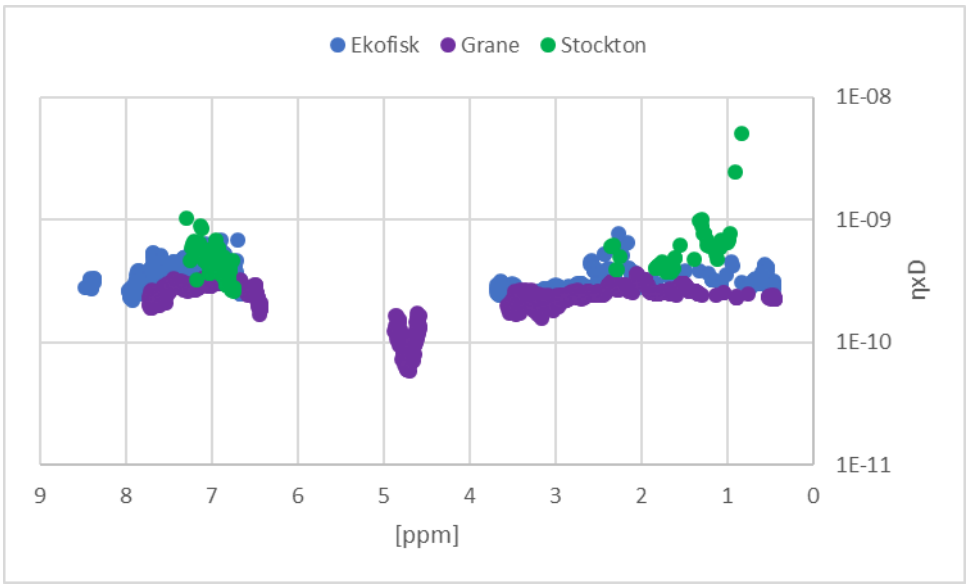

Figure 6.5.3: Comparison of the diffusion measurements of the non-diluted crude oils. Normalized with respect to viscosity.

6.5.2: T_1 relaxation measurements

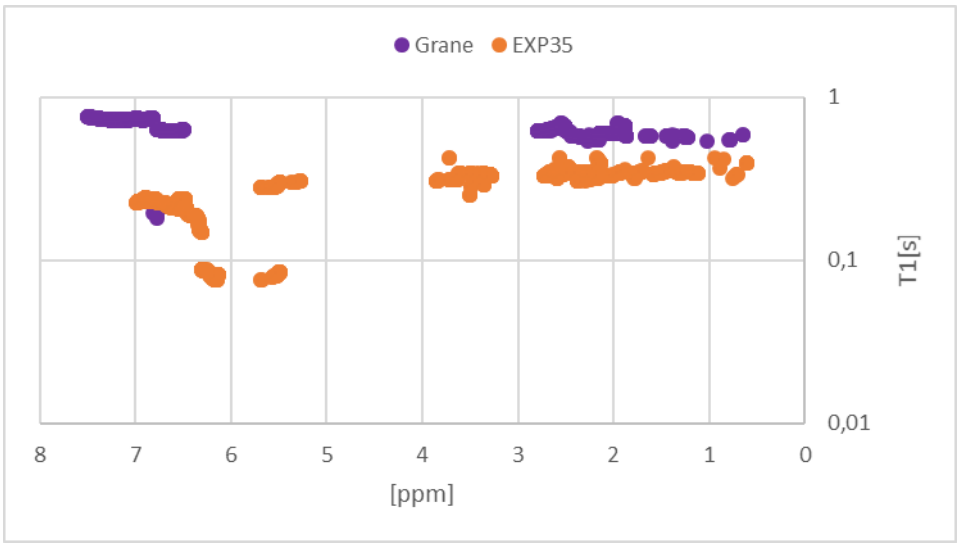

Figure 6.5.4: Comparison of T_1 relaxation times of the non-diluted Grane and EXP35 samples.

The T_1 comparison show that the Grane crude have longer T_1 relaxation times than the EXP35 biooil in both regions. However, the difference is more notable in the aromatic region than in the aliphatic region.

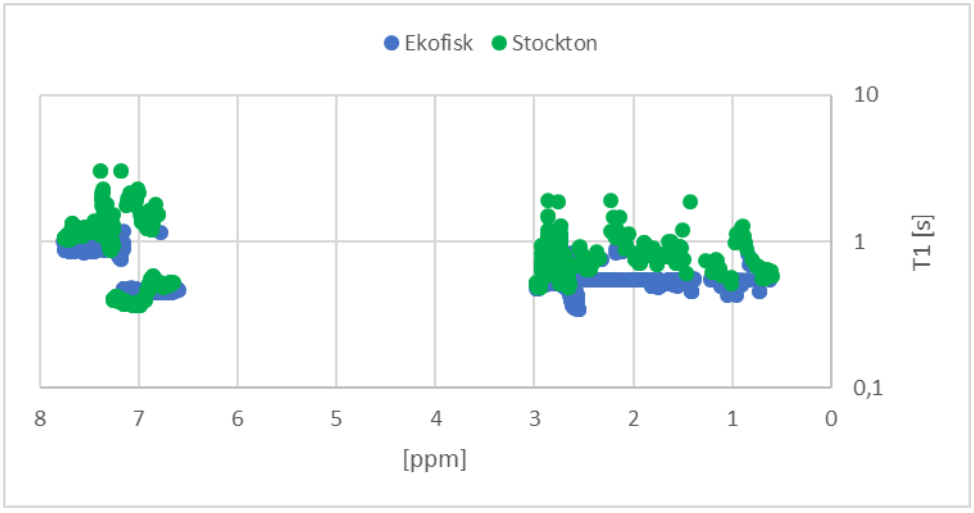

Figure 6.5.5: Comparison of T_1 relaxation times of the non-diluted Ekofisk and Stockton samples.

The comparison of T_1 relaxation times of the Ekofisk and Stockton crude show that the Stockton crude have equal or longer T_1 relaxation times than the Ekofisk crude in both regions.

6.5.3: T_2 relaxation measurements

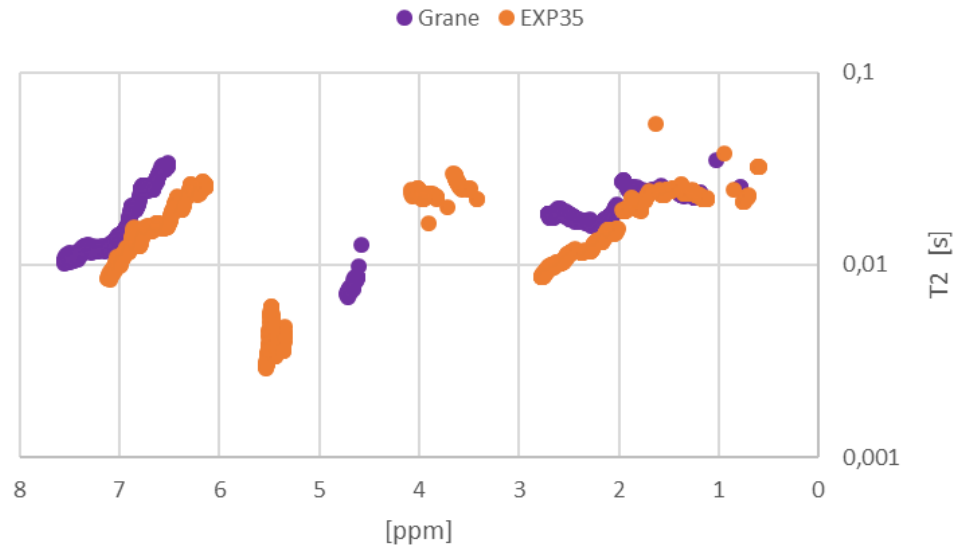

Figure 6.5.6: Comparison of T_2 relaxation times of the non-diluted Grane and EXP35 samples.

The comparison of T_2 of the Grane crude and the EXP35 biooil show that the T_2 relaxation times are slightly higher for the Grane crude than those of the EXP35 biooil. Both oils show a decline of T_2 relaxation times in the most electronegative part of both the aliphatic and aromatic region.

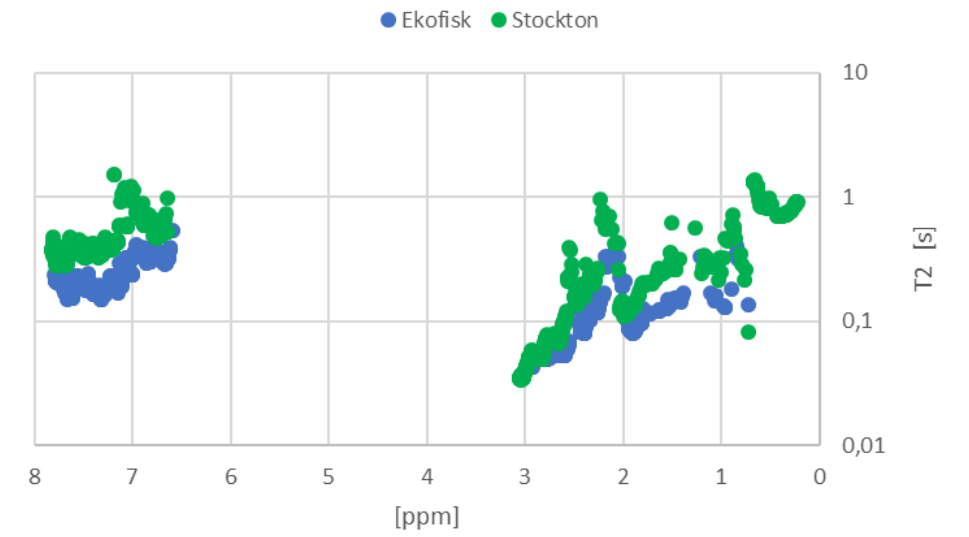

Figure 6.5.7: Comparison of T_2 relaxation times of the non-diluted Ekofisk and Stockton samples.

In the comparison of T_2 relaxation times of the Ekofisk and the Stockton crude it shows that the Stockton crude have longer T_2 relaxation times than those of the Ekofisk crude. As was seen for the Grane crude and the EXP35 biooil, the shortest relaxation times are found at the most electronegative part of both the aliphatic and aromatic region. However, for the Stockton and Ekofisk crude the shortest relaxation times are found in the most electronegative part of the aliphatic region.

6.5.4: T_1-T_2 correlation measurements

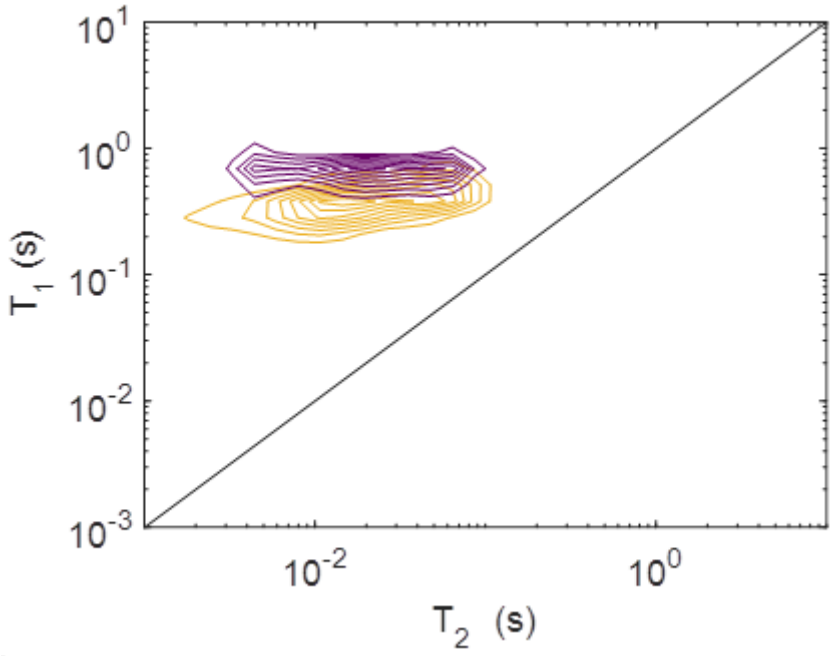

Figure 6.5.8: Overlapping T_1-T_2 correlation plot of the non-diluted Grane (purple) and EXP35 (orange) samples.

In the overlapping T_1-T_2 correlation plots of the Grane crude and the EXP35 biooil both oils share the same range of T_2 relaxation times. However, the T_1 relaxation times of the Grane crude are greater than those of the EXP35 biooil which was also seen in the T_1 comparison (Figure 6.5.4)

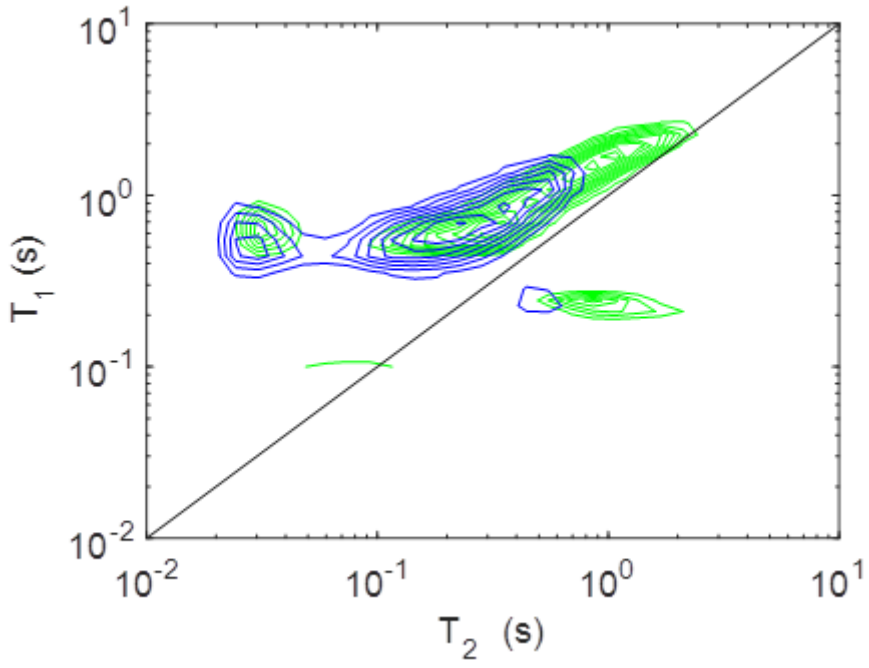

Figure 6.5.9: Overlapping T_1-T_2 correlation plot of the non-diluted Ekofisk (blue) and Stockton (green) samples.

The overlapping T_1-T_2 correlation plot of the Ekofisk and Stockton crude show that the two oils have mostly overlapping T_1-T_2 correlation distributions. However, the Stockton crude have higher T_1 and T_2 values than the Ekofisk crude in the distribution close to the T_1=T_2 diagonal. This was also seen in the T_1 comparison (figure 6.5.5) and the T_2 comparison (figure 6.5.7) where the Stockton crude showed longer relaxation times.

Chapter 7

Discussion

7.1: Standard samples.

The spectral relaxation measurements performed on the standard samples showed the expected trend for both T_1 and T_2 relaxation times. A decrease in both T_1 and T_2 relaxation were observed, which is consistent with the theory. However, the T_1/T_2 ratio of the hexadecane methyl groups is noticeably higher than the T_1/T_2 ratio calculated from the hexadecane methylene groups as well as the T_1/T_2 ratio of both functional groups of heptane.

The T_1-T_2 correlation measurements of the standard samples showed no variation along the T_2-axis, and differences was only seen along in the T_1 dimension. According to the theory both T_1 and T_2 are dependent on molecular size, however T_2 is more strongly dependent due to the contribution from J(0) (Eq.2.21). Within the extreme narrowing limit the T_1-T_2 correlation should move more diagonally from higher relaxation times to lower relaxation times along the T_1=T_2 diagonal line. The heptane sample had longer T_1 relaxation times resulting in a higher T_1/T_2 ratio for the heptane sample than for the hexadecane sample. This is the opposite of what is expected, as the T_1/T_2 ratio of heptane should be less than or equal to the T_1/T_2 ratio of hexadecane, since hexadecane is a larger molecule. The heptane sample show much higher T_1/T_2 ratio in the T_1-T_2 correlation measurement than what was seen from the spectral relaxation measurements.

The overlapping T_1-T_2 correlation plot of all the standard samples (Figure 4.3.7) show that the hydrocarbon distribution of the mixture sample is a combination of the distributions seen in the T_1-T_2 correlation plots of the individual solutions (Figure 4.3.4 and Figure 4.3.6). Again, the variation is found in the T_1 dimension. The T_1/T_2 ratio of the mixture is higher than what was seen for the hexadecane standard, but lower than what was seen for the heptane standard due to the unrealistic value for heptane. Error in acquisition or error in processing is unlikely since the same effect is seen for both the heptane standard and the mixture standard. The underlying reason was not investigated further as this was not the focus of the thesis.

7.2: Concentration series of the oils.

The diffusion measurements of the concentration series showed an increase in molecular radius in the aliphatic region of the EXP35 biooil ranging from 3,5-4,2ppm when the concentration was increased. This region corresponds to electronegative aliphatic species (i.e ethers) and conjugating species and the increase in molecular radiuses can be explained by a reduction of molecular mobility due to hydrogen bonding. An increase in molecular radius was also seen in the aromatic region of the EXP35 biooil in the range 7,5-8,2ppm, although this increase was to a less extent than what was seen in the aliphatic region.

The spectral relaxation measurements of the oil concentration series showed a decrease in T_1 relaxation times highly dependent on the viscosity of the oil in solution. This shift towards shorter T_1 relaxation times were therefore seen to a much greater extend in the most viscous oils, which are EXP35 and Grane. The same was also seen for the T_2 where the least viscous oils, Ekofisk and Stockton, had overlapping T_2 relaxation times and the T_2 relaxation times of the two more viscous oils were shifted towards shorter T_2 relaxation times. In the aromatic region of both EXP35 and Grane the highest concentration of both the oils showed a larger decrease in T_2 relaxation times resulting in a higher T_1/T_2 ratio for the highest concentration in this region. The most likely explanation for this is the increase in molecular size due to aggregating effects.

One of the most substantial weaknesses of Dynamics Center in the analysis of complex systems is the lack of fitting capability of broad peaks with medium to low intensity. Therefore, no results for the EXP35 biooil in the region 3,5-4,2ppm are included. In this region, the diffusion measurements showed a substantial increase in molecular radius.

In the T_1-T_2 correlation plots of the crude oil concentration series it is seen that the distributions of the lowest concentrations appear to move away from the T_1=T_2 diagonal line in the region with the shortest T_2 relaxation times. A possible explanation for this is that the sample is more aromatic in character, since the intensity ratio I(aromatic)/I(aliphatic) is higher for the lowest concentration sample due to the solvent being aromatic. Similar shapes of T_1-T_2 correlation plots for aromatic components are shown by Jia *et al.* [19], although the deviations from the T_1=T_2 diagonal there show a broader interval of T_1 relaxation times. The T_1-T_2 correlation plots did not present the changes in T_1/T_2 ratio that was seen in the spectral relaxation measurements.

Table 7.1: Ranking of diffusion coefficients and relaxation times received from the spectral measurements of the oil concentration series.

Rank	r_x/r_{TMS}	T_1	T_2	T_1/T_2
Lowest	Ekofisk	Grane and EXP35	EXP35	Stockton
Second lowest	Stockton		Grane	Ekofisk
Second highest	EXP35	Ekofisk		EXP35
Highest	Grane	Stockton	Stockton and Ekofisk	Grane

Table 7.2: Ranking of relaxation times received from the T_1-T_2 correlation measurements of the oil concentration series.

Rank	T_1	T_2	T_1/T_2
Lowest	Grane and EXP35	EXP35	Stockton and Ekofisk
Second lowest		Grane	
Second highest	Stockton		Grane
Highest	Ekofisk	Stockton and Ekofisk	EXP35

As seen in table 7.1 and 7.2 the T_1/T_2 ratio ranking is not consistent between the T_1-T_2 correlation measurement and the spectral relaxation measurements.

7.3: Non-diluted oils.

The spectral diffusion measurements of the non-diluted oils show low to moderate variation between the functional groups. The viscosity normalized plot (figure 6.5.3) show that the Grane crude have larger molecules than the two other crude oils in the aliphatic region, which is consistent with the previous analysis' performed on the crude oils. These analysis' can be found in Appendix A. The diffusion coefficient is expected to decrease with increasing T_1/T_2 ratio due to an increase in molecular radiuses. No clear trend of diffusion decreasing with increased T_1/T_2 is seen when comparing the average diffusion coefficients and T_1/T_2 ratio within the spectral regions (Tables 6.2.1,

6.3.1 and 6.4.1). An exception is the Ekofisk crude (table 6.1.1), where the Dynamics Center diffusion coefficients and T_1/T_2 ratio follows the expected trend. However, the rankings seen in table 7.3 shows that over the sum of all frequencies the diffusion coefficient is inversely proportional to the T_1/T_2 ratio as expected.

In the spectral relaxation measurements of the non-diluted crude oils with lowest viscosity (Ekofisk and Stockton) there was a large variation of both T_1 and T_2 relaxation times. The shortest T_2 relaxation times was found in the most electronegative part of the aliphatic region. This coincides with the most electronegative components of the aliphatic region being more susceptible to aggregation through hydrogen bonding. Unlike what was seen in the concentration series of Ekofisk and Stockton, the distribution with high T_1/T_2 ratio in the T_1-T_2 correlation plot can be explained using the spectral relaxation measurements.

In the spectral relaxation measurements of the non-diluted oils with highest viscosity (Grane and EXP35) no variation of T_1 relaxation times are seen in the aliphatic region. In the aromatic region, there is more variation, especially for the EXP35 biooil. In the T_2 relaxation measurements there were less variation for the Grane crude in the aliphatic region than what was seen for the EXP35 biooil. As for the relaxation measurements of the crude oils with the lowest viscosity, the shortest T_2 relaxation times were found in the most electronegative of this region. A low variation in T_1 relaxation times and a large variation of the T_2 relaxation times is also replicated in the T_1-T_2 correlation plot.

Table 7.3: Ranking of diffusion coefficients and relaxation times received from the spectral measurements of the non-diluted oils.

Rank	Diffusion	T_1	T_2	T_1/T_2
Lowest	Grane	EXP35	EXP35	Ekofisk and Stockton
Second lowest	EXP35	Grane	Grane	
Second highest	Ekofisk	Ekofisk	Ekofisk	EXP35
Highest	Stockton	Stockton	Stockton	Grane

Table 7.4: Ranking of relaxation times received from the T_1-T_2 correlation measurements of the non-diluted oils

Rank	T_1	T_2	T_1/T_2
Lowest	EXP35	EXP35	Stockton
Second lowest	Grane	Grane	Ekofisk
Second highest	Ekofisk	Ekofisk	EXP35
Highest	Stockton	Stockton	Grane

Unlike for the concentration series, table 7.3 and 7.4 shows that the rankings of T_1/T_2 ratios are the same for both the T_1-T_2 correlation measurement and the spectral relaxation measurements.

Chapter 8

Conclusion

In the diffusion experiment optimization improvement was seen in the diffusion dimension with increasing number of gradient steps. The largest improvement was seen when increasing from 16 to 32 gradient steps. An improvement was also seen when increasing from 32 to 64 gradient steps, however the increased resolution to time ratio was not as great due to the exponentially increasing experiment times. A number of 32 gradient steps (td(F1)=32) was found to be the optimal with respect to experimental time and resolution.

Convection was present in the samples with Toluene-d8 as a solvent. The double stimulated echo sequence compensated well for convection. It is important to note that this sequence does not have bipolar gradients, and therefore does not compensate for internal gradients.

The spectral measurements of the hydrocarbon standards showed that the T_1/T_2 followed the expected trend for the methylene groups. T_1-T_2 correlation measurements greatly underestimated the T_2 relaxation times of heptane, raising questions about the correlation measurement's capability to accurately determine T_1-T_2 correlations of simple solutions.

In the concentration series, an increase in molecular sizes was only seen for the EXP35 biooil. Results pointing towards larger molecular sizes are found in the aromatic region with both relaxation measurements as well as the diffusion measurement. An increase in molecular sizes was also seen in the most electronegative part of the aliphatic region of the EXP35 biooil. Relaxation measurements could not support this further due to problems with calculating relaxation times of broad peaks.

The diffusion measurements of the non-diluted oils showed low variation. Normalization with respect to viscosity showed that Grane contained the largest molecules, which is consistent with previous analysis.

The relaxation measurements of the non-diluted oils show low variation in T_1 relaxation times over the functional groups. The T_2 relaxation times show great variance. The shortest T_2 relaxation times and highest T_1/T_2 ratios are found in the most electronegative part of the aliphatic and aromatic region, corresponding to the aggregating components. The T_1-T_2 correlation measurements of the non-diluted oils show the same results as the spectral relaxation measurements.

Analysis performed on non-diluted samples show that the EXP35 biooil has a similar molecular size distribution as the Grane crude. The chemical composition of the biooil differs greatly to the chemical composition of the crude oils (figure 5.1.1, 5.2.1, 5.3.1 and 5.4.1). These compositional differences cause the most electronegative functional groups of the biooil to increase in molecular size at lower concentration than the crude oils.

8.1: Further work.

- Achieve a better relaxation model covering a larger range of molecular sizes.
- Attempt a more linear molecule as internal standard in diffusion measurements to achieve a more accurate $r_x/r_{standard}$ ratio for aliphatic molecules.
- Examine biooils and crude oils with D-T_2 correlation measurements.
- Perform diffusion and relaxation measurements on non-diluted biooils with known viscosity – ideally parallel to other compositional analysis.

Litterature

[1] Vogt, M.H., *Kvantitativ analyse av biooljer fra LtL-prosessen ved bruk av GC-FID.* 2013; 107

[2] Liu, H. *et al. Heavy oil component characterization with multi-dimensional unilateral NMR.* Petroleum Science, 2013; **10**(3); 402-407.

[3] Herzberg, A., *Edle metaller på alumina som katalysator I LtL-processer; Effekter på utbytte, produktsammensetning og reaksjonsbetingelser*, 2013

[4] Antalek, B., *Using PGSE NMR for chemical mixture analysis: Quantitative aspects*. Concepts in Magnetic Resonance Part A, 2007; **30**(5); 219-235

[5] Price, W.S., *NMR Studies of Translational Motion. Principles and Applications.* 2009. Cambridge University Press; 56

[6] Keeler, J., *Understanding NMR Spectroscopy 2nd edition.* 2010. John Wiley & Sons, Ltd; 253-258

[7] Sanchez-Minero, F. *et al*. *Predicting SARA composition of crude oil by means of NMR.* Fuel, 2013; **110**; 318-321

[8] Suatoni, J.C., Swab, R.E., *Rapid Hydrocarbon Group-Type Analysis by High Performance Liquid Chromatography.* Joirnal of Chromatographic Science, 1975; **13**(8); 361-366

[9] Ali, M.A., Nofa, W.A., *APPLICATION OF HIGH PERFORMANCE LIQUID CHROMATOGRAPHY FOR HYDROCARBON GROUP TYPE ANALYSIS OF CRUDE OILS.* Petroleum Science and Technology, 1994; **12**(1); 21-33

[10] Radke, M., *et al. Preparative hydrocarbon group type determination by automated medium pressure liquid chromatography.* Analytical Chemistry, 1980; **52**(3); 406-411

[11] Bollet, C., *et al. Rapid separation of heavy petroleum products by high-performance liquid chromatography.* Journal of Chromatography, 1981; **206**(2); 289-300

[12] Win Lee, S., Glavinecevski, N., *NMR method for detemination of aromatics in middle distillate oils.* Fuel Processing Technology, 1999; **60**(1); 81-86

[13] Yang, Y., *et al. Study on relationship between the concentration of hydrocarbon groups in heavy oils and their structural parameter from ^{1}H NMR spectra.* Fuel, 2003; **82**(6); 721-727

[14] Kapur, G.S., *et al. Determination of aromatics and naphthenes in straight run gasoline by ^{1}H NMR spectroscopy. Part I.* Fuel, 2000; **79**(9); 1023-1029

[15] https://www.statoil.com/content/dam/statoil/documents/crude-oil-assays/Statoil-GRANE-BLEND-2016-10.xls Downloadable Excel file as, retrieved 25.04.2017

[16] https://www.statoil.com/content/dam/statoil/documents/crude-oil-assays/Statoil-EKOFISK%202015%2006.xls Downloadable Excel file, retrieved 25.04.2017

[17] Freed, D.E., *Dependence on chain length of NMR relaxation times in mixtures of alkanes.* The Journal of Chemical Physics, 2007; **126**(17)

[18] Mutina, A.R., Hürlimann, M.D., *Effect of oxygen on the NMR relaxation properties of crude oils.* Applied Magnetic Resonance, 2005; **29**(3); 503-513

[19] Jia, Z. *et al. Molecular dynamics and composition of crude oil by low-field nuclear magnetic resonance*, 2016; **54**(8); 650-655

[20] Hansen, H.T.F., *Karakterisering av biooljer ved hjelp av NMR-spektroskpi.* 2015; 16-19

[21] Abraham, R.J., Mobil, M., *Modelling ^{1}H NMR Spectra of Organic Compounds: Theory, Applications and NMR Prediction Software.* 2008. John Wiley & Sons, Ltd; 1¨

[22] http://chem.libretexts.org/@api/deki/files/9529/Zeeman_modified.png?revision=1 Retrieved 19.01.17

[23] http://chemistry.umeche.maine.edu/CHY431/NMR/NMR-9.jpg Retrieved 19.01.17

[24] Keeler, J., *Understanding NMR Spectroscopy 2nd edition.* 2010. John Wiley & Sons, Ltd; 241-250

[25] Hahn, E.L., *Spin echoes.* Physics Today, 1950; **3**(12); 21

[26] Stilbs, P., *Automated CORE, RECORD and GRECORD processing of multi-component PGSE NMR diffusometry data.* European Biophysics Journal, 2013; **42**(1); 25-32

[27] Ernst, R.R., Anderson, W.A. *Application of Fourier Transform Spectroscopy to Magnetic Resonance.* Reviewing of Scientific Instruments, 1966; **37**(1); 93-102

[28] Berger, F., *NMR techniques employing selective radiofrequency pulses in combination with pulsed field gradients.* Progress in Nuclear Magnetic Resonance Spectroscopy, 1997; **30**(3); 137-156

[29] Price, W.S., *NMR Studies of Translational Motion. Principles and Applications.* 2009. Cambridge University Press; 10

[30] Price, W.S., *NMR Studies of Translational Motion. Principles and Applications.* 2009. Cambridge University Press; 2

[31] Cabrita, E.J., Berger, S. *DOSY studies of hydrogen bond association: tetrametylsilane as a reference compound for diffusion studies.* Magnetic resonance in chemistry, 2001; **39**; 142-148

[32] Johnson Jr., C.S., *Diffusion ordered nuclear magnetic resonance spectroscopy: principles and applications.* Progress in Nuclear Magnetic Resonance Spectroscopy, 1998; **34**; 207-209

Appendix A – Previous analyses of the crude oils.

Stockton analysis.

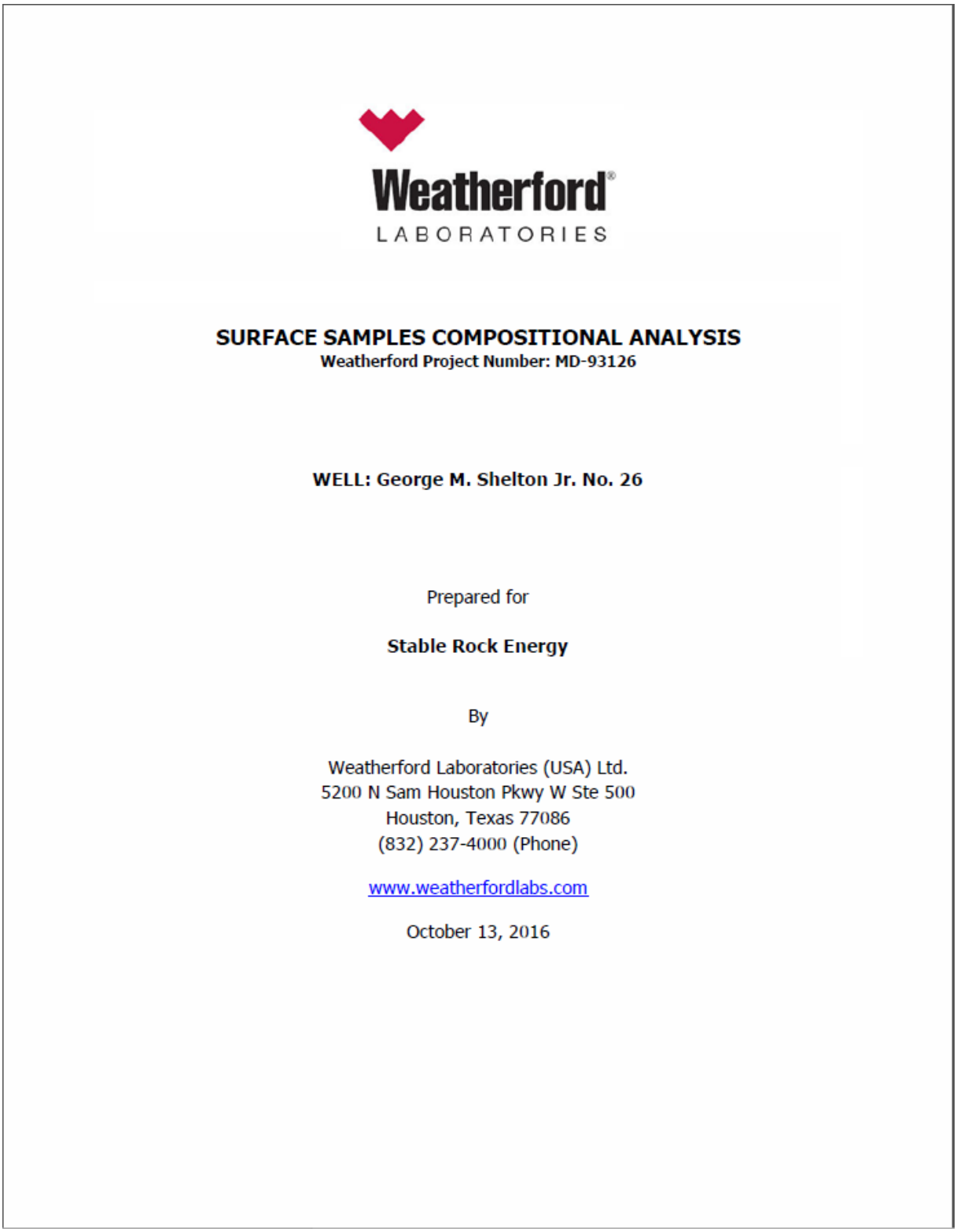

Weatherford®
LABORATORIES

SURFACE SAMPLES COMPOSITIONAL ANALYSIS
Weatherford Project Number: MD-93126

WELL: George M. Shelton Jr. No. 26

Prepared for

Stable Rock Energy

By

Weatherford Laboratories (USA) Ltd.
5200 N Sam Houston Pkwy W Ste 500
Houston, Texas 77086
(832) 237-4000 (Phone)

www.weatherfordlabs.com

October 13, 2016

Description of Experiment

Tables

DESCRIPTION OF EXPERIMENT

The Surface Sample Compositional Report was conducted on separator fluid samples collected from the well George M. Shelton Jr. No. 26.

Compositional analyses were performed on the atmospheric separator oil and separator gases using gas chromatography methods. The molecular weight and density of the flashed liquid phase were measured.

Stable Rock Energy-George M. Shelton Jr. No. 26

TABLE 1

Sample Inventory

Client	Stable Rock Energy
Well	George M. Shelton Jr. No. 26
Location	Pecos co., TX
Formation	N/A
Sample Type	Surface
Sampled By	Client
Sampled Date	N/A
Producing Depth (ft)	N/A
Reservoir Temperature (°F)	N/A
Reservoir Pressure (psig)	N/A

Weatherford Reference Number	Cylinder Number	Sampling Time	Sample Type	Sampling Pressure (psig)	Sampling Temperature (°F)	Opening Pressure (psig @72°F)	Saturation Pressure (psig @Tsep)	Initial Sample Volume (cc)	Remaining Sample Volume (cc)
MD-93126-01	319	2:45:00 PM	Separator Gas	50	80	40	N/A	300	300
MD-93126-02	323	3:45:00 PM	Separator Gas	50	80	5	N/A	300	300
MD-93126-03	383	4:45:00 PM	Separator Gas	50	80	5	N/A	300	300
MD-93126-04	IATA	5:45:00 PM	Separator Oil	50	80	N/A	N/A	5 Gallon	5 Gallon

TABLE 2
Compositional Analysis of Atmospheric Separator Oil MD-93126-04

Component Name	Chemical Symbol	Mol %	Weight %	Calculated Properties	
Nitrogen	N_2	0.000	0.000	**Total Sample**	
Carbon Dioxide	CO_2	0.000	0.000		
Hydrogen Sulphide	H_2S	0.000	0.000	Molecular Weight	223.78
Methane	C_1	0.000	0.000		
Ethane	C_2	0.119	0.016		
Propane	C_3	0.442	0.087	**C_{6+} Fraction**	
i-Butane	i-C_4	0.270	0.070		
n-Butane	n-C_4	0.993	0.258	Molecular Weight	231.05
i-Pentane	i-C_5	1.250	0.403	Mole Fraction	0.9565
n-Pentane	n-C_5	1.281	0.413	Density (g/cc)	0.8591
Hexanes	C_6	3.070	1.182		
Heptanes	C_7	7.973	3.570	**C_{7+} Fraction**	
Octanes	C_8	10.068	5.139		
Nonanes	C_9	7.965	4.565	Molecular Weight	235.85
Decanes	C_{10}	6.477	4.118	Mole Fraction	0.9258
Undecanes	C_{11}	6.003	3.943	Density (g/cc)	0.8618
Dodecanes	C_{12}	5.210	3.748		
Tridecanes	C_{13}	5.228	4.088	**C_{12+} Fraction**	
Tetradecanes	C_{14}	4.405	3.740		
Pentadecanes	C_{15}	4.016	3.697	Molecular Weight	315.39
Hexadecanes	C_{16}	3.104	3.079	Mole Fraction	0.5409
Heptadecanes	C_{17}	2.939	3.112	Density (g/cc)	0.8957
Octadecanes	C_{18}	3.034	3.403		
Nonadecanes	C_{19}	2.688	3.159	**C_{30+} Fraction**	
Eicosanes	C_{20}	2.072	2.546		
Heneicosanes	C_{21}	1.862	2.421	Molecular Weight	662.14
Docosanes	C_{22}	1.716	2.339	Mole Fraction	0.0919
Tricosanes	C_{23}	1.543	2.193	Density (g/cc)	0.9887
Tetracosanes	C_{24}	1.404	2.076		
Pentacosanes	C_{25}	1.289	1.987	**C_{36+} Fraction**	
Hexacosanes	C_{26}	1.193	1.914		
Heptacosanes	C_{27}	1.129	1.887	Molecular Weight	853.07
Octacosanes	C_{28}	1.058	1.834	Mole Fraction	0.0487
Nonacosanes	C_{29}	1.008	1.810	Density (g/cc)	1.0304
Tricontanes	C_{30}	0.886	1.647		
Hentriacontanes	C_{31}	0.863	1.658		
Dotriacontanes	C_{32}	0.756	1.500		
Tritriacontanes	C_{33}	0.691	1.414		
Tetratriacontanes	C_{34}	0.560	1.181		
Pentatriacontanes	C_{35}	0.564	1.224		
Hexatriacontanes plus	C_{36+}	4.872	18.572		
		100.00	**100.00**		

Physical Properties calculated based on GPA 2145-00 physical constants

TABLE 3
Compositional Analysis of Separator Gas MD-93126-01

Component Name	Chemical Symbol	Mole %			GPM
		As Analyzed	Acid Gas Free	With Oxygen	
Oxygen	O_2			0.000	
Nitrogen	N_2	2.214	2.227	2.214	
Carbon Dioxide	CO_2	0.265	0.000	0.265	
Hydrogen Sulphide	H_2S	0.320	0.000	0.320	
Methane	C_1	78.115	78.575	78.115	
Ethane	C_2	7.232	7.275	7.232	1.929
Propane	C_3	5.160	5.190	5.160	1.418
i-Butane	i-C_4	0.923	0.929	0.923	0.301
n-Butane	n-C_4	2.345	2.358	2.345	0.737
i-Pentane	i-C_5	0.900	0.905	0.900	0.328
n-Pentane	n-C_5	0.682	0.686	0.682	0.246
Hexanes	C_6	0.814	0.819	0.814	0.334
Heptanes	C_7	0.760	0.764	0.760	0.350
Octanes	C_8	0.202	0.204	0.202	0.103
Nonanes	C_9	0.064	0.064	0.064	0.036
Decanes	C_{10}	0.004	0.004	0.004	0.003
Undecane	C_{11}	0.000	0.000	0.000	0.000
Dodecanes Plus	C_{12+}	0.000	0.000	0.000	0.000
Total		**100.000**	**100.000**	**100.000**	**5.294**
Propanes Plus	C_{3+}	10.823	10.887	10.823	3.365
Butanes Plus	C_{4+}	5.663	5.697	5.663	1.947
Pentanes Plus	C_{5+}	2.395	2.410	2.395	0.909

Calculated Gas Properties @ Standard Conditions			Calculated Pseudocritical Properties		
Molecular Weight	22.65 kg/kmol	22.65 lb/lb-mol	Ppc	654.0 psia	4.51 MPa
Specific Gravity	0.7820 (Air = 1)	0.7820 (Air = 1)	Tpc	406.5 R	225.8 K
MW of C7+	101.11 kg/kmol	101.11 lb/lbmol	Ppc*	650.8 psia	4.49 MPa
Density of C7+	0.7294 g/cc	729.4 kg/m3	Tpc*	404.5 R	224.7 K

Calculated Gross Heating Value @ Standard Conditions			Calculated Net Heating Value @ Standard Conditions		
Dry	1,318.8 Btu/scf	49.23 MJ/m3	Dry	1,198.5 Btu/scf	44.74 MJ/m3
Wet	1,295.9 Btu/scf	48.37 MJ/m3	Wet	1,177.6 Btu/scf	43.96 MJ/m3

Standard Conditions: 60°F(288.7 K) @ 14.696 psia (0.101325 MPa)

TABLE 4
Compositional Analysis of Separator Gas MD-93126-02

Component Name	Chemical Symbol	Mole %			GPM
		As Analyzed	Acid Gas Free	With Oxygen	
Oxygen	O_2			0.000	
Nitrogen	N_2	2.871	2.886	2.871	
Carbon Dioxide	CO_2	0.324	0.000	0.324	
Hydrogen Sulphide	H_2S	0.194	0.000	0.194	
Methane	C_1	73.574	73.957	73.573	
Ethane	C_2	8.130	8.173	8.130	2.169
Propane	C_3	7.316	7.354	7.316	2.010
i-Butane	i-C_4	1.277	1.284	1.277	0.417
n-Butane	n-C_4	3.277	3.294	3.277	1.030
i-Pentane	i-C_5	1.024	1.029	1.024	0.373
n-Pentane	n-C_5	0.726	0.729	0.726	0.262
Hexanes	C_6	0.634	0.637	0.634	0.260
Heptanes	C_7	0.466	0.468	0.466	0.214
Octanes	C_8	0.135	0.135	0.135	0.069
Nonanes	C_9	0.047	0.047	0.047	0.026
Decanes	C_{10}	0.007	0.007	0.007	0.004
Undecane	C_{11}	0.000	0.000	0.000	0.000
Dodecanes Plus	C_{12+}	0.000	0.000	0.000	0.000
Total		**100.000**	**100.000**	**100.000**	**6.522**
Propanes Plus	C_{3+}	14.252	14.327	14.252	4.353
Butanes Plus	C_{4+}	6.937	6.973	6.937	2.343
Pentanes Plus	C_{5+}	2.383	2.396	2.383	0.896

Calculated Gas Properties @ Standard Conditions			Calculated Pseudocritical Properties		
Molecular Weight	23.63 kg/kmol	23.63 lb/lb-mol	Ppc	651.8 psia	4.49 MPa
Specific Gravity	0.8159 (Air = 1)	0.8159 (Air = 1)	Tpc	416.9 R	231.6 K
MW of C7+	101.72 kg/kmol	101.72 lb/lbmol	Ppc*	649.1 psia	4.48 MPa
Density of C7+	0.7303 g/cc	730.3 kg/m3	Tpc*	415.2 R	230.7 K

Calculated Gross Heating Value @ Standard Conditions			Calculated Net Heating Value @ Standard Conditions		
Dry	1,360.0 Btu/scf	50.76 MJ/m3	Dry	1,237.0 Btu/scf	46.17 MJ/m3
Wet	1,336.3 Btu/scf	49.88 MJ/m3	Wet	1,215.5 Btu/scf	45.37 MJ/m3

Standard Conditions: 60°F(288.7 K) @ 14.696 psia (0.101325 MPa)

TABLE 5
Compositional Analysis of Separator Gas MD-93126-03

Component Name	Chemical Symbol	Mole %			GPM
		As Analyzed	Acid Gas Free	With Oxygen	
Oxygen	O_2			0.000	
Nitrogen	N_2	2.889	2.913	2.889	
Carbon Dioxide	CO_2	0.273	0.000	0.273	
Hydrogen Sulphide	H_2S	0.552	0.000	0.552	
Methane	C_1	73.397	74.007	73.397	
Ethane	C_2	8.118	8.185	8.118	2.165
Propane	C_3	7.356	7.417	7.356	2.021
i-Butane	i-C_4	1.289	1.300	1.289	0.421
n-Butane	n-C_4	3.316	3.343	3.316	1.043
i-Pentane	i-C_5	1.033	1.042	1.033	0.377
n-Pentane	n-C_5	0.724	0.730	0.724	0.262
Hexanes	C_6	0.571	0.575	0.571	0.234
Heptanes	C_7	0.358	0.361	0.358	0.165
Octanes	C_8	0.087	0.088	0.087	0.044
Nonanes	C_9	0.027	0.028	0.027	0.015
Decanes	C_{10}	0.010	0.011	0.010	0.006
Undecane	C_{11}	0.000	0.000	0.000	0.000
Dodecanes Plus	C_{12+}	0.000	0.000	0.000	0.000
Total		**100.000**	**100.000**	**100.000**	**6.523**
Propanes Plus	C_{3+}	14.289	14.408	14.289	4.358
Butanes Plus	C_{4+}	6.933	6.991	6.933	2.336
Pentanes Plus	C_{5+}	2.328	2.347	2.328	0.873

Calculated Gas Properties @ Standard Conditions			Calculated Pseudocritical Properties		
Molecular Weight	23.57 kg/kmol	23.57 lb/lb-mol	Ppc	652.4 psia	4.50 MPa
Specific Gravity	0.8137 (Air = 1)	0.8137 (Air = 1)	Tpc	417.0 R	231.6 K
MW of C7+	101.37 kg/kmol	101.37 lb/lbmol	Ppc*	648.3 psia	4.47 MPa
Density of C7+	0.7297 g/cc	729.7 kg/m3	Tpc*	414.3 R	230.2 K

Calculated Gross Heating Value @ Standard Conditions			Calculated Net Heating Value @ Standard Conditions		
Dry	1,354.5 Btu/scf	50.56 MJ/m3	Dry	1,231.9 Btu/scf	45.98 MJ/m3
Wet	1,330.9 Btu/scf	49.68 MJ/m3	Wet	1,210.5 Btu/scf	45.18 MJ/m3

Standard Conditions: 60°F(288.7 K) @ 14.696 psia (0.101325 MPa)

Grane analysis.

Crude: **GRANE BLEND 2016 10**

Reference: **GRANEBLEND201610**

Crude Summary Report

General Information		Molecules (% wt on crude)		Whole Crude Properties	
Name:	GRANE BLEND 2016 10	methane + ethane	0,00	Density @ 15°C (g/cc)	0,892
Reference:	GRANEBLEND201610	propane	0,30	API Gravity	27,1
Traded Crude:	Grane	isobutane	0,21	Total Sulphur (% wt)	0,69
Origin:	Norway	n-butane	0,73	Pour Point (°C)	-6
Sample Date:	05 October 2016	isopentane	0,50	Viscosity @ 20°C (cSt)	28
Assay Date:	18 November 2016	n-pentane	0,68	Viscosity @ 40°C (cSt)	13
Issue Date:	23 November 2016	cyclopentane	0,09	Nickel (ppm)	3,6
Comments:		C_6 paraffins	1,19	Vanadium (ppm)	11,1
		C_6 naphthenes	0,90	Total Nitrogen (ppm)	2087
		benzene	0,15	Total Acid Number (mgKOH/g	1,20
		C_7 paraffins	1,03	Mercaptan Sulphur (ppm)	10
		C_7 naphthenes	1,46	Hydrogen Sulphide (ppm)	-
		toluene	0,53	Reid Vapour Pressure (psi)	6,1

Cut Data			Atmospheric Cuts									Vacuum Cuts			
Start (°C)	IBP	IBP	C5	65	100	150	200	250	300	350	370	370	450	500	550
End (°C)	FBP	C4	65	100	150	200	250	300	350	370	FBP	450	500	550	FBP
Yield (% wt)		1,2	1,9	3,0	5,4	5,6	7,2	9,7	10,6	3,6	51,7	13,6	8,7	7,9	21,5
Yield (% vol)		2,0	2,6	3,7	6,1	6,2	7,6	10,0	10,6	3,6	47,5	13,1	8,2	7,4	18,8
Cumulative Yield (% wt)		1,2	3,1	6,2	11,5	17,1	24,3	34,0	44,7	48,3	100,0				
Density @ 15°C (g/cc)	#####		#####	#####	0,776	0,802	0,836	0,866	0,890	0,907	0,969	#####	0,940	0,954	1,017
API Gravity	27,1		88,2	64,4	50,9	44,9	37,6	31,9	27,5	24,4	14,5	21,2	19,0	16,7	7,6
UOPK	11,8				11,5	11,6	11,5	11,5	11,5	11,5	11,7	11,6	11,7	11,8	11,7
Total Sulphur (% wt)	0,69		#####	#####	0,003	0,015	0,054	0,183	0,470	0,66	1,15	0,74	0,88	1,04	1,56
Mercaptan Sulphur (ppm)	10		0,2	1,1	2,5	3,8	1,9	0,8							
Total Nitrogen (ppm)	2087						33	83	173	384	3954	944	1671	2769	7225
Basic Nitrogen (ppm)	589						3,09	15	57,5	151	1114	324	442	738	2026
Total Acid Number (mgKOH/g	1,20		0,00	0,00	0,00	0,01	0,03	0,11	0,72	1,24	1,59	1,50	2,05	2,30	1,21
Viscosity @ 20°C (cSt)	28,1					1,27									
Viscosity @ 40°C (cSt)	12,9					0,95	1,68	3,14	6,83	15,7					
Viscosity @ 50°C (cSt)	9,42						1,44	2,57	5,21	10,9	1193	37,5	105	359	
Viscosity @ 60°C (cSt)											554	24,4	61,5	187	
Viscosity @ 100°C (cSt)											60,9	6,82	12,9	28,8	4236
Viscosity @ 130°C (cSt)															602
RON (Clear)			78,1	59,9	64,9	38,9									
MON (Clear)			77,3	57,6	61,4	36,9									
Paraffins (% wt)	31,5		95,2	53,0	35,3	40,7									
Naphthenes (%wt)	32,3		4,8	42,1	38,8	35,6									
Aromatics (% wt)	36,2		0,0	5,0	25,9	23,7									
Pour Point (°C)	-6						-52	-32	-7	8	26	24	38	46	44
Cloud Point (°C)							-51	-32	-7						
Freeze Point (°C)						-64	-48	-26							
Smoke Point (mm)						22	18	15							
Cetane Index						33	38	43	47	49					
Naphthalenes (% vol)						0,3	3,5	8,3	12,4						
Aniline Point (°C)					44,0	46,9	54,6	59,5	63,1	68,0		75,3	79,5	81,0	
Hydrogen (% wt)			16,5	15,0	13,5	13,8	13,3	12,9	12,6	12,5		12,4	12,2	12,1	
Wax (% wt)	6,7										10,5	14,1	14,5	12,7	5,7
C_7 Asphaltenes (% wt)	1,1										2,0		0,0	0,0	4,9
Micro Carbon Residue (% wt)	4,1										7,9		0,1	1,4	18,5
Rams. Carbon Residue (% wt	3,4										6,6		0,1	1,2	15,3
Vanadium (ppm)	11,1										21,4		0,0	0,0	51,6
Nickel (ppm)	3,6										7,0		0,0	0,0	16,9
Iron (ppm)	14,0										27,1		0,0	0,0	65,2

Statoil

Reference: **GRANEBLEND201610**
Crude: **GRANE BLEND 2016 10**

Yield Distribution

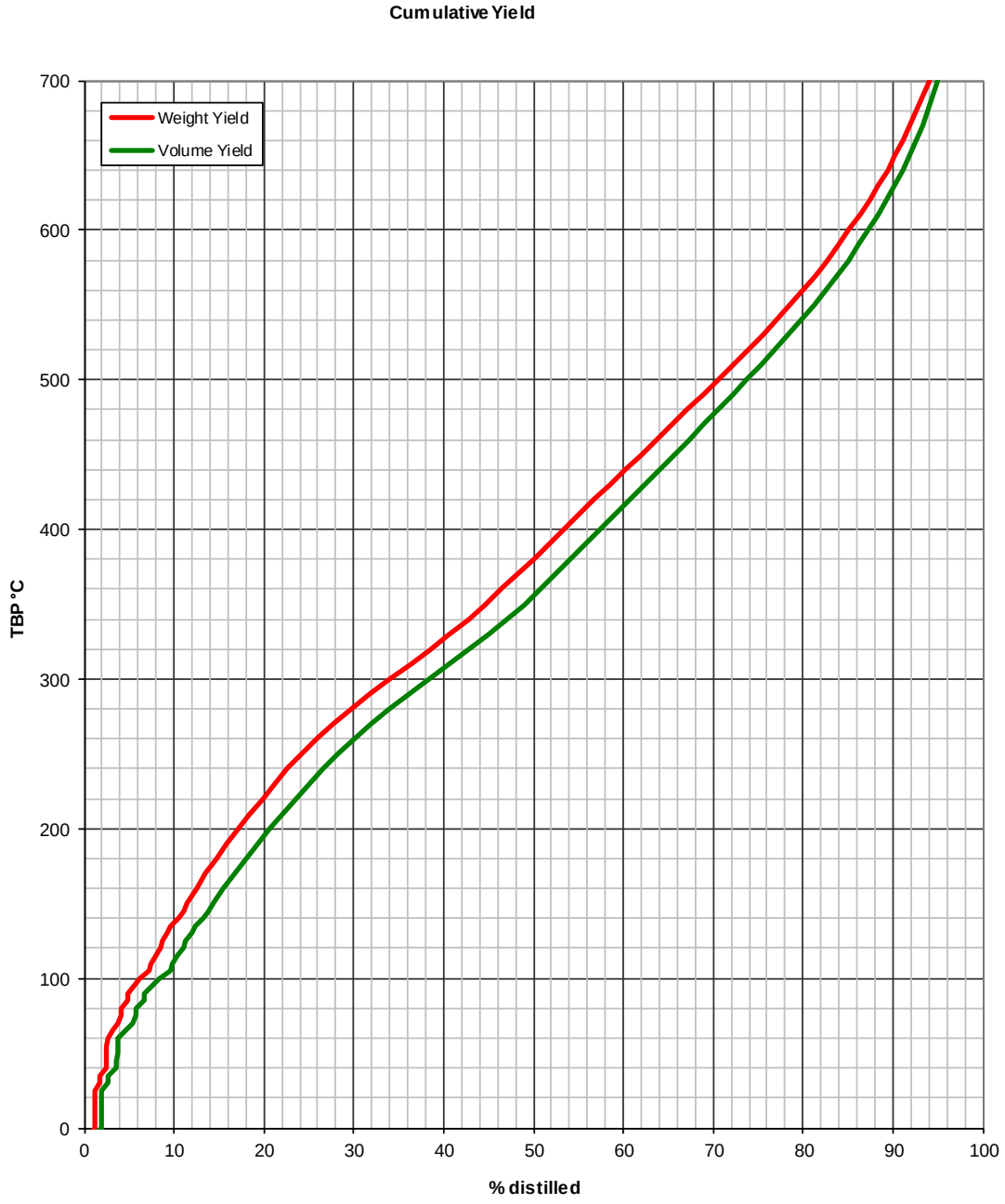

Ekofisk analysis.

Crude: **EKOFISK 2015 06**

Reference: **EKOFISK201506**

Crude Summary Report

General Information		Molecules (% wt on crude)		Whole Crude Properties	
Name:	EKOFISK 2015 06	methane + ethane	0,01	Density @ 15°C (g/cc)	0,830
Reference:	EKOFISK201506	propane	0,05	API Gravity	38,9
Traded Crude:	Ekofisk	isobutane	0,48	Total Sulphur (% wt)	0,21
Origin:	Norway	n-butane	1,92	Pour Point (°C)	-3
Sample Date:	17 July 2015	isopentane	1,07	Viscosity @ 20°C (cSt)	6
Assay Date:	29 September 2015	n-pentane	1,73	Viscosity @ 40°C (cSt)	4
Issue Date:	07 October 2015	cyclopentane	0,17	Nickel (ppm)	3,0
Comments:		C_6 paraffins	2,83	Vanadium (ppm)	1,9
		C_6 naphthenes	1,09	Total Nitrogen (ppm)	1168
		benzene	0,35	Total Acid Number (mgKOH/	0,10
		C_7 paraffins	2,16	Mercaptan Sulphur (ppm)	0
		C_7 naphthenes	1,73	Hydrogen Sulphide (ppm)	-
		toluene	0,98	Reid Vapour Pressure (psi)	7,6

Cut Data			Atmospheric Cuts									Vacuum Cuts			
Start (°C)	IBP	IBP	C5	65	100	150	200	250	300	350	370	370	450	500	550
End (°C)	FBP	C4	65	100	150	200	250	300	350	370	FBP	450	500	550	FBP
Yield (% wt)		2,5	4,3	5,7	10,4	8,1	9,1	9,3	8,9	3,4	38,3	12,1	6,4	5,4	14,3
Yield (% vol)		3,5	5,5	6,7	11,3	8,6	9,2	9,2	8,6	3,2	34,1	11,3	5,8	4,8	12,2
Cumulative Yield (% wt)		2,5	6,8	12,5	22,9	31,0	40,1	49,4	58,3	61,7	100,0				
Density @ 15°C (g/cc)	#####		#####	#####	0,762	0,782	0,813	0,836	0,857	0,871	0,929	#####	0,914	0,929	0,972
API Gravity	38,9		88,7	67,3	54,3	49,3	42,4	37,6	33,6	30,9	20,8	27,5	23,2	20,8	14,0
UOPK	12,2				11,8	11,9	11,9	11,9	12,0	12,0	12,1	12,0	12,1	12,1	12,2
Total Sulphur (% wt)	#####		#####	#####	0,002	0,006	0,023	0,073	0,172	0,234	0,456	#####	0,360	0,437	0,65
Mercaptan Sulphur (ppm)	0		0,0	0,1	0,0	0,0	0,0	0,0							
Total Nitrogen (ppm)	1168						2	19	153	372	2976	782	1742	2798	5451
Basic Nitrogen (ppm)	357						2,23	18,8	87,5	169,7	893	311	588	864,6	1531
Total Acid Number (mgKOH/g	0,10		0,00	0,00	0,00	0,00	0,01	0,04	0,12	0,16	0,21	0,16	0,18	0,22	0,26
Viscosity @ 20°C (cSt)	6,30					1,27									
Viscosity @ 40°C (cSt)	3,83					0,91	1,55	2,89	5,80	9,91					
Viscosity @ 50°C (cSt)	3,10						1,31	2,34	4,53	7,46	150	15,1	51,4	155	
Viscosity @ 60°C (cSt)											90,8	11,2	34,3	93,2	
Viscosity @ 100°C (cSt)											20,3	4,43	10,1	20,6	294
Viscosity @ 130°C (cSt)															79,6
RON (Clear)			77,3	54,6	53,3	31,5									
MON (Clear)			76,7	53,2	49,2	36,1									
Paraffins (% wt)	44,9		96,1	63,9	50,6	55,3									
Naphthenes (%wt)	30,4		3,9	29,9	30,3	27,5									
Aromatics (% wt)	24,7		0,0	6,1	19,1	17,2									
Pour Point (°C)	-3						-44	-20	4	15	35	26	35	37	37
Cloud Point (°C)							-41	-18	4						
Freeze Point (°C)						-61	-39	-15							
Smoke Point (mm)						29	27	24							
Cetane Index						42	48	55	62	67					
Naphthalenes (% vol)						0,1	1,7	5,5	9,6						
Aniline Point (°C)					52,2	56,6	63,8	71,0	78,4	83,5		89,6	95,0	97,0	
Hydrogen (% wt)			16,5	15,1	14,1	14,3	13,7	13,4	13,2	13,0		12,8	12,5	12,3	
Wax (% wt)	7,7										13,7	11,6	12,7	13,6	16,0
C_7 Asphaltenes (% wt)	0,0										0,1		0,0	0,0	0,3
Micro Carbon Residue (% wt)	1,7										4,3		0,0	0,4	11,4
Rams. Carbon Residue (% wt	1,4										3,7		0,0	0,4	9,8
Vanadium (ppm)	1,9										4,9		0,0	0,0	13,0
Nickel (ppm)	3,0										7,8		0,0	0,0	20,9
Iron (ppm)	0,5										1,3		0,0	0,0	3,4

Statoil

Reference: **EKOFISK201506**
Crude: **EKOFISK 2015 06**

Yield Distribution

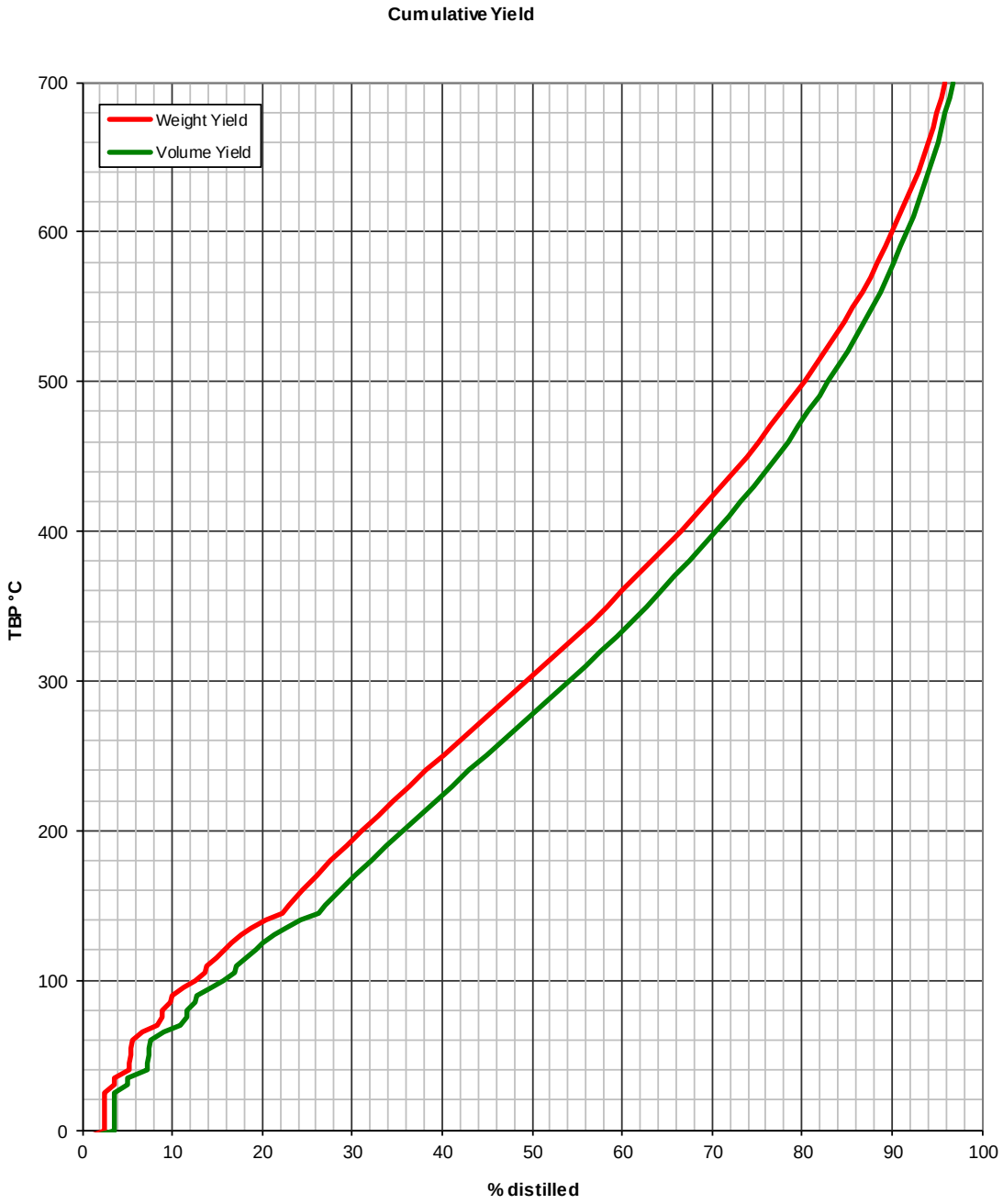

Appendix B - Vd-lists used in T_1-measurements

	Standard samples [s]	Diluted oil samples [s]	Non-diluted oil samples [s]
Time #1	0.001	0.001	0.001
Time #2	0.05	0.05	0.05
Time #3	0.1	0.07	0.07
Time #4	0.2	0.1	0.1
Time #5	0.3	0.12	0.12
Time #6	0.4	0.15	0.15
Time #7	0.5	0.17	0.17
Time #8	0.6	0.2	0.2
Time #9	0.7	0.25	0.25
Time #10	0.8	0.3	0.3
Time #11	0.9	0.35	0.35
Time #12	1	0.4	0.4
Time #13	1.2	0.45	0.45
Time #14	1.3	0.5	0.5
Time #15	1.5	0.6	0.6
Time #16	1.7	0.7	0.7
Time #17	2	0.8	0.8
Time #18	2.2	0.9	0.9
Time #19	2.5	1	1
Time #20	2.7	1.1	1.1
Time #21	3	1.2	1.2
Time #22	4	1.5	1.5
Time #23	5	1.7	1.7
Time #24	6	2	2
Time #25	7	2.2	2.2
Time #26	8	2.5	2.5
Time #27	10	2.7	2.7

Time #28	12	3	3
Time #29	15	4	4
Time #30	20	5	5
Time #31	25	6	6
Time #32	30	7	7

Appendix C – Vc-lists used in T_2-measurements

	Standard samples [ms]	Diluted oil samples [ms]	Non-diluted oil samples [ms]
Time #1	2	2	2
Time #2	10	5	5
Time #3	20	10	10
Time #4	50	20	15
Time #5	100	30	20
Time #6	150	50	25
Time #7	200	70	30
Time #8	250	100	40
Time #9	300	120	50
Time #10	350	150	60
Time #11	400	170	70
Time #12	450	200	80
Time #13	500	250	100
Time #14	550	300	120
Time #15	600	350	150
Time #16	650	400	170
Time #17	800	450	200
Time #18	1000	500	250
Time #19	1100	550	300
Time #20	1200	600	350
Time #21	1300	650	400

Time #22	1500	750	450
Time #23	1700	800	500
Time #24	2000	900	600
Time #25	2500	1000	700
Time #26	3000	1100	800
Time #27	5000	1200	900
Time #28	10000	1300	1100
Time #29	15000	1500	1200
Time #30	20000	1700	1500
Time #31	25000	2000	2000
Time #32	30000	2500	2500

Appendix D – MatLab Scripts

T1_T2_500_ir.m

```
%Program (or function) for procssing data obtained using the bp11_cpmg_2D
or bp11_intg_cpmg_2D
%pulse sequence on the %500 MHz instrument at UiB. Final result is a
matrice
%with T2-decays (magnitude) at different diffusion weightings.
%function [] = bp11_G0_T2_500
close all
clear all
fid=fopen('ser','r','l');
data=fread(fid,'int32');

td1=32;
td2=size(data);
td2=td2(1);
td3=0.5*td2/td1;

ser_r=data(2:2:td2);
ser_i=data(1:2:td2);


figure(1)
plot(ser_r,'b*')
hold on
plot(ser_i,'ro')
hold off

%Phase adjustment does not work yet.
%choose the phase based on a good T2-decay (the second one)
%ser_rss=ser_r(td3+1:2*td3)
%ser_iss=ser_i(td3+1:2*td3)
%ser_ttt=ser_rss+i*ser_iss;

%phi=angle(ser_ttt);
%phi=mean(phi(50:100))

%loop for correction of each ser
k=1 %in order to remove the first point in cpmg decay
td4=td3
for i=1:td1
    ser_rs=ser_r(k:td4);
    ser_is=ser_i(k:td4);
ser_t=complex(ser_rs,ser_is);

%Magnitude of the complex signal
if ser_rs(10) >= 0
ser_tt(:,i)=abs(ser_t);
else
    ser_tt(:,i)=-abs(ser_t);
end

%Phasing of the signal
%ser_tt(:,i)=ser_t.*exp(-i*phi);
```

```
figure(2)
plot(ser_tt)
hold on
k=k+td3
    td4=td4+td3
end


figure(3)
plot(imag(ser_tt))
hold on
plot(real(ser_tt),'r')
%plot(-ser_r,'g')
%plot(-ser_i,'c')
hold off

%cpmg time vector
t = [1:1:td3];
tau=input('What is the echo spacing (ms) in the CPMG train? (d20)');
t=t.*tau*1e-3;
t=t';


%inv rec time vector
x = load('vdlist');
x=x(1:td1)

n=size(x);
p=size(t)

ser_tt_mod=ser_tt(:,1:32); %to remove the first T1 point

data_real=real(ser_tt);
save -ascii -tabs T1_T2_data.txt ser_tt_mod
save -ascii -tabs t_cpmg.txt t
save -ascii -tabs t_ir.txt x
t1t2fix
```

T1_T2_500_sr.m

```
%Program (or function) for procssing data obtained using the bp11_cpmg_2D
or bp11_intg_cpmg_2D
%pulse sequence on the %500 MHz instrument at UiB. Final result is a
matrice
%with T2-decays (magnitude) at different diffusion weightings.
%function [] = bp11_G0_T2_500
close all
clear all
fid=fopen('ser','r','b');
data=fread(fid,'int32');

td1=32;
td2=size(data);
td2=td2(1);
td3=0.5*td2/td1;

ser_r=data(2:2:td2);
ser_i=data(1:2:td2);



figure(1)
plot(ser_r,'b*')
hold on
plot(ser_i,'ro')
hold off

%Phase adjustment does not work yet.
%choose the phase based on a good T2-decay (the second one)
%ser_rss=ser_r(td3+1:2*td3)
%ser_iss=ser_i(td3+1:2*td3)
%ser_ttt=ser_rss+i*ser_iss;

%phi=angle(ser_ttt);
%phi=mean(phi(50:100))

%loop for correction of each ser
k=1 %in order to remove the first point in cpmg decay
td4=td3
for i=1:td1
    ser_rs=ser_r(k:td4);
    ser_is=ser_i(k:td4);
ser_t=complex(ser_rs,ser_is);

%Magnitude of the complex signal
if ser_rs(10) >= 0
ser_tt(:,i)=abs(ser_t);
else
    ser_tt(:,i)=abs(ser_t);
end

%Phasing of the signal
%ser_tt(:,i)=ser_t.*exp(-i*phi);

figure(2)
plot(ser_tt)
hold on
k=k+td3
```

```
    td4=td4+td3
end


figure(3)
plot(imag(ser_tt))
hold on
plot(real(ser_tt),'r')
%plot(-ser_r,'g')
%plot(-ser_i,'c')
hold off

%cpmg time vector
t = [1:1:td3];
tau=input('What is the echo spacing (ms) in the CPMG train? (d20)');
t=t.*tau*1e-3;
t=t';


%inv rec time vector
x = load('vdlist');
x=x(1:td1)

n=size(x);
p=size(t)

ser_tt_mod=ser_tt(:,1:32); %to remove the first T1 point

data_real=real(ser_tt);
save -ascii -tabs T1_T2_data.txt ser_tt_mod
save -ascii -tabs t_cpmg.txt t
save -ascii -tabs t_ir.txt x
t1t2fix
```

plotfig_T1T2_500.m

```
load T1_T2_data_inv.txt.out
data=T1_T2_data_inv_txt
load t_ir.txt.out
load t_cpmg.txt.out

logT1=log10(t_ir_txt);
logT2=log10(t_cpmg_txt);

figure(102); contour(t_cpmg_txt,t_ir_txt,data');colormap hot
xlabel('T_2 (s)');ylabel('T_1 (s)')
set(gca,'xscale','log')
set(gca,'yscale','log')
set(gca,'fontsize',16)
set(findall(gca,'Type','Text'),'FontSize',16)
hold on
x=[0.001;0.01;0.1;1;10;100];
y=[0.001;0.01;0.1;1;10;100];
%manually adjust the x- and y-values based on the range used
%in the nnls-smoothing
plot(x,y,'k-');
```

Appendix E – Pulse programs

^{1}H measurement (zg)

```
;zg
;avance-version (12/01/11)
;1D sequence
;
;$CLASS=HighRes
;$DIM=1D
;$TYPE=
;$SUBTYPE=
;$COMMENT=


#include <Avance.incl>


"acqt0=-p1*2/3.1416"


1 ze
2 30m
  d1
  p1 ph1
  go=2 ph31
  30m mc #0 to 2 F0(zd)
exit


ph1=0 2 2 0 1 3 3 1
ph31=0 2 2 0 1 3 3 1


;pl1 : f1 channel - power level for pulse (default)
;p1 : f1 channel -  high power pulse
;d1 : relaxation delay; 1-5 * T1
;ns: 1 * n, total number of scans: NS * TD0



;$Id: zg,v 1.11 2012/01/31 17:49:31 ber Exp $
```

^{1}H DOSY (ledbpg2s)

```
;ledbpgp2s
;avance-version (12/01/11)
;2D sequence for diffusion measurement using stimulated
;   echo and LED
;using bipolar gradient pulses for diffusion
;using 2 spoil gradients
;
;D. Wu, A. Chen & C.S. Johnson Jr.,
;   J. Magn. Reson. A 115, 260-264 (1995).
;
;$CLASS=HighRes
;$DIM=2D
;$TYPE=
;$SUBTYPE=
;$COMMENT=


#include <Avance.incl>
#include <Grad.incl>
#include <Delay.incl>


define list<gradient> diff=<Difframp>


"p2=p1*2"


"DELTA1=d20-p1*2-p2-p30*2-d16*2-p19-d16"
"DELTA2=d21-p19-d16-4u"


"acqt0=-p1*2/3.1416"


1 ze
2 d1
  50u UNBLKGRAD
  p1 ph1
  p30:gp6*diff
  d16
  p2 ph1
  p30:gp6*-1*diff
  d16
  p1 ph2
  p19:gp7
  d16
  DELTA1
  p1 ph3
  p30:gp6*diff
  d16
  p2 ph1
  p30:gp6*-1*diff
  d16
```

```
  p1 ph4
  p19:gp8
  d16
  DELTA2
  4u BLKGRAD
  p1 ph5
  go=2 ph31
  d1 mc #0 to 2 F1QF(calgrad(diff))
exit


ph1= 0
ph2= 0 0 2 2
ph3= 0 0 0 0 2 2 2 2  1 1 1 1 3 3 3 3
ph4= 0 2 0 2 2 0 2 0  1 3 1 3 3 1 3 1
ph5= 0 0 0 0 2 2 2 2  1 1 1 1 3 3 3 3
ph31=0 2 2 0 2 0 0 2  3 1 1 3 1 3 3 1


;pl1 : f1 channel - power level for pulse (default)
;p1  : f1 channel -  90 degree high power pulse
;p2  : f1 channel - 180 degree high power pulse
;p19: gradient pulse 2 (spoil gradient)
;p30: gradient pulse (little DELTA * 0.5)
;d1  : relaxation delay; 1-5 * T1
;d16: delay for gradient recovery
;d20: diffusion time (big DELTA)
;d21: eddy current delay (Te)              [5 ms]
;ns: 8 * n
;ds: 4 * m
;td1: number of experiments
;FnMODE: QF
;        use xf2 and DOSY processing


;use gradient ratio:    gp 6 : gp 7   : gp 8
;                       100  : -17.13 : -13.17

;for z-only gradients:
;gpz6: 100%
;gpz7: -17.13% (spoil)
;gpz8: -13.17% (spoil)

;use gradient files:
;gpnam6: SMSQ10.100
;gpnam7: SMSQ10.100
;gpnam8: SMSQ10.100

;use AU-program dosy to calculate gradient ramp-file Difframp



;$Id: ledbpgp2s,v 1.8 2012/01/31 17:49:27 ber Exp $
```

^{1}H DOSY (leddste)

```
;diffDste
;new version using built in gradient functions as shapes 14.12.2007
KLZ
;pl2 --> pl12, lock during DELTA removed, comments improved
29.05.2008 KLZ
;1D mode included 22.08.08 KLZ
;variable gradient amplitude ramp included 30.09.09 KLZ
;new mc syntax and use of ZGOPTNS rather than loop counters 26.07.11
KLZ
;ZGOPTNS corrected 22.12.2011 KLZ
;spoilRec included 28.01.2013 KLZ
;
;$CLASS=diff
;$DIM=2D
;$TYPE=exp


#include <Grad.incl>
#include <Avance.incl>
#include <Grad_Pulse.incl>

define list<gradient> diff_ramp=<$GPNAM31>

"acqt0=0"
;----------------------------------------------------------------
----------

ze
10u
5m pl1:f1       ;set rf power level

start,      100u
#ifdef DEC
               1u pl12:f2                  ; decoupler use pl12
            1u do:f2                    ; decoupler off during d1
#endif
#ifdef LOCK
          d1 LOCKH_OFF                ; lock on during d1
               d11 UNBLKGRAD             ; unblank gradient
amplifier, lock hold during experiment
#endif
#ifndef LOCK
               d1  H2_PULSE
               d11 UNBLKGRAMP              ; unblank gradient
amplifier
#endif
;------------------------ Spoiler recovery sequence ---------------
---------------
#ifdef SpoilRec
               p1:f1 ph11
               p23:gp23             ;(10m:1=18 G/cm)
               d2
               p1:f1 ph12
               p24:gp24             ;(1m:-5=-90 G/cm)
```

```
                d2
                d23  ;BLKGRAMP
                d11 UNBLKGRAMP             ; unblank gradient
amplifier
#endif
;-------------------------- Start of dummy gradient loop -----------
----------------
#ifdef dummyGrad
                dummy, 1u
                     gradPulse( cnst1, cnst2, cnst3, d17, d18, d16,
l8, l9, diff_ramp)
                     d2                            ; gradient
stabilisation time
                     d9 BLKGRAMP                    ; tau
#ifdef spoil
                d11 UNBLKGRAMP             ; unblank gradient
amplifier
                          p19:gp5                          ; spoiler
gradient, sine shape
                          d2                       ; gradient
stabilisation time
#endif
                     d5 BLKGRAMP                    ; long tau
                     d11 UNBLKGRAMP             ; unblank gradient
amplifier
                lo to dummy times l13       ; l13 number of dummy
gradient pulses
#endif
;-------------------------- Start of experiment --------------------
---------------
                p1:f1 ph1                     ; 90 degree pulse
            gradPulse( cnst1, cnst2, cnst3, d17, d18, d16, l8, l9,
diff_ramp)
                d2                                ; gradient
stabilisation time
                d9 BLKGRAMP                       ; tau
                p1:f1 ph2                     ; 90 degree pulse
#ifdef spoil
                d11 UNBLKGRAMP             ; unblank gradient
amplifier
                     p19:gp5                          ; spoiler
gradient, sine shape
                     d2                       ; gradient
stabilisation time
#endif
                d5 BLKGRAMP                       ; long tau
                d11 UNBLKGRAMP                ; unblank gradient
amplifier
                p1:f1 ph3                     ; 90 degree pulse
            gradPulse( cnst1, cnst2, cnst3, d17, d18, d16, l8, l9,
diff_ramp)
                d2                                ; gradient
stabilisation time
                d9 ;ph0                           ; tau
            gradPulse( cnst1, cnst2, cnst3, d17, d18, d16, l8, l9,
diff_ramp)
```

```
                d2                                  ; gradient
stabilisation time
                d9 BLKGRAMP                         ; tau
                p1:f1 ph4                       ; 90 degree pulse
#ifdef spoil
                d11 UNBLKGRAMP              ; unblank gradient
amplifier
                     p19:gp5*0.7                            ; spoiler
gradient, sine shape
                     d2                         ; gradient
stabilisation time
#endif
                d5 BLKGRAMP                         ; long tau
                d11 UNBLKGRAMP                  ; unblank gradient
amplifier
                p1:f1 ph5                       ; 90 degree pulse
             gradPulse( cnst1, cnst2, cnst3, d17, d18, d16, l8, l9,
diff_ramp)
                d2                                  ; gradient
stabilisation time
                d10 BLKGRAMP                ; tau
;               d10 ph0 BLKGRAMP                ; tau
;--------------------------- Start of LED module  -------------------
----------------
#ifdef LED
             p1:f1 ph6
#ifdef spoil
             d11 UNBLKGRAMP                     ; unblank gradient
amplifier
                p19:gp5*-1                          ; spoiler
gradient, sine shape
#endif
                d2                                  ; gradient
stabilisation time
             d19 BLKGRAMP
             p1:f1 ph7
#endif
;--------------------------- End of LED module  ---------------------
--------------
#ifdef DEC
           go=start ph31 cpd2:f2            ; start acquisition with
decoupling
#endif
#ifndef DEC
           go=start ph31                    ; start acquisition
#endif
           100u mc #0 to start F1QF(calgrad(diff_ramp))
#ifdef DEC
         100m do:f2                       ; wait for data storage,
decoupler off
#endif
#ifndef DEC
         100m                             ; wait for data storage
#endif
#ifdef LOCK
      100m rf #0 LOCKH_OFF           ; reset file pointer, lock on
```

```
#endif
#ifndef LOCK
     100m rf #0                                   ; reset file pointer
#endif
     lo to start times l1                  ; l1 = Number of
repetitions
exit

ph0=0
ph1= 0 1 2 3
ph2= 0
ph3= 2 3
ph4= 2 2 2 2 0 0 0 0
ph5= 0
ph6= 0
ph7= 0
ph11= 0
ph12= 1
#ifdef LED
     ph31=2 2 0 0 0 0 2 2
#endif
#ifndef LED
     ph31=0 0 2 2 2 2 0 0
#endif

;pl1: f1 channel - power level for pulse (default)
;p1: f1 channel -  90 degree pulse
;d17: gradient ramp up time
;d16: gradient ramp down time
;d18: gradient duration
;p19: spoil gradient duration - 2*p17
;d1: relaxation delay; 1-5 * T1
;d2: gradient stabilisation time
;d5: DELTA/2 remainder
;d9: tau remainder
;d10: tau remainder, used to shift trigger position
;d11: gradient amplifier unblank delay 200 us

;ns: 8 * n
;td1: number of experiments
;l1: Repetitions of the whole experiment



;$Id: diffDste,v 1.9 2013/02/11 15:37:34 ber Exp $
```

^{1}H T_1 measurement (t1ir)

```
;t1ir
;avance-version (12/01/11)
;T1 measurement using inversion recovery
;
;$CLASS=HighRes
;$DIM=2D
;$TYPE=
;$SUBTYPE=
;$COMMENT=


#include <Avance.incl>


"p2=p1*2"
"d11=30m"


"acqt0=-p1*2/3.1416"


1 ze
2 d1
  p2 ph1
  vd
  p1 ph2
  go=2 ph31
  d11 wr #0 if #0 ivd
  lo to 1 times td1
exit


ph1=0 2
ph2=0 0 2 2 1 1 3 3
ph31=0 0 2 2 1 1 3 3


;pl1 : f1 channel - power level for pulse (default)
;p1 : f1 channel -  90 degree high power pulse
;p2 : f1 channel - 180 degree high power pulse
;d1 : relaxation delay; 1-5 * T1
;d11: delay for disk I/O                             [30 msec]
;vd : variable delay, taken from vd-list
;ns: 8 * n
;ds: 4
;td1: number of experiments = number of delays in vd-list
;FnMODE: undefined

;define VDLIST

;this pulse program produces a ser-file (PARMOD = 2D)


;$Id: t1ir,v 1.13 2012/01/31 17:49:28 ber Exp $
```

^{1}H T_2 measurement (cpmg)

```
;cpmg
;avance-version (12/01/11)
;T2 measurement using Carr-Purcell-Meiboom-Gill sequence
;
;$CLASS=HighRes
;$DIM=2D
;$TYPE=
;$SUBTYPE=
;$COMMENT=


#include <Avance.incl>


"p2=p1*2"
"d11=30m"


1 ze
2 d1
  p1 ph1
3 d20
  p2 ph2
  d20
  lo to 3 times c
  go=2 ph31
  d11 wr #0 if #0 ivc
  lo to 1 times td1
exit


ph1=0 0 2 2 1 1 3 3
ph2=1 3 1 3 0 2 0 2
ph31=0 0 2 2 1 1 3 3


;pl1 : f1 channel - power level for pulse (default)
;p1 : f1 channel -  90 degree high power pulse
;p2 : f1 channel - 180 degree high power pulse
;d1 : relaxation delay; 1-5 * T1
;d11: delay for disk I/O                                [30 msec]
;d20: fixed echo time to allow elimination of diffusion
;     and J-mod. effects
;vc : variable loop counter, taken from vc-list
;ns: 8 * n
;ds: 16
;td1: number of experiments = number of values in vc-list

;define VCLIST

;this pulse program produces a ser-file (PARMOD = 2D)

;d20: d20 should be << 1/J ,but > (50 * P2)
;vc : vc should contain even numbers to provide
```

```
;     for cancellation of 180 degree pulse errors


;$Id: cpmg,v 1.11 2012/01/31 17:49:22 ber Exp $
```

^{1}H T_1-T_2 correlation measurement (t1sr_cpmg_all_echoes)

```
;Inversion recovery combined with single shot T2 experiment
;sample on all echoes and optimized by JGS 29.10.2009.
;using single point acquisition 11.02.2009 KLZ
;use qsim and analog mode
;adjust ph30 for absorption
;for t1/t2 processing use slice increment 2, expdec, auto,
; increment = 2*d20, pft2

;$CLASS=
;$DIM=1D
;$TYPE=install
;$OWNER=Bruker

;dwellmode explicit

#include <Avance.incl>
#include <Grad.incl>
#include <De.incl>

"l1=td/2"
"p2=2*p1"
"d21=d20-p2"
"d22=(d21/2-1u)/2"
1  ze                 ; initialize
start,  d1
       p1 ph6
  d3
  p28:gp10
  d4
  p1 ph7
  d8
  p29:gp11
  d9
     vd
        ACQ_START(ph30,ph31)                          ; start
acquisition
        10u REC_BLK
        10u sytra
        p1 ph1
cpmg,   d22 REC_BLK
        d22 sytra
        p2 ph2
        d22 syrec
        d22 REC_UNBLK
        1u DWL_CLK_ON
        1u DWL_CLK_OFF
    lo to cpmg times l1
    10u REC_BLK
rcyc=start
100m
1s wr #0 if #0 ivd
lo to 1 times td1
exit
```

```
ph1=0 0 2 2 1 1 3 3
ph2=1 3 1 3 0 2 0 2
ph6=0
ph7=1
ph30=0
ph31=0 0 2 2 1 1 3 3

;d1:    Relaxation delay
;d20:   Echo time, use 2*d20 for auto increment
;p1:    90 degree pulse
;p2:    180 degree pulse
```

^{1}H T_1-T_2 correlation measurement (t1ir_cpmg_all_echoes)

```
;Inversion recovery combined with single shot T2 experiment
;sample on all echoes and optimized by JGS 29.10.2009.
;using single point acquisition 11.02.2009 KLZ
;use qsim and analog mode
;adjust ph30 for absorption
;for t1/t2 processing use slice increment 2, expdec, auto,
; increment = 2*d20, pft2

;$CLASS=
;$DIM=1D
;$TYPE=install
;$OWNER=Bruker

;dwellmode explicit

#include <Avance.incl>
#include <Grad.incl>
#include <De.incl>

"l1=td/2"
"p2=2*p1"
"d21=d20-p2"
"d22=(d21/2-1u)/2"

"anavpt=8"
1  ze                ; initialize
start,  d1
     p2 ph12
     vd
        ACQ_START(ph30,ph31)                          ; start
acquisition
        10u REC_BLK
        10u sytra
        p1 ph1
cpmg,   d22 REC_BLK
        d22 sytra
        p2 ph2
        d22 syrec
        d22 REC_UNBLK
        1u DWL_CLK_ON
        1u DWL_CLK_OFF
    lo to cpmg times l1
    10u REC_BLK
rcyc=start
100m
1s wr #0 if #0 ivd
lo to 1 times td1
exit

ph12=0 0 2 2
ph1=0 0 2 2 1 1 3 3
ph2=1 3 1 3 0 2 0 2
ph30=0
ph31=0 0 2 2 1 1 3 3
```

```
;d1:    Relaxation delay
;d20:   Echo time, use 2*d20 for auto increment
;p1:    90 degree pulse
;p2:    180 degree pulse
```